# WEAR AND TRIBOFILM FORMATION WITH ZINC-FREE ANTIWEAR ADDITIVES

by

PRADIP SAIRAM PICHUMANI

Presented to the Faculty of the Graduate School of

The University of Texas at Arlington in Partial Fulfillment

of the Requirements

for the Degree of

MASTER OF SCIENCE IN MATERIALS SCIENCE & ENGINEERING

THE UNIVERSITY OF TEXAS AT ARLINGTON

December 2012

ACKNOWLEDGEMENTS

In any research work, that one undertakes, one cannot rule out the significant contributions, guidance and assistance from others. I wish to express my gratitude to all the people who have contributed through their support and knowledge to this work.

My warmest thanks go to Dr. Pranesh B. Aswath for being my research advisor and guiding me throughout my MS degree. He has been my strong support towards my research work. He has always inspired me to provide perfect, accurate and efficient work. I would like to take this opportunity to thank Dr. Fuqiang Liu & Dr. Daejong Kim for assisting me and being my committee members.

I am very grateful to all the faculty members of the Department of Materials Science and Engineering at the University of Texas at Arlington for providing me their constant support and knowledge. I would like to thank the MSE staff, Mrs. Jennifer Standlee, who has always been the first person who comes to my mind when I need help and Mrs. Libia Cuauhti for assisting me with the administrative tasks.

I would like to thank Dr. Jiecho Jiang and Dr. David Yan for training me on various equipment in the Characterization Center for Materials and Biology.

I thank all my friends & colleagues, Dr. Mihir Patel, Dr. Xin Chen, Sujay Bagi, Megen Velten, Vibhu Sharma and all others in Dr. Aswath's group for making my Master's degree experience an amazing part of my life.

I would like to thank my parents, Pichumani Sethuraman and Kamala Pichumani for providing me the support and opportunity to pursue my Masters in the US. I wish to express all my respect to them.

December 3, 2012

ABSTRACT

WEAR AND TRIBOFILM FORMATION WITH ZINC-FREE ANTIWEAR ADDITIVES

Pradip Sairam Pichumani, M.S.

The University of Texas at Arlington, 2012

Supervising Professor: Pranesh B. Aswath

Engine oil is used in all internal combustion engines to lubricate the moving parts & mitigate the wear due to friction. Along with the mentioned two functions, engine oil also serves to protect the engine from corrosion, clean debris, improves sealing and serves in thermal conductivity. Engine oil is either derived from petroleum derivatives or made synthetically. A number of additives are added to the engine oil (Base oil) to improve its performance and longevity. Antioxidants, pour point depressants, viscosity index improvers, antifoaming agents, corrosion inhibitors, etc are some of the additives that are added to improve the engine oil's performance.

The main goal of this study is to understand the mechanism of formation of tribofilms from combining ashless additives, their synergistic and antagonistic properties and wear performance with different blends of these additives. Wear tests were performed using high frequency reciprocating rig in order to map the effects of wear and tribological properties of ashless antiwear additives on 52100 steel at 100°C and 1 Kg load. X-ray absorption near edge structure spectroscopy (XANES) was performed on the tribofilms in order to investigate the chemical properties of films generated by the combination of ashless fluorothiophosphates and ashless dialkyl dithiophosphates ashless antiwear additives.

TABLE OF CONTENTS

LIST OF ILLUSTRATIONS

Figure Page

LIST OF TABLES

# CHAPTER 1

## INTRODUCTION

The development of machinery and equipment to cater to every field of automation in the early 1960 was rapidly evolving. This progress brought steep increases in the reported failures of plant and machinery due to wear and its associated failure, resulting in heavy financial loss and the cost of operating machinery was increasing. Numerous papers were published based on this issue by specialists involved in the subjects of friction, wear and lubrication [1-4]. However this issue caught attention only after October 1964's Conference on Iron and Steel Works Lubrication & Wear Group of the Institution of Mechanical Engineers [1]. This issue called for a better understanding of the situation and research on a global scale. As a result, a group was setup to investigate the present state of lubrication education and research. Three principal reasons for investigating a field which was widely neglected in the past, despite its technological importance:

1. The importance of the field spans across wide areas of engineering, physics, metallurgy and chemistry.
2. Research into only the advancement of production or automation has been carried out.
3. To better understand the terminology "Lubrication" as it has been falsely understood as a medium of transference of force from one moving surface onto another when the surfaces are in relative motion.

The term "Tribology" was coined by Dr. H. Peter Jost [5]. Chairman of the Working Group from the Greek word *Tribos,* meaning rubbing and *Logos* meaning Logic or principle. Tribology was defined as "the science and technology of interacting surfaces in relative motion and of related subjects and practices". On March 9, 1966, the British Government published the

Working Group's report which confirmed its prognosis that prompted its establishment. The report found a direct correlation between the theoretical understanding of the field (tribology education and research) and the progress in the industrial research and development to support production. This laid a strong foundation to this field of study and the British government could not afford to overlook its economic and commercial advantages. On Sept 26, 1966, the Committee on Tribology was introduced at a press conference, chaired by Wedgewood Benn.

The field of tribology can be differentiated into two main branches, namely tribotechnology and triboscience. Tribotechnology covers the technical aspects of certain basic units and sets, while triboscience is aimed at clarifying the fundamental processes occurring during friction and wearing processes and establishing universally valid laws. Triboscience regards tribophysical and tribochemical processes, that is, processes connected with the occurrence of friction, which take place under the influence of mechanical energy [6].

### 1.1 Tribochemical Challenges

Tribology, being an essential field in combating wear, has motivated research in many practical and real life scenarios. The fundamental understanding of friction, wear and lubrication is yet to be uncovered completely. Changes in material properties during friction; strengthening of engineering materials and surfaces; innovative approach to protect, repair and maintain engineering surfaces are some of the aspects that still mesmerizes researchers. The principle reason/basis of the mentioned observations is yet to be satisfactorily proved. Therefore an approach to improve chemical and mechanical properties of metal surfaces used in industries is an ongoing research. The practical approach to improving the performance of lubricants used between interacting surfaces is by the addition of additives. These additives on the other hand must be environmentally friendly and must not damage the machine in which it is being used in any way. In the case of internal combustion engines, engine oils must not hinder the fuel

economy of the vehicle. In fact, it should raise the fuel economy, durability and all other environment related issues. Inefficient lubrication brings about wear and tear, high friction and reduction in the vehicle life. To cater the above mentioned requirements, there is a need for high efficient lubricants and a strong fundamental understanding of tribochemical interactions and surface properties.

## 1.2 Chemical Additives

Lubricants and lubrication technology are essential components of modern industries. Lubrication contributes to the reduction in wear and control/mitigation of friction. Modern machines create extreme operating conditions such as high temperatures, loads and speeds. Lubricants used must be able to operate in the above mentioned conditions while delivering the optimum performance. Many liquids including water have been used as lubricants to reduce friction & heat between two contacting surfaces. Today Lubricant oil or Lube oil is the most commonly used lubricant because of its availability in natural state and its wide range of possible applications. When the crude oil basestocks arrived on the scene, the stage was set for chemical additives to take on the task of improving petroleum-based lubricants. Additive compounds are added to lube oils to increase the performance in various aspects. The most common chemical additives are antiwear, antioxidants, friction modifiers, foam depressants, viscosity Index improvers and other chemical additives.

One of the most common additives used in engine oil is Zinc Dialkyldithiophosphate (ZDDP). ZDDP has been used for many years as an antioxidant and an anti-wear additive in the engine lubricant formulations [7]. ZDDP is contained in fully formulated oils with Phosphorus content of less than 0.1% and it the most vital additive that inhibits oxidation of metal parts and form sacrificial film called the “Tribofilm” that reduces the wear of the interacting surfaces considerably. A number of mechanisms have been proposed to explain the formation of

Tribofilms (film formation) from ZDDP. Although not completely understood, it is widely accepted that the Antiwear (AW) films are formed by the decomposition products of ZDDP [7-11]. The antiwear (AW) films consist mainly of phosphates and sulfides and the average film thickness is about 100nm [7,12]. The main chemical state of sulfur in Tribofilms from ZDDP is zinc sulfide (at high rubbing period between two load bearing surfaces). At low rubbing period, there are two kinds of sulfide formed: 1. iron sulfide, 2. Zinc sulfide. Iron sulfide is present in small quantities and close to the load bearing surface. This is due to the fact that, iron facilitates the formation of Tribofilm during the initial stages. This could also be explained thermodynamically. Sulfur being a soft base, prefers to react with borderline soft acid (Zinc). Iron ($Fe^{2+}$ and $Fe^{3+}$) are hard acids and in the presence of soft acids, sulfur reacts with Zinc forming ZnS [13]. The tribofilm formed by ZDDP is made of multiple layers. X Ray Absorption near Edge Spectroscopy (XANES) is used to find the chemical makeup of the Tribofilms. Total Electron Yield (TEY) is used to obtain the surface information as the penetration depth for this type is low (about 50nm). The upper layers of ZDDP are made up of long chain polyphosphates [14]. Fluorescent Yield (FY) is used to obtain chemical information from the bulk of the Tribofilm (penetration depth > 800nm). The bulk of the Tribofilm is made up of short chain polyphosphates. ZDDP has multiple merits as an antioxidant and as an Antiwear (AW) additive but it causes catalytic poisoning by deposition of degraded products. In addition to this, additive containing metal are susceptible to hydrolysis (Zn in the case of ZDDP).

The presence of water affects the performance of ZDDP [15]. It reduces the chain length of phosphate in the tribofilm, thereby reducing the reaction layer thickness of the wear scar. Water is considered to be a contaminant that enters the engine or the oil through absorption, condensation, heat exchangers and water entry during the addition of additives. Water is reported to have a detrimental influence on the physical and chemical aspects of the engine oil and as well as the parts that are being lubricated [16]. Moisture presence in the

lubricated parts can cause corrosion, hydrogen embrittlement, wear caused due to loss of oil films or hard water deposit. In the case of lubricating oils, it can cause accelerated oxidation of the oil, deplete oxidation inhibitors and demusifiers, can cause the additives to precipitate and most importantly causes ZDDP to destabilize at temperatures of over 83ºC [15]. These reactions cause clogging of filter, depositing ash forming elements on the substrate leading to degraded performance.

Ashless additives have been found to have potential as Antiwear/EP additives, a viable replacement to the current additives that contain metal (such as ZDDP). Ashless antiwear additives do not contain metal elements due to which, it does not cause catalytic poisoning. Ashless neutral Dialkyldithiophosphate (DDP-1), Acidic Dialkyldithiophosphate (DDP-2), Alkylated Triphenyl Phosphorothionate (A-TPPT), Butylated triphenyl phosphororthionate (B-TPPT), Triphenyl phosphororthionate (H-TPPT) are some of the Ashless additives.

## 1.3 Laws of Friction

Friction can be defined as the force that resists motion. This is experienced when one body slides over another. Friction force is a resistive that acts parallel to the direction of motion. When two solid bodies are loaded together and a tangential force is applied, the value of the tangential force which is required to begin sliding is known as the ‘static friction force’. The tangential force required to maintain sliding is called the ‘kinetic (or dynamic) friction force’. The magnitude of kinetic friction is generally lower than static friction.

There are two basic laws of friction. The laws of friction are accepted over a wide range of conditions (proven experimentally), however there are a few notable exceptions. The laws of friction are empirical in nature and in cases where the laws of friction don’t obey, no basic principles are violated. The first law states that friction is independent of the apparent area of contact between the contacting bodies and second, that the friction force is proportional to the

normal load between the bodies. These laws are often referred to as 'Amontons laws' after the French engineer Amontons who presented them in 1699 [17].

Coulomb (1785) introduced a third law, that kinetic friction is nearly independent of the speed of sliding, but this law has a smaller range of applicability than the first two. The second law of friction enables ones to define a coefficient of friction. The law states that the friction force F is proportional to the normal load W [17].

## 1.4 Mechanism of Lubrication

A Lubrication system consists of two load bearing surfaces separated by a film of lubrication. The lubricant medium can be a solid (such as graphite, $MoS_2$), liquid (such as base oil with additives), A liquid-liquid dispersion (such as greases) or gas. Lubricants primary functions are to mitigate friction, wear reduction, thermal conductivity and suspension of contaminants. The additives in lubricant oil also serve to protect from oxidation and corrosion. The physical and chemical properties of the lubricating fluid play a crucial role in lubrication. Physical properties such as density, viscosity, heat capacity and thermal conductivity influence the ability of the lubricant to perform under elasto-hydrodynamic (EHD) and hydrodynamic (HD) lubrication. Chemical properties that are crucial in successful boundary lubrication include solvency, dispersancy, detergency, antiwear, anticorrosion & frictional properties. Some properties are controlled by the chemical composition of the base oils, and some properties are controlled by chemical additives designed for that purpose.

There are three types of lubrication regimes:

1. Hydrodynamic (HD) Lubrication: This kind of lubrication occurs when the two load-bearing surfaces are separated by a lubrication film. There is no metal-to-metal contact and the machine life depends on the oil cleanliness. Elasto-Hydrodynamic (EHD) lubrication is a condition that occurs when the load between the two load-bearing

surfaces are high that it induces high fluid pressures (~500,000 psi) and cause the oil to act like an elastic solid. EHD is usually observed between gears and bearing elements.

2. Boundary Lubrication: This type of lubrication is the most common and important type of regime where the interacting surfaces comes in close contact at their asperities. Heat is developed at this interface by the local pressure and causes a condition known as “Stick-Slip”. Stick-Slip causes some of the asperities to break away. At elevated temperature and pressure, the chemically reactive constituents of the lubricant, react with the surface forming a highly resistant, surface film. This surface film is capable of supporting the moving solid surfaces from major and minor wear and breakdown is avoided. In this regime, load is carried by the asperities rather than the lubricant.
3. Mixed Film Lubrication: In this type of lubrication, the load-bearing surfaces come in contact in certain regions even though there is a lubricating film present in between them. The lubrication film is thicker than in boundary lubrication. It is a combination of hydrodynamic and boundary lubrication.

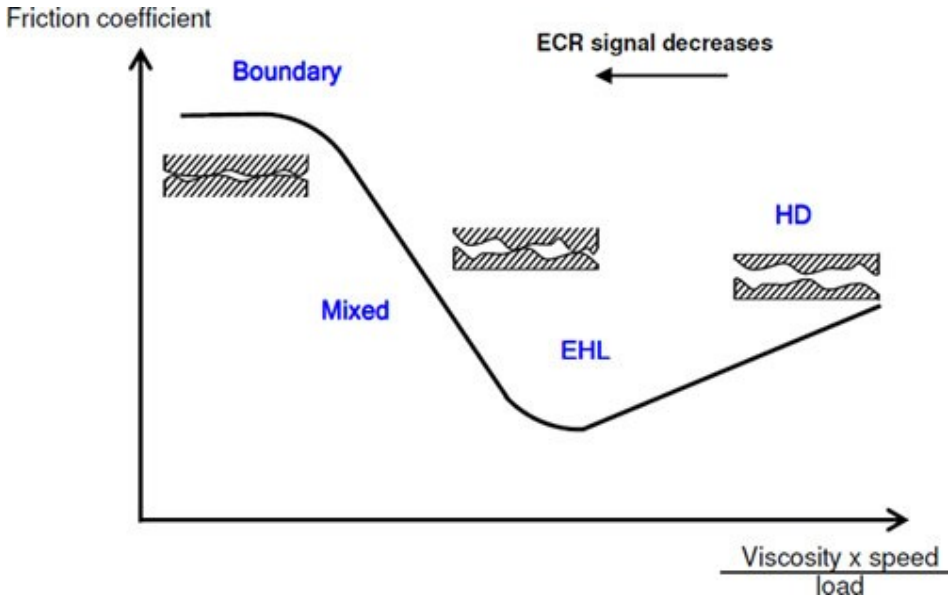


Figure 1.1: Stribeck curve showing the lubrication regimes

## 1.5 Motivation for this research

Tribology is an amalgamation of multiple fields of study. It has a high economic impact on the industries. About a third of world's energy consumption is wasted in friction. While friction may be required in certain aspects (such as welding, brake discs, etc), it is not desirable in most applications. Reduction in friction is highly beneficial in terms of monetary savings, longevity and the performance of the equipment. Zinc dialkyldithiophosphate is the principal Antiwear/Extreme Pressure additive used in engine oils that promotes effective surface protection by developing homogenous surface film or Tribofilm. Along with its merits, there are also equally damaging demerits. Zinc based dialkyldithiophosphate additives are known to poison the catalytic converters. This antioxidant contains phosphorus which is an important component that aids in the formation of the antiwear films and also forms stable compound with the washcoat components in the catalytic converters thereby hindering its performance. Ceria and Zirconia are the major components of automotive washcoats. Alumina is used as a binder. Ceria is known to promote its catalytic functions in numerous ways. Oxygen Storage Capacity (OSC) is one of the functions of Ceria. During rich conditions, it releases O as $Ce^{4+}$ is reduced to $Ce^{3+}$; during lean conditions, O is taken up and the reverse reaction occurs [18]. The lean and rich conditions are determined by the Air - Fuel ratio (AFR). Air – Fuel ratio is the ratio of mass of air to fuel present in the internal combustion engine. Phosphorus combines with alumina forming aluminum phosphate [19]. When the temperature rises, aluminum phosphate dissociates and it combines with cerium forming cerium phosphate. The OSC mechanism is hindered when cerium phosphate is formed. Oxalic acid wash is the commonly used method of washing the washcoat components. Oxalic acid wash gets rid of all the impurities and compounds, thereby enhancing the catalytic performance. Aluminum phosphate and Cerium Phosphate are so stable that it is difficult to remove even with oxalic acid wash. The zinc content in ZDDP is susceptible to hydrolysis in the presence of moisture, especially at high

temperatures. This leads to breakage of bonds in zinc oxide thereby leading to filter clogging & clogging of catalytic converters. All the above mentioned side effects of using ZDDP results in emission of harmful gases into the environment, degraded performance of the engine, constant replacement of numerous engine parts and filters. Thus research into the development of additives that are Zinc free & environment friendly is necessary.

## 1.6 Objective of this research

Zinc dialkyldithiophosphate is the most successful lubricant additive ever to be developed. It has been in continuous use for the past 60 years. There has been a lot of effort to develop a replacement and so far, it has been proved impossible to come up with a replacement for ZDDP with comparable performance. It has been proved by a number of researchers that ZDDP forms a thick Tribofilm on the metal surface, favoring the mitigation of friction and wear [20,21]. ZDDP contains phosphorus and sulfur in the ratio of 1:2 [P:S], but the Tribofilm was shown to have [P:S] ratio higher than 8:1. Although there is a wealth of knowledge about ZDDP and its tribological antiwear performance, lot of questions still remain unanswered such as its Tribofilm formation mechanism, the reacting species that builds the Tribofilm, the kinetics involved, etc. [7]. Therefore, the main objective of this research is to develop a fundamental understanding of how Ashless additives aid in Tribofilm formation, its synergism on combining two Ashless additives and a comparative study with ZDDP.

CHAPTER 2

BACKGROUND

## 2.1 Function of an Engine Oil

Engine oil or Motor oil is used in internal combustion engines for lubrication. It lubricates every moving part of the engine and protects them from wear. Engine oil forms a protective film (also known as Tribofilm) which reduces friction and essentially keeps metal moving parts from every coming in contact with each other. An in-depth understanding of surface processes such as friction and wear is crucial in developing an optimum design where engineering components come into close tribological contact [22]. This is especially significant in modern day engines. Figure 2.1 shows the schematic of modern day internal combustion engine.

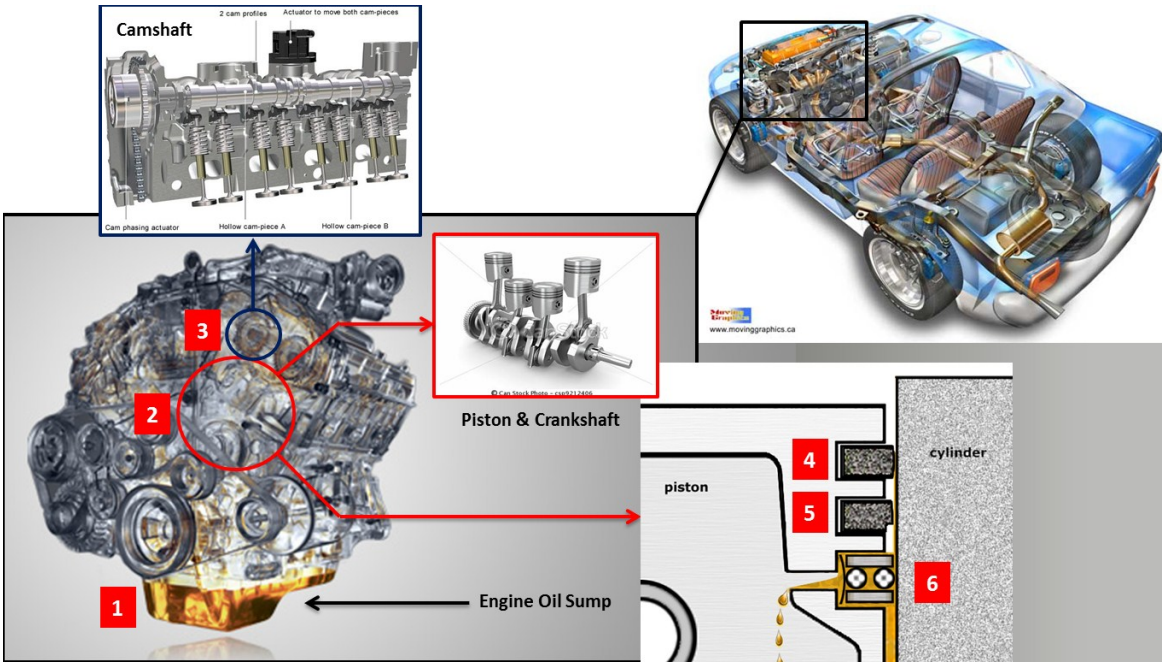


Figure 2.1: Schematic of an internal combustion engine [23-25].

The internal combustion engine has numerous moving parts. The engine oil is stored in the oil sump (Location 1 in Figure 2.1). The engine oil then travels from the sump through the oil ways into the oil pump. It is forced through an oil filter to remove any foreign contaminant. The filter removes any large particles that could cause wear and blockages. The oil is then supplied to the crankshaft to lubricate the bearings (Location 2). The oil is sprayed onto the underside of the piston and cylinder walls to provide essential cooling and wear protection. The oil travels up through the oils ways to the top of the engine where it lubricates the camshafts (Location 3) to ensure smooth contact with their followers. This ensures smooth movement of the valves [24]. Additives such as detergents are added to the lubricant oil to clean the contaminated particles off the engine surface. The detergents suspend the contaminants in the motor oil and hold them in globules till the next engine oil replacement.

Engines do not usually consume oil. Oil is consumed within the engine due to the reasons mentioned below:

1. Leakage or seepage from the front valve cover or oil pan gasket, front seals, rear main seals. Leakage is sometimes observed around the vehicle's timing belt covers.
2. Wear in the engine surface. The piston rings are worn if the lubrication is not adequate. When the engine's rings wear down this is indicative of a compression drop, the oil starts seeping past and is consumed in the gas/air explosion. During the initial stages, the consumption is only noticed by the oil quantity. When this condition worsens, blue or black smoke is noticed at startup.

Piston rings are used to seal the piston to the cylinder. There is very little gap between the steel rings and the cylinder and it rides on a very thin film of engine oil (boundary lubrication). This boundary lubrication prevents cylinder wear and since the film is very thin, contamination and debris causes the performance of the oil to decrease and will promote wear. This also reduces the power of the engine. Thus regular oil replacement is crucial to the

longevity of the engine. Piston ring placement and the number of rings vary depending on the performance of the engine. Most engines use three piston rings. The ring farthest from the combustion chamber (Location 6 in Figure 2.1) is the oil ring. The oil ring is made up of multiple parts and its function is to scrape away most of the engine oil from the cylinder wall. The oil from the crankcase is sprayed onto the cylinder wall. This oil passes through the oil ring and it is returned to the crankcase through an opening in the piston (present in location 6 in Figure 2.1). Small amount of oil is retained which lubricates the upper rings (Location 4 & 5). The upper ring (location 4) serves to form a tight seal for the combustion chamber. It seals the combustion chamber from engine oil & other debris seeping into it. The middle ring (location 5) has a scraper built in and it leaves almost no oil behind. What little oil remains, stays between the upper rings and serves as lubrication [25]. Modern day engines places greater stresses on the lubricant while at the same time, calling for low wear rates and reduced friction. In the regime of boundary lubrication, protection is given by the formation of Tribofilms through the action of lubricant additives.

## 2.2 Lubricant Additives

Engine oil contains several additives dissolved and dispersed in the hydrocarbon base oil. Hydrocarbon base oils are divided into two groups: Mineral and synthetic oils. Mineral oils are obtained from crude oil after a number of processes to filter out debris and other unwanted components. The composition of mineral oil is highly complex and consists of hydrocarbons with hundreds of aliphatic and aromatic compounds. The type of hydrocarbon present, determines the lubrication properties [26]. Lubricants used today contain a number of additives. Additives are added to enhance the lubricant performance. Additives are of different chemical functionalities to meet many service requirements. Among them are friction modifiers (FM), extreme pressure (EP) additives and antiwear (AW) additives. Additives made from organic or

organometallic compounds containing surface film forming active elements (P, S, N, Cl, Zn, Mo & B) are added to the base oils at low concentrations. The performance of base oil is enhanced by these additives. Additives add new properties to the lubricant. Lubricant additives are classified into two categories: Chemically-inert and chemically-active. Chemically inert additives modify the physical properties of the base oil. Viscosity modifiers, foam inhibitors, and pour point depressants are some of the physically inert additives. Tribochemical properties and the antiwear/EP properties are imparted by the chemically active additives.

Lubricant additives can be classified according to their chemical compositions: Sulfur compounds, Ashless phosphorus compounds, heterocyclic compounds, Dialkyldithiophosphate complexes of metals (MDTPs), dialkyldithiocarbamate complexes of metals (MDTCs), Chlorine compounds, boron compounds and ionic liquids. Each of the additives added is meant to perform one or multiple functions. The functions may or may not be related to the antiwear and friction. Additives that are not related to friction and wear performance may contribute to the efficiency of the antiwear additives. Ashless lubricating oil does not contain ash forming metal additives, such as Barium, Calcium, Zinc and Magnesium.

## 2.3 Extreme Pressure and Antiwear Additives

These kinds of additives prevent seizure and decrease wear-out during friction. These additives are especially useful in boundary conditions, where the lubrication film tend to break due to the partial high pressure and high temperature. The main application of Antiwear and extreme pressure additive is in gear oil, cutting oil, engine oil or machine oil. AW/EP additives contain functional groups in the molecule that can react with the metal surface forming boundary lubrication film. This film protects the surface from further wear. The requisite for the boundary lubrication film is that, it has to be soft and ductile, and also mechanically and chemically stable. These requirements are met by containing sulfur, chlorine, phosphorus and

other elements in the additive molecule. Every boundary lubrication film that is formed is different from each other and hence, multiple additives are combined to obtain their synergistic effects.

Initially it was believed that sulfurized fatty oils and lead soap were effective EP/AW additives. A number of compounds were developed in 1930 after the hypoid-gear spread for rear axles of cars. From around 1940, reports concerning the reaction mechanism of EP / AW additives started to appear and a lot of patents also appeared, including for tricresylphosphate (TCP) and zinc dialkyldithiophosphate (ZnDTP). Since then, an EP / AW additive containing phosphorus, sulfur and chlorine (1959) and an EP / AW additive containing phosphorus and sulfur (1961) have been developed, and a lot of new compounds are still being reported [27].

## 2.4 Types of Extreme Pressure and Antiwear Additives

The EP/AW additives are divided into four types: Sulfur compound type, Chlorine compound type, Phosphorus compound type and organo-metallic compound type. EP/AW sulfur based additives are usually sulfurized fatty oils and sulfurized olefin. These are used in gear oil along with phosphorus compound based EP/AW additives and also used in cutting oil alone or together with the chlorine compound type EP/AW additives. Chlorinated esters, chlorinated paraffin and chlorinated fatty oils are some of the chlorine based EP/AW additives used in lubricants. In the case of Phosphorus based compounds, TCP and amine phosphates are typically used.

| | |
|---|---|
| **Sulfur compound type** | |
| Sulfurized fatty oil | 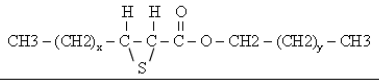 |
| Sulfurized terpene | 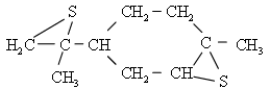 |
| Sulfurized olefin | 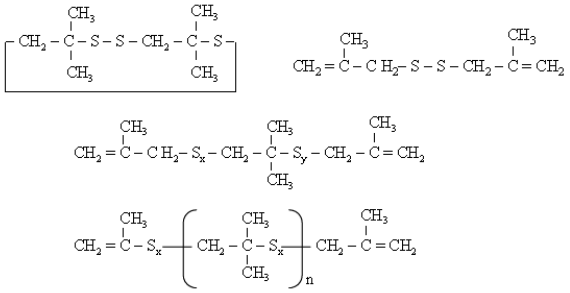 |
| Sulfide | 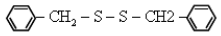 |
| **Chlorine compound type** | |
| Chlorinated paraffin<br>Chlorinated fatty oil | 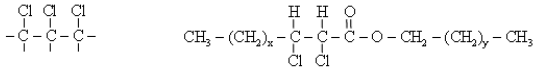 |
| **Phosphorus compound type** | |
| Phosphite |  |
| Phosphate |  |
| Amine phosphate | 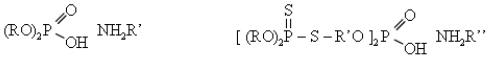 |
| **Organo-metallic compound type** | |
| Dialkyldithiophosphate | 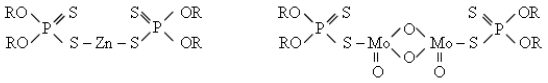 |
| Dialkyldithiocarbamate | 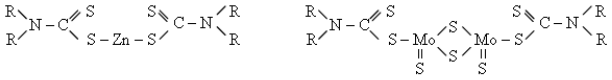 |
| Naphtanate | 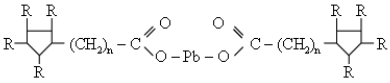 |

Figure 2.2: Typical EP/AW Additives [27].

*2.4.1 Sulfur Compounds*

Addition of additives to inhibit oxidation of oil dates back to 1800s. One of the earliest methods of mitigating oil oxidation was by the addition of elemental sulfur and heating the mixture to produce a nonoxidizing mixture [28]. But, the main disadvantage of using the sulfurized oil is that, it initiates corrosion when brought in contact with copper. Oil with corrosion inhibition characteristics was developed by sulfurizing sperm oil [28]. This methodology was extended by sulfurizing terpenes and polybutene. Sulfur based compounds are prepared from Paraffin wax.

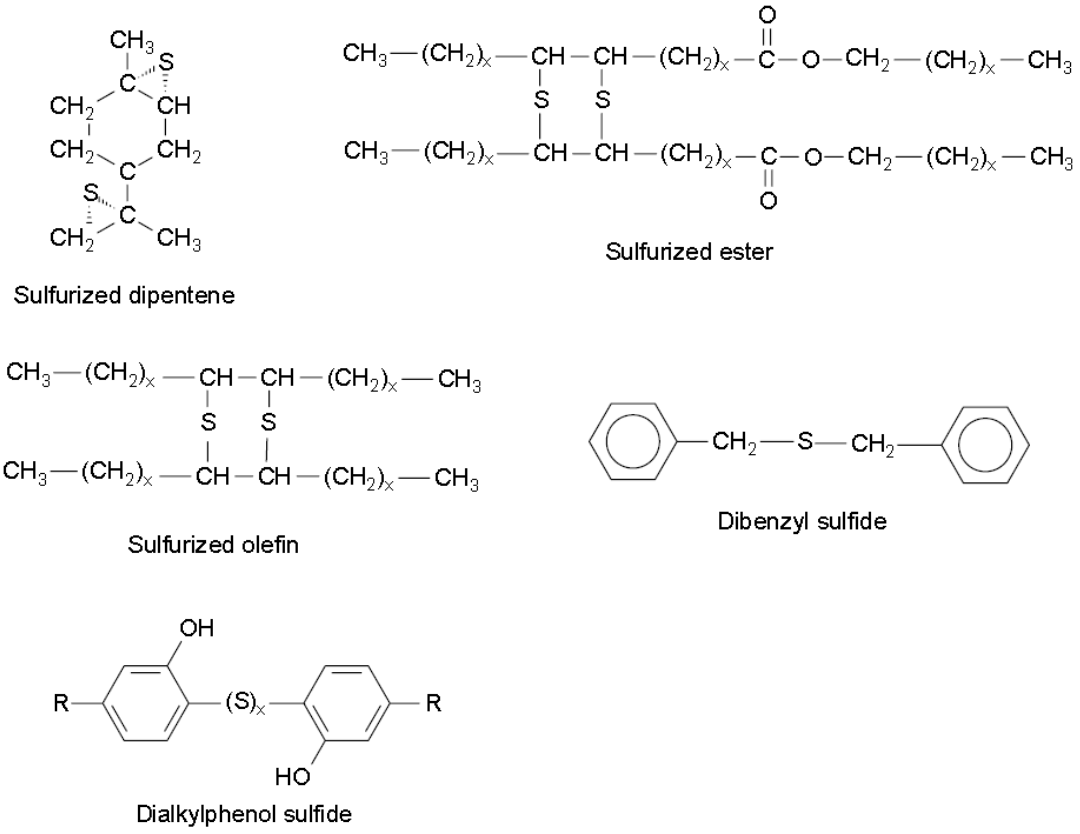


Figure 2.3: Sulfur bearing compounds [29].

Compounds of sulfur and aromatic sulfides can be chemically complex in nature. Aromatic sulfides are also used as oxidation and corrosion inhibitors. Dibenzyl sulfide and

dixylyl disulfide are examples of simple sulfides. Benzyl sulfide is an aromatic based sulfur compound (shown in Figure 2.3); have sulfur attached to carbon atoms in the alkyl side groups. Alkyl based sulfides have sulfur attached to the carbon atoms in the aromatic rings. By testing various sulfur based compounds in multiple lubricants, alkyl phenol sulfide chemistry appears to have superior antioxidant properties in many types of lubricants [29]. Monoalkyldiphenyl sulfides and dialkyldiphenyl sulfides were demonstrated to have powerful antioxidant properties and capable of usage in high temperature lubricants (especially synthetic base stocks). They are prepared by reacting diphenyl sulfide with C10-C18 alpha-olefins in the presence of Aluminum Chloride [30]. Metal elements can be added to alkyl phenol sulfides by replacing its hydroxyl groups to form oil soluble metal phenates. Metal phenates perform the role of an antioxidant and as a detergent. Multifunctional additive compounds can be prepared with heterocyclic structures by sulfurizing norbornene, 5-vinylnorbornene dicyclopentadiene or dicyclopentadiene dimer [31]. N-alkyl 2-thiazoline disulfide is a heterocyclic compound which on combination with ZDDP (Zinc Dialkyldithiophosphate) exhibited excellent antioxidant performance. This test was carried out in the laboratory engine test [32].

Organo monosulfides, polysulfides, elemental sulfur and other wide variety of sulfurized fats and hydrocarbons are some of the sulfur containing additives. The anti-wear (AW) and extreme pressure (EP) properties of a series of organic disulphides have been investigated by Allum and Forbes in late 1960s [33]. Their research shows that the Extreme Pressure (EP) additive property depends on the ease of cleavage of the Carbon-Sulfur (C-S) and Sulfur-Sulfur (S-S) bonds. Additives with S-S bond impart good antiwear properties because S-S bonds cleave easily at high pressures [2,34]. Figure 2.4 shows the antiwear and extreme pressure (EP) mechanism of sulfur compounds.

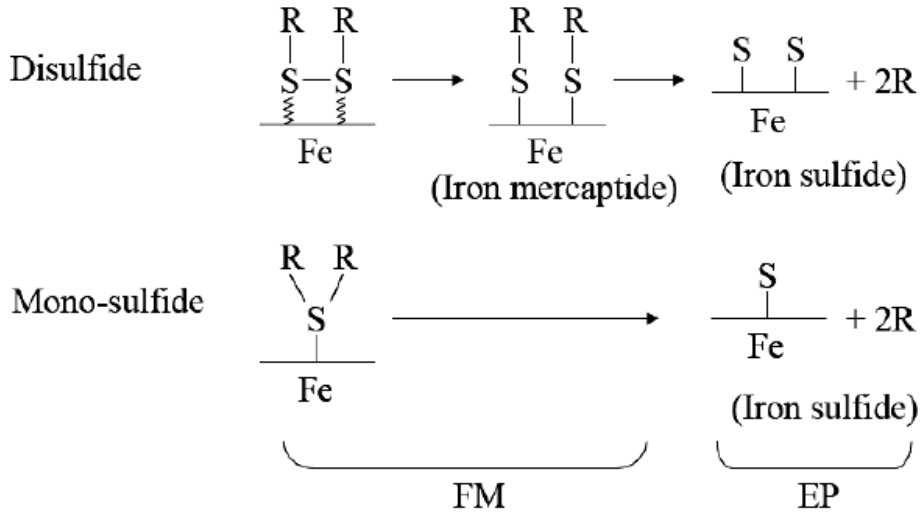


Figure 2.4: Tribofilm formation of sulfur at iron surface by sulfur compounds [35].

Sulfur based compounds get adsorbed on the iron surface (load bearing surfaces) and reacts with the Fe active sites forming Iron Sulfide films. A mono-sulfide additive, on physisorption forms iron sulfide, while a disulfide additive forms iron sulfide films through the formation of iron mercaptides [35,36]. Sulfur in the form of sulfides, is an effective Tribofilm. Sulfides form soft, ductile film on the surface which acts as a sacrificial layer during movement of the load bearing surfaces. Elemental sulfur is an effective EP additive when combined with mineral oils [37,38]. The reactivity of elemental sulfur with steel surface is found to be higher than organic sulfides [39,40].

*2.4.2 Phosphorus Compounds*

Phosphorus exhibits properties required for the formation of Tribofilms. Its performance in lubricant oil as an oxidation inhibitor was identified early on in lubrication science. The use of elemental phosphorus to reduce sludge formation in oils has been described [41]. Elemental phosphorus, like elemental sulfur has corrosive effects on many nonferrous metals and alloys.

Hence phosphorus is never incorporated in oils in the elemental form. It is included with oil in the form of oil – soluble organic compounds. Phosphorus in its naturally occurring form (as lecithin) has been utilized as antioxidants. Many patents have been issued on these materials for single use or in combination with other additives [42-45]. Lecithin contains phosphorus in the form of phosphatide. It is produced commercially as a by-product from the processing of crude soybean oil. The antioxidant property of synthetic neutral and acid phosphite esters has been known for some time. Alkyl and aryl phosphites such as tributyl phosphite and triphenyl phosphite are efficient antioxidants in some petroleum base oils, and many patents have been issued on such compositions [46,47]. The aluminum, calcium, or barium salts of alkyl phosphoric acids are another type of phosphorus compound that displays antioxidant properties.

*2.4.3 Catalytic Converter poisoning*

Big cities in the United States have thousands of vehicles on the road and each one is a source of air pollution. To control the effects of pollution, governing bodies created clean-air laws that restrict the amount of pollution that vehicles produce. In 1975, automakers started installing an interesting small device known as the catalytic converter [48]. Phosphorus has long been known for its detrimental effect on catalytic converters. Catalytic converters are attached at the end of the engine (exhaust system) and it is a vehicle emission control device.

It converts toxic byproducts of combustion in the exhaust of an internal combustion engine to less toxic substances by the way of catalyzed chemical reactions. The type of reaction depends on the catalyst present and most present day vehicles contain three way converters. It is so named because it converts three harmful pollutants to less harmful gases before it is let out. Carbon Monoxide, unburned hydrocarbons and oxides of nitrogen are the three pollutants

that are converted to less harmful Carbon Dioxide, Nitrogen and water [49]. Phosphorus causes the reduction in the performance of the catalysts present over time.

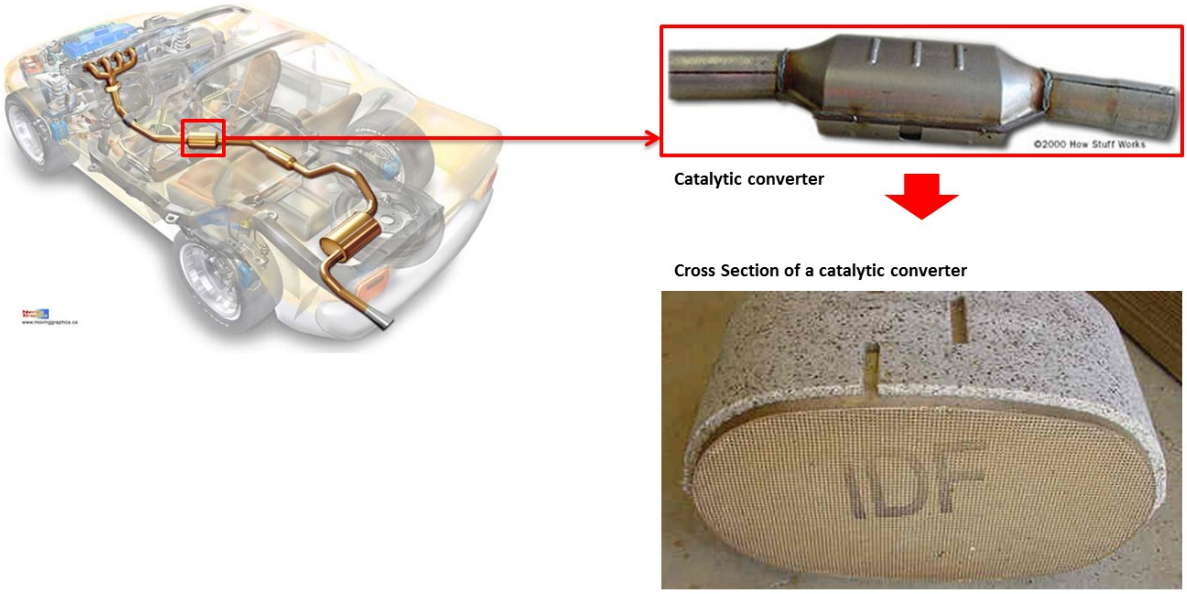


Figure 2.5: Catalytic converter [23,25].

Phosphorus is introduced to the catalyst through the engine oil. The washcoat in the catalytic converters are responsible for control of the vehicle emission. The washcoats are made up of Ceria or Zirconia. Alumina is used as the washcoat binder. Phosphorus reacts with the washcoat components to form aluminum and cerium phosphates [19,48,49]. Ceria provides the Oxygen Storage Capacity (OSC) that aide in the catalytic conversion. Ceria is poisoned by phosphates that lead to the reduction or loss of OSC. Cerium phosphate is highly stable compound and even on washing with oxalic acid, it is found to remain. Oxalic acid wash is a known technique that is known to improve the catalytic activity of phosphorus contaminated catalysts [49].

*2.4.4 Chlorine Compounds*

Chlorine based EP/AW additives form boundary lubrication film by thermal decomposition and results in the formation of iron chloride ($FeCl_2$, $FeCl_3$, FeOCl) on the iron surface. The film thus formed has a stratified structure and this prevents wear and seizure [50-54].

$$RCl_x + Fe \rightarrow FeCl_2 + RCl_{x-2}$$

$$RCl_x \rightarrow 2HCl + R'Cl_{x-2}$$

$$HCl + Fe \rightarrow FeCl_2 + H_2$$

Figure 2.6: Formation of Iron Chloride on the steel surface [51].

Chlorine based EP/AW additive thermally decomposes on the iron surface forming a film comprising a layer of iron chloride which also incorporates nano-sized carbon particles in accordance with the above equation [52,54]. Chlorine based compounds exhibit good lubricity with properties of anti-seizure in a tribologically severe condition. This additive applies to applications in metal forming process. It is used or included in cutting oils or press forming oils. They are not used as much in other application because chlorine based compounds have a high hydrolysis property and their boundary lubrication films are apt to hydrolyze themselves in iron hydroxide or iron oxide [55]. Chlorine based compounds have harmful effects on human body and hence their use is nowadays restricted.

*2.4.5 Zinc Dialkyldithiophosphates (ZDDP)*

Sulfur and phosphorus are powerful antioxidants and are capable of forming a protective film on the metal surface even at high temperature and pressure. This has led to the

formation of oil-soluble antioxidants, having both elements in one molecule. A number of papers have been published on the combined effect of phosphorus and sulfur and they have also been used commercially [56-63]. It has been proved that phosphorus and sulfur combined gives better antiwear properties than base stocks containing phosphorus and sulfur individually. The most common class of additives that have phosphorus and sulfur together is the metal dialkyldithiophosphates. Metal dialkyldithiophosphates are prepared by the reaction of phosphorus pentasulfide with alcohols to form dithio-phosphoric acid, which is then followed by the neutralization of the acids with an appropriate metal compound. Many types of alcohols have been used to bring about this reaction such as aliphatic, cyclic [58], and phenolic derivatives. High molecular weight alcohols are preferred because they bring about sufficient thermal stability to the final products while rendering sufficient solubility in oils. For the neutralization of the acids, Zinc, Molybdenum, or Calcium oxides are usually chosen. For many years, zinc salts of dialkyldithiophosphates have been used because of its superior antioxidant capability. It is also cost effective antioxidant to be produced and therefore have been included as a key component in many oxidation inhibitor packages for engine oils and transmission fluids. ZDDP functions as an antioxidant and an antiwear additive. Its antiwear properties are attributed to the fact that ZDDP decomposes to form sulfide and phosphate films in the valve train area through corrosive reactions on the metal surface. It undergoes a series of chemical reactions to form organo-substituted phosphates, thiophosphates and phosphoric acids. These form the precursors for surface films or Tribofilms. These precursors undergo a series of polymerization and exchange reactions. These films can provide protection against friction and corrosive attack from organic acids formed during the oxidation process. Multiple salts of dialkyldithiphosphoric acids have been developed and tested, among which salts of C4/C5 diphosphoric acids have better properties. A broad range of other alkyl derivatives have been developed to meet special needs (for instance, protection at high temperatures).

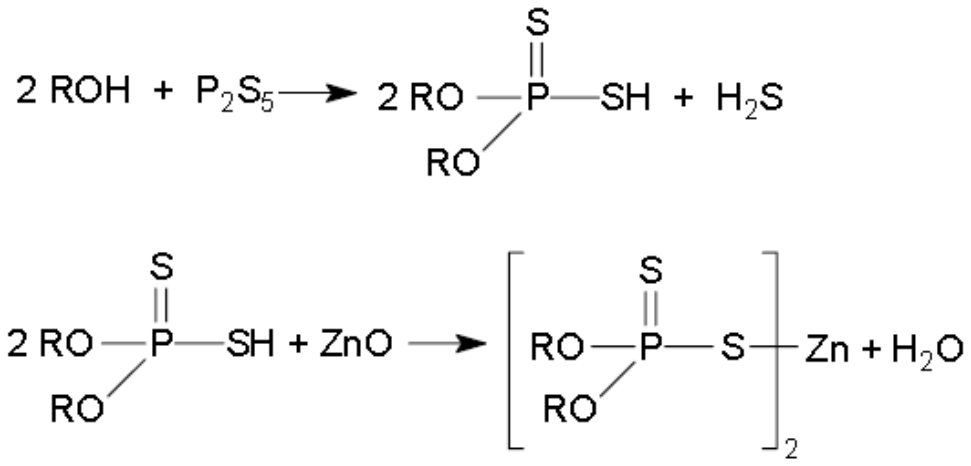


Figure 2.7: Reaction scheme of making ZDDP [63].

The reaction involved in the formation of ZDDP is shown in Figure 2.7. Condensation reaction of phosphorus pentasulfide is carried out with unsaturated organic compounds such as terpenes, polybutenes, wax olefins, fatty acids, fatty esters and sperm oil. This results in the formation of high molecular weight intermediate products [60]. During these reactions, hydrogen sulfide is liberated as a byproduct which is acidic and highly corrosive. The acidic intermediates are neutralized by the treatment with alkaline earth oxides or hydroxides to form metal salts. Calcium, Barium or potassium based salts are the most preferred products. Some additives may also display detergency characteristics. Alkyl and aryl based phosphites are added to ZDDP to reduce the staining effect on the metal parts. ZDDP causes sludge deposition and eventual poisoning of catalytic converters and it is also affected by the presence of moisture. ZDDP becomes unstable at temperature of over 83ºC in the presence of moisture. Metal Dialkyldithiophosphates have multiple merits, but owing to the increasing concerns of its usage due to toxicity, waste disposal, filter clogging, pollution, etc., there have been extensive research activities on the use of Ashless technologies for both industrial and automotive applications.

## 2.5 Ashless Additives

Ashless additives have started gaining popularity in the automotive and heavy engineering applications because of lesser sludge formation and environmental considerations for substituting ZDDP (Zinc Dialkyldithiophosphate) with additives containing Zinc free, low phosphorus and low sulfur. A number of Ashless compounds have been tested based on derivatives of dialkylphosphorodithioic acids. These derivatives have been reported as multifunctional additives. Diisoamylphosphorodithioic acid is reacted with primary and secondary amines to produce eight alkylamino phosphorodithioates with varying chain length from C5 to C18. They were found to possess excellent antiwear and antioxidant properties as compared to ZDDP. ZDDP becomes unstable in the presence of moisture at temperatures of about 83ºC. Alkylamino phosphorodithioates is obtained by reacting heptylated or octylated or nonylated phosphorodithioic acids with ethylene diamine, morpholine, or tert-alkyl (C12-C14) amines. This Ashless additive is found to have similar antioxidant and antiwear efficiency as that of ZDDP and also immune to moisture presence [36].

### *2.5.1 Ashless Phosphorus Compounds*

A number of phosphorus compounds have been investigated for possible application in tribology and replacement for ZDDP, but only a small percentage of phosphorus compounds are commonly used in industry [64]. These include Ashless thiophosphates, Ashless dithiocarbamates, and phosphorus free triazine derivatives. Ash consists of metallic solid, salt particles which originate from ZDDP (Zinc). Schumacher and Zinke studied the antiwear behavior of several additive compounds based on the atomic structure of dithiophosphates. They studied the wear behavior and influence of phosphorus by replacing sulfur with oxygen atoms and varying the length and branching of alkyl groups [65]. The antiwear properties for both monothiophosphates and dithiophosphates were found to be comparable. A clear

correlation was found between the presence of phosphorus in the antiwear film and lower wear rate. On the other hand, there was no correlation between wear rate and sulfur content in additives.

Additives with phosphorus have increased thermal stability and maintain good performance at high temperatures. Thermal instability is a key precursor for the reaction to begin for the Tribofilm formation. Hence a certain amount of thermal instability is usually preferred and required to allow the compound to react and form protective antiwear Tribofilms.

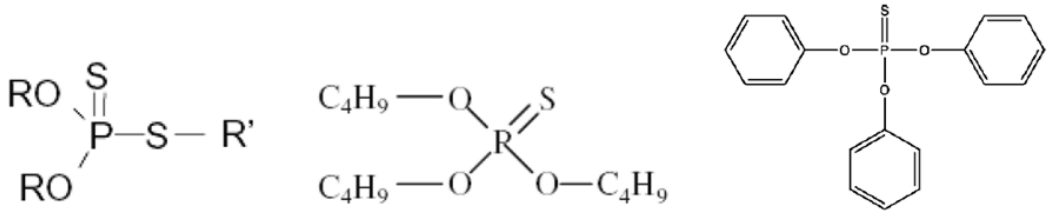


Figure 2.8: (Left) General Structure of Dithiophosphate, (Middle) Tributyl thiophosphate (TBT), (Right) Triphenyl Phosphorothionate (TPPT) [65].

The reactivity of alkylated phosphorothionates was investigated by Heuberger et al with steel surface [62]. They observed the cleavage of P=S bonds occurs under the impact of a high contact pressure and a frictional heat, and sulfur reacts with iron forming Iron Sulfide.

*2.5.2 Heterocyclic Compounds*

In the recent few decades, additives containing Nitrogen, Sulfur and Oxygen are being looked into as a potential additive in lubricants because of their promising friction and antiwear properties [66-74].

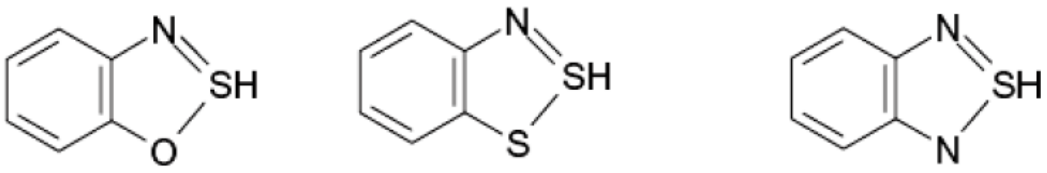


Figure 2.9: Sulfur, Nitrogen-Heterocyclic compounds general molecular structure [74].

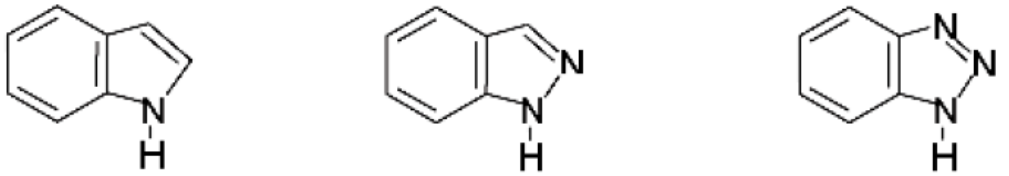


indole indazole benzotriazole

Figure 2.10: Nitrogen – Heterocyclic Compounds general molecular structure [75].

Heterocyclic compounds containing Nitrogen have a high affinity for free iron. They readily adsorb on the surface of steel, leading to formation of antiwear Tribofilm. The number of Nitrogen atoms in the molecular structure influences the properties of the formed Tribofilm. The antiwear property of the Tribofilm increases with the increase in the Nitrogen atom in the molecular structure. Benzotriazole has better antiwear properties compared to Indole or Indazole. This was observed by Ren et al [75]. Fe reacts with the three Nitrogen atoms in Benzotriazole forming an effective antiwear film compared to other antiwear additives in this class of compounds. XPS analysis of these N-heterocyclic compounds showed the same spectra for surfaces rubbed in solution and immersed in solution without rubbing. This showed that these compounds do not change chemically during rubbing.

## 2.6 Effect of combining multiple Antioxidants

Modern engine oils must meet more and more stringent challenges from oxidative degradation as the performance of engines are increasing rapidly and research into alloying engine material makeup to reduce weight and cost are underway. Hence the use of one or two types of antioxidant alone is fast becoming less and less effective. Antioxidant synergism describes the outcome of combined use of multiple antioxidants in lubricant base stock. This offers practical solutions to conditions where single antioxidant is inadequate.

Several commercial passenger car engine oils were analyzed, which determined that four types of antioxidants are generally employed in various combinations in modern engine oils. The four general antioxidant types are hindered phenol, aromatic amine, sulfur compounds, and organomolybdenum compounds. According to oxidation mechanisms, these antioxidants can be classified according to three major modes of action: (1) hindered phenol and aromatic amine antioxidants are recognized as radical scavengers, (2) sulfur compounds are classified as hydroperoxide decomposers, and (3) molybdenum compounds are known as antioxidation synergists.

Synergistic effects of combining multiple antioxidants can be classified in three categories [76]:

[A]. Homosynergism: This condition occurs when two or more antioxidants with similar properties and mechanisms interact. An example of this kind of synergism is ADPA (Alkylated Diphenyl Amine) in combination with HP (Hindered Phenolic Compounds).

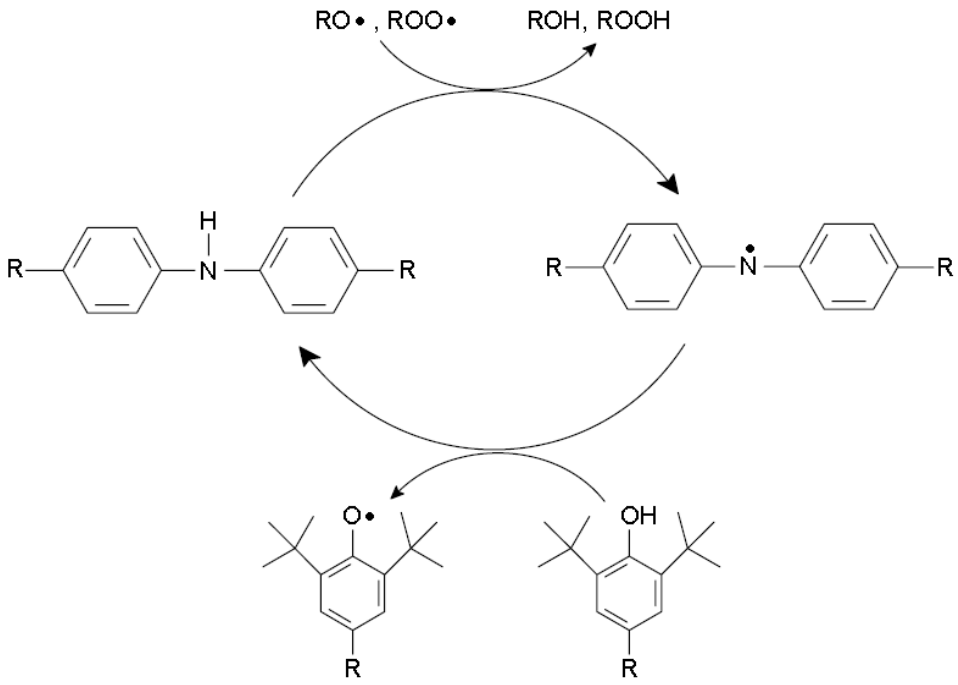


Figure 2.11: Synergism between ADPA and HP [76].

Figure 2.11 shows the mechanism of synergism between ADPA and HP. The amine is first converted to an aminyl radical, which is relatively stable. This unstable aminyl radical accepts a hydrogen atom from HP to regenerate the alkylated amine. As a result, HP is converted to a phenoxy radical. This mechanism of regeneration cycle is driven by the fact that ADPA is more reactive than HP. Phenoxy radical tends to be more stable than the aminyl radical. The reactivity of the regeneration cycle starts to deplete as the HP is being consumed. By addition of more reactive amine, the overall effectiveness of the system is enhanced. This leads to extended life of the useful antioxidant.

[B]. Heterosynergism: This condition occurs when the antioxidants used are of different properties and tend to complement each other. This type of synergism leads to categorizing antioxidants based on its properties and reactivity. Antioxidants in heterosynergism are

classified into primary antioxidant and secondary antioxidant. The primary antioxidant functions as a scavenger of radicals, while the secondary antioxidant decomposes hydroperoxides. Hydroperoxides are decomposed into more stable alcohols by the process of reduction. These reactions reduce chain propagation. A representative example of a heterosynergism is an aminic antioxidant in combination with a ZDDP.

[C]. Autosynergism: This type of synergism results from two different antioxidant functions in the same molecule. Usually, antioxidants having functional groups that provide radical scavenging and hydroperoxide decomposing functions exhibit autosynergy. Examples of this type of antioxidants are sulfurized phenols and phenothiazines.

## 2.7 XANES (X-Ray Absorption near Edge Spectroscopy)

The mode of decomposition of lubricant oil between rubbing surfaces is crucial for understanding how additives work. Until 1986, X-ray Absorption spectroscopy was an unexplored territory in the investigation of tribological contacts [77]. X-ray Absorption Fine Structure methodology is used to understand how x-rays are absorbed by an atom at energies near and above the core level binding energies of that atom. Specifically, XAFS is the modulation of an atom's x-ray absorption probability due to the chemical and physical state of the atom. This method can be used to understand the chemical makeup of the sample as it is very sensitive to formal oxidation state, coordination chemistry, and the distances, coordination number and species of the atoms immediately surrounding the selected element. This dependence provides a practical approach to determine the chemical state and local atomic structure for a selected atomic species. This method is frequently used in wide range of scientific fields, including biology, environmental science, catalyst research, and Materials Science. The spectra allow for the collection of set of data that provides details on the chemical

changes that result from the rubbing of the metal surfaces with lubricant running between them. XAFS spectra can be obtained for essentially every element on the periodic table. Crystallinity is not a mandatory requirement for XAFS measurements, making it one of the few methodologies available for noncrystalline and highly disordered materials, including solutions. X-rays are highly penetrating in matter and hence XAFS studies are not limited to the surface. But special measurement techniques can be applied to enhance XAFS's surface sensitivity. XAFS measurements can also be made on elements found in trace concentration in the sample. In practice, to obtain XAFS measurements and spectra, synchrotron facility is required. The history and developments of XAFS closely parallels that of synchrotron radiation. The x-ray absorption spectrum is divided into two regimes: X-Ray Absorption near Edge Spectroscopy (XANES) and X-Ray Absorption Fine-Structure Spectroscopy (EXAFS). The two regimes have the same origin; the distinction is for the convenience of interpretation of spectra. XANES is sensitive to formal oxidation state and coordination chemistry of the absorbing atom (octahedral, tetrahedral coordination), while EXAFS is used to obtain information on atomic distances, coordination number, and species of neighbors of the absorbing atoms [78]. XANES has an absorption edge in the range of 50~100eV and oscillation regions for about 1000eV or more above the edge is the Extended X-ray Absorption Fine Structure (EXAFS).

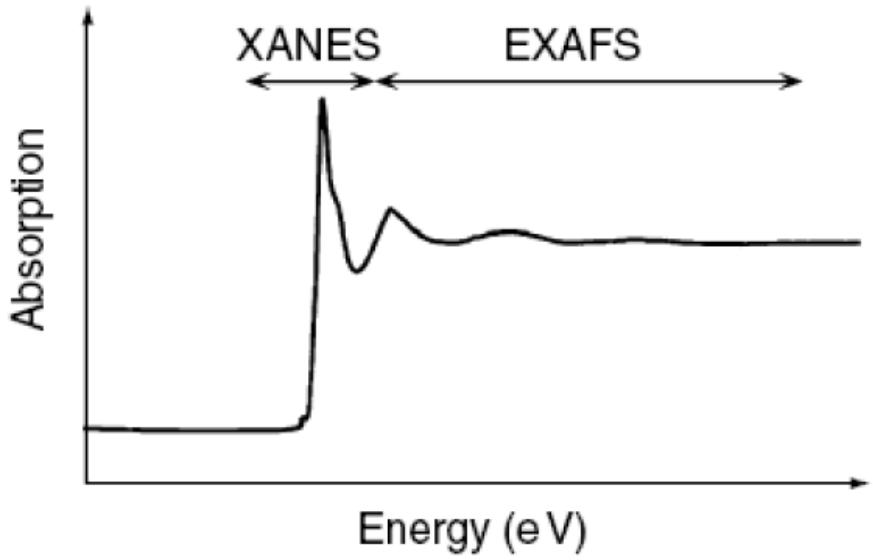


Figure 2.12: Schematic Illustration of X-ray Absorption Spectrum [78].

Developments in the field of nanotechnology and constant research into the miniaturization of all the day today equipment have demanded an improvement in the spatial resolution of many of surface analytical techniques, XAS being the first to succumb to this pressure. XAS has welcomed these advancements and has made some very significant achievements towards providing spatially resolved chemical speciation to less than 100nm spatial resolution [79-81]. The first use of XAS in tribology (X-ray Photoelectron Emission Spectroscopy – X-PEEM) was published on the reaction films formed from organo-molybdenum compounds in a tribo-contact in 1997 [82].

The use of X-Ray Absorption near Edge Spectroscopy and X-Ray Photoelectron Emission Spectroscopy gained importance in the Lubricant sector after a chance meeting at an Ontario Centre for Materials Research (OCMR) meeting in 1990. At the meeting, G. M. Bancroft and M. Kasrai from the University of Western Ontario (UWO) introduced XANES to a major lubricant manufacturer, Imperial Oil. After this chance event, a number of papers were

published and at the root of these publications is the ability of XANES spectroscopy to explain the phenomenon of Tribofilm formation, its composition, determine mechanisms by which certain oil additives perform. It also explains the antiwear behavior at a fundamental chemical level.

### *2.7.1 Physics of X-ray Absorption*

X-ray is form of electromagnetic radiation that is ionizing in nature and has sufficient energy to eject a core electron from an atom. Each core shell has a characteristic binding energy and hence the spectrum of ejected electron is plotted in terms of X-ray absorption vs. energy. When X-ray is irradiated on a sample through the binding energy of a core shell, there is abrupt increase in absorption cross- section. This is known as absorption edge. Each absorption edge represents a different core-electron binding energy [83-86]. The absorption edges are classified according to the principle quantum number of the electron that is excited (for n=1, L, for n=2, M, for n=3, N).

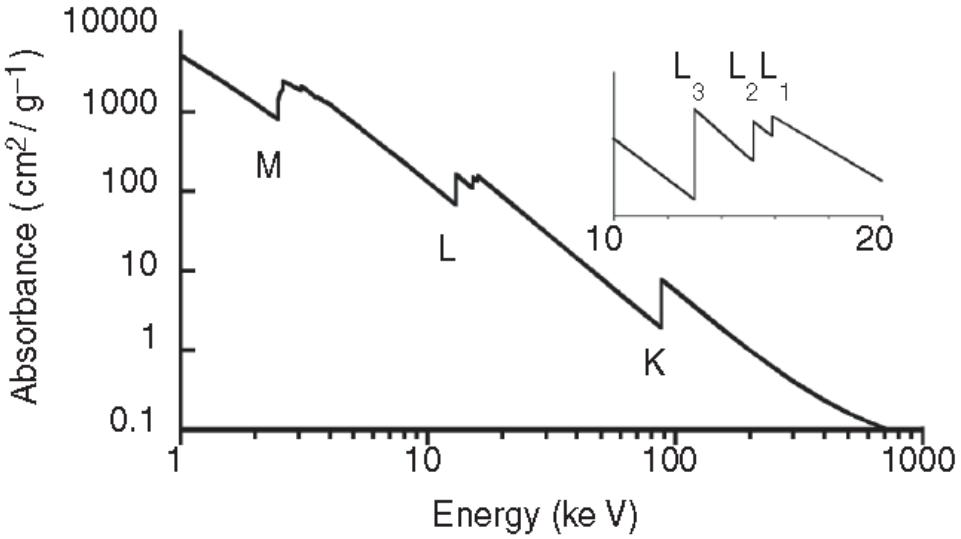


Figure 2.13: Low-resolution X-ray absorption spectrum for Pb. Three major transitions are seen (K, L, and M edges), corresponding to excitation of an electron from n = 1, 2, and 3 shells, respectively [87].

*2.7.2 X-Ray Fluorescence*

X-ray absorption results in the ejection of a photoelectron, which results in the development of a vacancy in the core-hole state. The relaxation of the atom results by a variety of mechanisms. The two most important mechanisms of relaxation are Auger electron fluorescence and X-ray Fluorescence. Auger emission is the dominant process in the case of low energy excitation and X-ray fluorescence is the dominant process in higher energy excitation. X-ray fluorescence curve is simple for light elements and large number of emission lines is observed in the case of heavier elements. The nomenclature used in identifying the

curves dates back before the modern quantum understanding. Hence the relation between the current knowledge and process of identification is not a simple one [88].

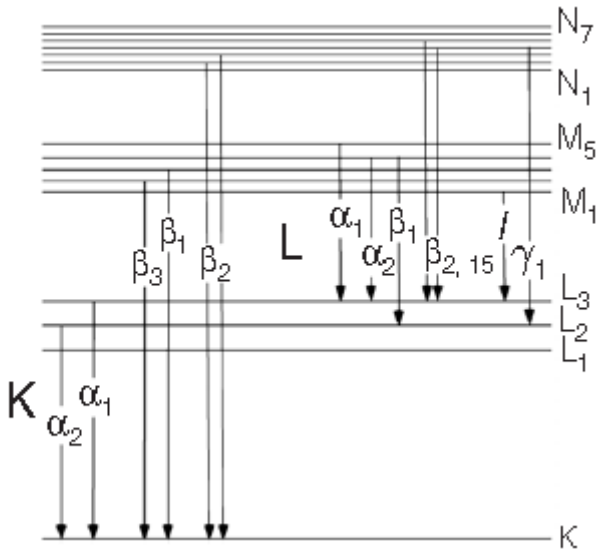


Figure 2.14: Nomenclature of X-ray emission lines [88].

The nomenclature of emission lines are shown in Figure 2.14. X-ray Fluorescence is governed by a series of selection rules that determine the emission. Thus only transitions known as diagram lines are allowed. Non diagram lines are observed in other spectroscopic studies [83].

### *2.7.3 Data Acquisition*

XANES data for the samples were acquired at two different synchrotron facilities depending on the energy range. DCM (Double Crystal Monochromator) beamline and VLS-PGM (Varied Line spacing Plane Grating Monochromator) beamline were used at the Synchrotron Radiation Centre at the University of Wisconsin – Madison (Stoughton, Wisconsin). The Double Crystal Monochromator covers an energy range of 1500 to 4000 eV. The step scan used for P & S (K edges) was 0.3 eV. The spot position is 241 mm beyond exit flange. The spot

size (horizontal x vertical) is 2 x 2 mm. the P & S L edges were acquired for the samples with the Varied Line Spacing Plane Grating Monochromator (VLS-PGM) beamline. This beamline has an energy range of 70 to 2000 eV. Low energy grating (LEG: 130-190eV) was used for P & S L edges. High energy grating (HEG: 500 to 775 eV) was used for Fe (700 – 775 eV) L edge & O (500 to 560 eV) K edge. Medium energy grating (MEG) was used for Ca L edge (340 – 365 eV) [89]. The other synchrotron facility used to obtain XANES data for the samples was the Canadian Light Source (CLS) facility in Saskatoon, Saskachewan, Canada. Varied Line Spacing Plane Grating Monochromator (VLS-PGM) beamline and High Resolution Spherical Grating Monochromator (SGM) was used. Varied Line Spacing Plane Grating Monochromator has an energy range of 5.5 to 250 eV. VLS PGM was used to obtain the P & S L edges. The VLS-PGM beam spot size is 500 μm by 500 μm. SGM beamline was used to obtain Zinc (Zn) L-edge, iron (Fe) L-edge, oxygen (O) K-edge, and fluorine (F) K-edges. It covers an energy range of 250 to 2000 eV with 0.1 eV scan step in 1000 μm by 100 μm spot size [90].

Each of the beamlines mentioned above has two detection modes; Total Electron Yield (TEY) and Fluorescent Yield (FY). The detection modes differ by the sampling depth. The TEY mode obtains information close to the surface. The sampling depth of TEY in K edge mode is about 50nm and FY is about 300 to 500nm. The L edge depth for TEY is about 5 to 7nm and FY is about 50nm. The Fluorescent Yield obtains information from the depths of the sample. The two modes provide information from various layers according to the depth. This is beneficial in studying the tribofilm's chain length, chemical composition, and structural environment variations [91].

## 2.8 Nano mechanical properties of Tribofilms

The efficiency of EP/AW additives can be related to their mechanical behavior inside the contact. Among the required properties, shear strength coupled with an adequate rate of

film formation to ensure continuous covering of the rubbing surface is also an important criterion. The shear strength of the film should be sufficiently low so that the shearing occurs inside the film and not inside the metallic parts when the two load bearing surfaces are rubbing against each other. The requirement is for the protective surface film to be continuous and uniform in thickness throughout, but practically the film formed is patchy and not uniform in thickness. Thus it is difficult to measure and assess the mechanical properties of the Tribofilms.

Nano indentation is an appropriate technique to measure the mechanical properties of patchy, inhomogeneous or continuous, uniform Tribofilms. It has been used in a number of publications on ZDDP tribofilms [92]. The hardness and young's modulus increases with the applied load irrespective of the external conditions such as temperature and strain rate. The phenomenon of increase in hardness and modulus is due to the fact that film is subjected to high applied pressure. The film is sandwiched between the indenter tip and the hard steel surface. This effect is known as the Anvil Effect.

The nanoindenter consists of a tandem piezoelectric ceramic scanning tube and a transducer. The piezoelectric ceramic material aids in the positioning of the indenter tip during testing. The transducer records the force/displacement data [93].

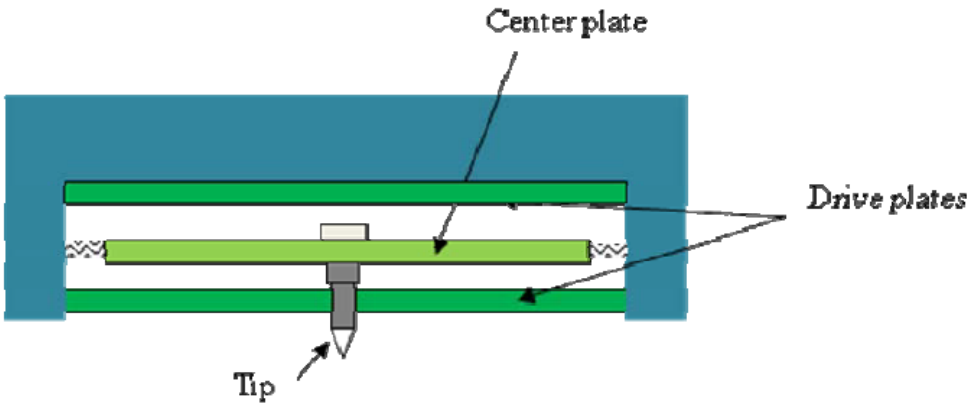


Figure 2.15: Transducer Cross Section. Hysitron Triboindenter [93].

The cross section of a transducer is shown in figure 2.15. On application of voltage, electrostatic attraction is produced between the center and bottom plates. Thus the center plate moves down toward the bottom plate and along with the tip moves down [93].

Hysitron Triboindenter is a high resolution nanoindenter which is an ideal instrument to study the mechanical properties of Tribofilms. Three types of nanomechanical tests that can be carried out by Hysitron Triboindenter are nano-indentation, nano-scratch, and scanning nano-wear. Scanning nano wear and nano scratch are relatively techniques to analyze mechanical properties of films. Nano-mechanical tests were performed at the University of Texas at Arlington on a Hysitron Ubi 1 nano mechanical testing system.

*2.8.1 Principle of Nano indentation test*

Nano mechanical tests are important source of information for mechanical properties of tribofilms. This equipment requires minimum sample preparation and an easy setup. Nanoindentation is considered to be non-destructive because it leaves a small imprint. Nanoindentation has a depth resolution on the nanoscale. A sharp tip is used to indent the sample and the corresponding load-displacement curve is recorded. Berkovich tip is the standard tip that is used in nanoindentation tests. The tip consists of three sides with a total included angle of 142.35º. Berkovich tips are made of diamond with a modulus of 1140 GPa. The compliance of the machine, the tip and the sample is recorded. The relation is expressed as [94]:

$$C = C_m + C_1$$

C: measured compliance

$C_m$: Compliance of the machine

$C_1$: Compliance of the sample and indenter

The compliance of the sample and the indenter is used to derive the reduced modulus. But to obtain accurate values of the sample's mechanical properties, the compliance of the machine has to be taken into consideration. The machine compliance is found out by carrying out indentation on quartz [93].

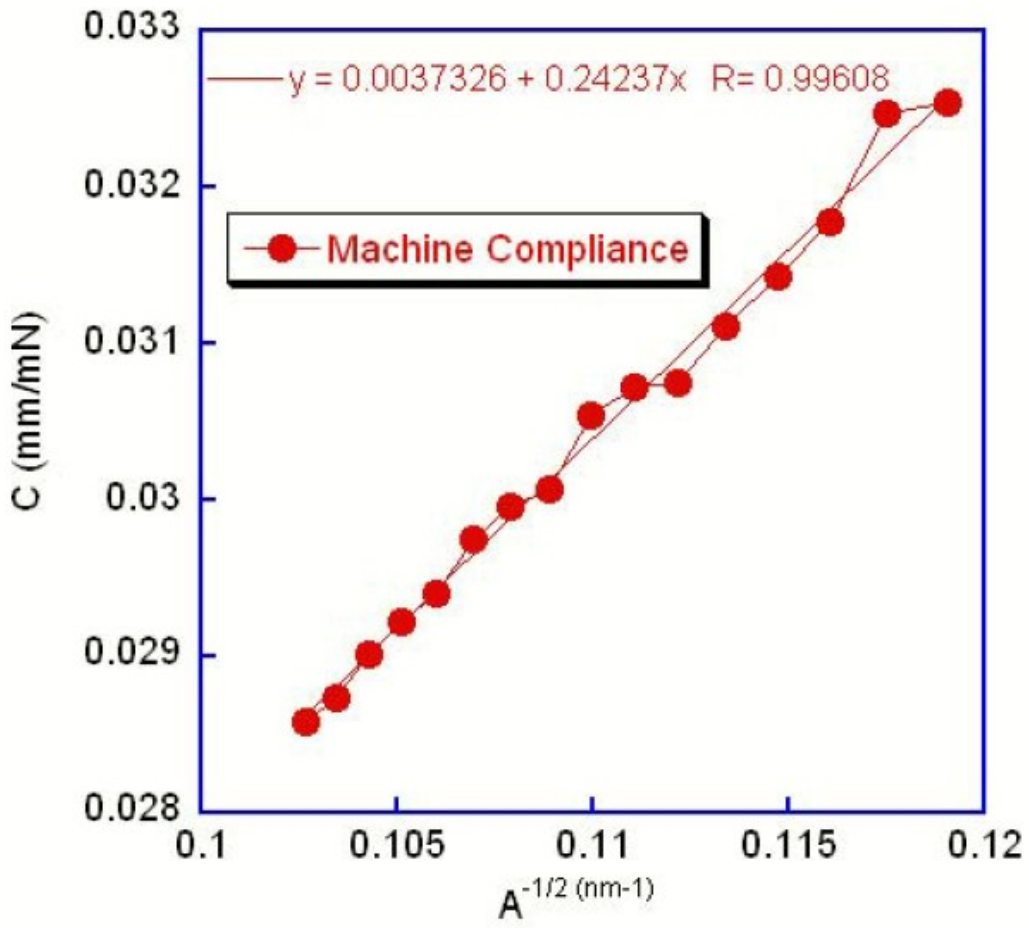


Figure 2.16: Machine Compliance curve [94].

The compliance of the machine is shown in Figure 2.16. The machine's response is given by the Y intercept which is inserted in the final compliance to remove the machine's influence. The common methodology implemented for calculating the mechanical properties of the sample is the Oliver-Pharr method [95].

$$\text{Stiffness} \quad S = dP / dh$$

$$P = q(\delta - \delta_{pl})^m$$

Where: q & m are the fitting parameters.

P: maximum load on the indentation test.

δ: Indentation depth from the unloading curve.

The contact depth is given by:

$$h_c = h_t - w\frac{P}{dP / dh}$$

$h_t$: Total Indentation depth

w: Indenter geometry factor

The reduced modulus is calculated from:

$$S = \beta\frac{2}{\pi}E_r\sqrt{A_C}$$

Ac: Contact area

β: Indenter geometry constant

The modulus of film of interest can be calculated as:

$$\frac{1}{E_r} = \frac{1-\nu_i^2}{E_i} + \frac{1-\nu_s^2}{E_S}$$

$E_i$ – Modulus of the Indenter

$E_s$ – Modulus of the sample

$\nu_i$ – Poission's ratio of the indenter

$v_s$ – Poission's ratio of the sample

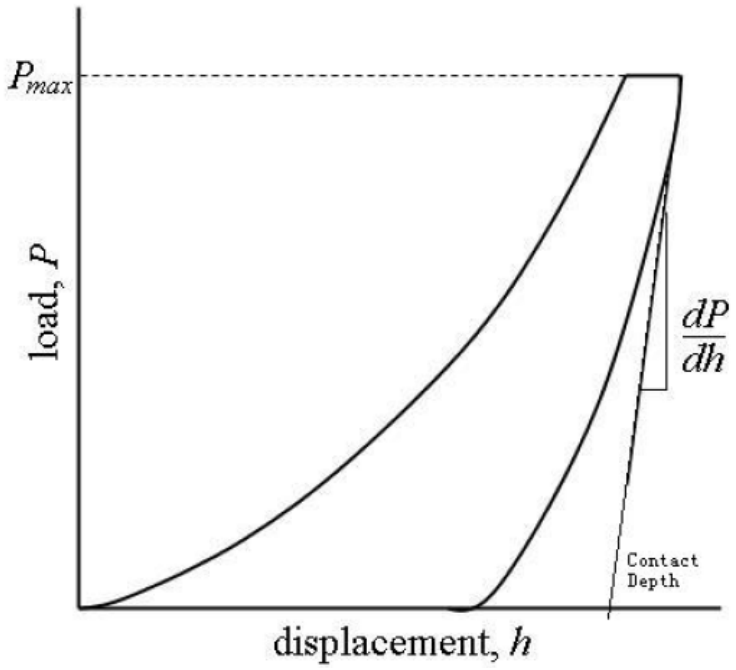


Figure 2.17: Typical Load vs. Displacement curve of a Nano indentation test [95].

## 2.9 Tribological Wear Tester

There are number of ways for evaluating the performance of lubricant oil. There are various factors that influence the outcome of a tribological test. Temperature of the setup, load being applied, type of lubricant used, contact geometry, surface roughness, environment in which test is carried out (air or Nitrogen), etc. are some of the factors that affect the outcome of lubricant evaluation [12]. Thus, initial planning and cautious monitoring the conditions of the test are crucial for obtaining reliable results that are close to real wear. The performance of lubricant oil varies between real life application and laboratory tests as a number of external factors play a role in the real life condition. Laboratory-scale tests are good methods to predict the performance of various lubricants to a certain extent [91]. There are a number of dependable

lubricant testers for the evaluation of lubricity of engine oil. High Frequency Reciprocating Rig, Ball-on-Cylinder Lubricity Evaluator (BOCLE), Surface Force Apparatus (SFA), 4-Ball Wear Tester (ASTM D-2266) are some of the equipment used widely. Wear tester in this study is the High Frequency Reciprocating Rig (HFRR).

*2.9.1 High Frequency Reciprocating Rig (HFRR)*

Modern engine oils are developed based on the drive for lower sulfur levels. This has led to the reduction in fuel lubricity. Low sulfur based fuels require additional additives to compensate for the reduced mechanical properties and provide adequate protection to the moving surfaces. A collaborative ISO/CEC work program in 1994 identified HFRR as the suitable testing equipment to evaluate the properties of the intermediate lubricity fuels. The High Frequency Reciprocating Test method measures the lubricity, or ability of a fluid to affect friction between, and wear to surfaces in relative motion under load. A number of tests were carried out and a number of modifications were done in order to derive a standard and to correlate the results with the wear in the fuel injection equipment. HFRR provides a fast, repeatable assessment of the performance of lubricants. It is particularly useful for simulating boundary lubrication conditions of engine oils, greases and other compounds. In order to simulate the engine conditions for the decomposition of engine oil and activating the surface film formation, a unique type of high frequency reciprocating ball (HFRB) testing unit was developed and built by the University of Texas at Arlington. The HFRB system consists of five major components: upper assembly, lower assembly, drive system, support structure and the control components (shown in Figure 3.1). The various components mentioned are illustrated in the figure below (Figure 2.18).

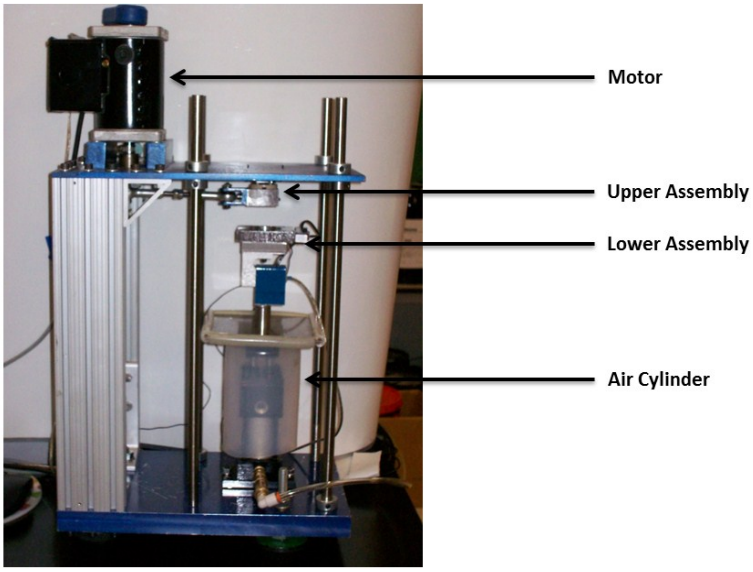


Figure 2.18: Home built High Frequency Reciprocating Rig (HFRR)

The upper assembly of the machine performs a reciprocating action. The upper assembly consists of the counter sample holder which houses a steel ball (ASTM 52100 Steel). The reciprocating action of the steel ball on the sample coupon (ASTM 52100 steel) generates the wear scar. The length of the wear scar generated is around 2.3mm. the lower assembly consists of the sample holder or oil bath, heating block with thermocouple and the steel sample coupon. The wear scar is generated on the steel coupon. The oil bath houses the heater, the test sample and a thermocouple. The test sample is placed in a small recess in the center of the oil bath. The oil bath mounts to two guide pins of the lower fixture. Then, the horizontal load cell and air cylinder are in order set up below lower fixture. In the drive system, a 1/7 Hp 12-24V DC motor is used to drive the slider crank mechanism, which provides the linear motion, the stroke and the frequency required of the machine. The drive system is controlled by an off the shelf controller, making the velocity dynamically controllable. The support structure consists of the top plate, bottom plate, vertical rods, rectangular aluminum tubing and base supports. The control

system of this machine includes three components: heating assembly, motor controller, and loading system. A high electrical resistance heater and an aluminum plate are used for heater. The heat controller, on/off relay, a maximum output of 15 VDC and 2.0 A DC power supply are used to control the temperature. For the motor control, an economical SCR variable speed control that is not pulse modulated is used. The SCR (silicon-controlled rectifier or semiconductor-controlled rectifier) is a 4-layer solid state device that controls current flow. In the loading system, the electrical pressure regulator is used as the means to apply the vertical load. To sum up, the key feature of the UTA-build HFRB tester is its ability to accurately control and measure input forces, output forces, temperature, angular velocity, and electrical resistance. By the lab-made HFRB, the precise evaluation and investigation of engine lubricants under boundary conditions can be accomplished.

# CHAPTER 3

# EXPERIMENTAL SECTION

## 3.1 Chemicals

Several additives are added to lubricants (base oil stock) to improve their efficiency. Antiwear/EP additives are crucial in the development of surface protective film. Antiwear/EP additives are added to base oil. Modern engines and equipment requirements have driven changes to mineral oil base stocks. There are three types of base oil stocks defined by the American Petroleum Institute (API) [96]:

Table 3.1: Types of Base Oil stock.

| Base Stock Type | Percentage of saturates | Sulfur content | Viscosity Index (VI) |
|---|---|---|---|
| Group I | <90% | >0.03% | 120>VI≤80 |
| Group II | >90% | ≤0.03% | 120>VI≤80 |
| Group III | ≥90% | ≤0.03% | ≥120 |

A step change in the performance of mineral oil based lubricant is observed on using Group II based base oil over Group I base oil. Group II based base oil contains significantly lower levels of aromatic compounds. Aromatic compounds are vulnerable to oxidation. Group I base oil contains high contents of aromatic compounds. Hence the oxidation resistance of group II is higher than group I. However, group II base oil has lower quantities of sulfur which acts as secondary oxidation inhibitors. The oxidation resistance of group II base oil can be improved by adding sulfur containing secondary oxidation inhibitors along with the combination of hindered phenols and diaryl amine primary antioxidants [97].

Extensive research into the development of Ashless (Zinc free) AW/EP additives is underway due to the environmental shortcomings in ZDDP. Ashless phosphorus containing

additives have been found to be particularly useful in reducing friction and wear [98]. Phosphates, thiophosphates, metal thiophosphates are some of the phosphorus additives that are used in the lubricant industry.

Lubricant formulation is achieved by combining two AW/EP additives in different proportions to group II base oil in order to understand their mechanical properties and their surface film formation nature. The base oil stock was supplied by Infenium and was used without any further purification. Two different Ashless additives were used. The first Ashless additive used was Ashless dialkyldithiophosphate and is referred to as SSC18. The second Ashless additive used was fluorothiophosphate and is referred to as PFC18. Other additives such as detergents (overbased calcium sulfonate), dispersants (Straight chain OCP) and antioxidants (alkylated diphenyl amine and hindered phenolic) were added to study the synergism in additives.

The chemical structure of SSC18 is given below (Figure 3.1):

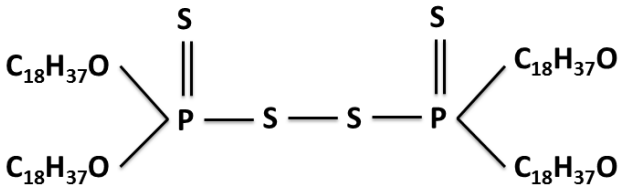


Figure 3.1: Ashless Dialkyldithiophosphate (SSC18)

Fluorinated organic compounds or partially fluorinated organic compounds are known to exhibit properties required by antiwear additives in lubricating oils. Fluorinated compounds especially esters and ethers have been used in lubricating oil as an AW additive for protecting surfaces that are magnetic [99-101]. Fluorinated compounds form metal fluorides through tribochemical reactions on the surface of the metal surface thereby protecting the metal. The chemical structure of Ashless fluorothiphosphate used in the lubricant formulation is given below (Figure 3.2).

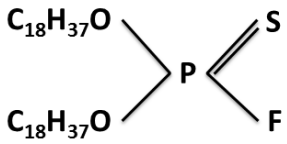


Figure 3.2: Chemical structure of Fluorothiophosphate (PFC18)

The properties of the mentioned additives in Group II base oil are compared with the fully formulated Oil (FFO) containing ZDDP, PFC18 & SSC18 in different concentrations. The lubricant formulation matrix is mentioned below.

Table 3.2: Experimental Base Oil Matrix

| Sr. No. | Mixture in Base Oil | Comment |
|---|---|---|
| 1 | 100PFC18 | AW only |
| 2 | 100SSC18 | AW only |
| 3 | 80PFC18-20SSC18 | AW only |
| 4 | 60PFC18-40SSC18 | AW only |
| 5 | 40PFC18-60SSC18 | AW only |
| 6 | 20PFC18-80SSC18 | AW only |
| 7 | 20PFC18-80SSC18 Calcium Sulphonate | AW + Detergent |
| Calcium Sulfonate is used as a detergent additive in engine oils. It is composed of inorganic salts in the core, surrounded by alkylbenzene sulfonate. It is also found to exhibit anti-wear, friction reducing and load carrying properties under boundary lubrication conditions [102]. | | |
| 8 | 20PFC18-80SSC18 DPA | AW + Antioxidant |
| Antioxidants are important additives in lubricants. Along with being AW/EP additives, it also retards ageing process. Among the several types of molecules that exhibit antioxidant activity, sulfur compounds, substituted phenols, ZDDP and alkylateddiphenylamines are the most common and most used in the industry [102-104]. The additives are classified into two families: peroxide decomposers and radical scavengers. Diphenylamine is the most commonly employed radical scavenger because of its high stoichiometric efficiency. | | |
| 9 | 20PFC18-80SSC18 Phenolic | AW + Antioxidant |
| Hindered phenols are the common antioxidants used in both polymers and lubricants. Hindered phenols protect polymers by increasing their process stability and their stability against oxidative degradation [105-107]. They protect lubricant oils and greases by acting as a barrier from the attack by oxygen. Oxidation degrades lubricants at high temperature. The auto oxidation has been observed and studied for many years. It is known to proceed via a series of radical processes. | | |
| 10 | 20PFC18-80SSC18 Straight OCP | AW + Viscosity modifier |
| Straight chain OCP (Olefin Copolymer): These are viscosity modifiers which are either in solid or liquid concentrates. The physical state of solids depends on numerous factors. The primary factor is the ethylene/propylene mass ratio (e/p mass ratio). When e/p ratio is in the 45/5-55/45 range, the material is amorphous and cold flows at room temperature. When e/p ratio is higher than 60/40, the copolymer becomes semi crystalline and does not col flow under ambient conditions | | |

## 3.2 Experimental Details

The friction and wear properties of the different formulated lubricants were evaluated with UTA's High Frequency Reciprocating Rig (HFRR).

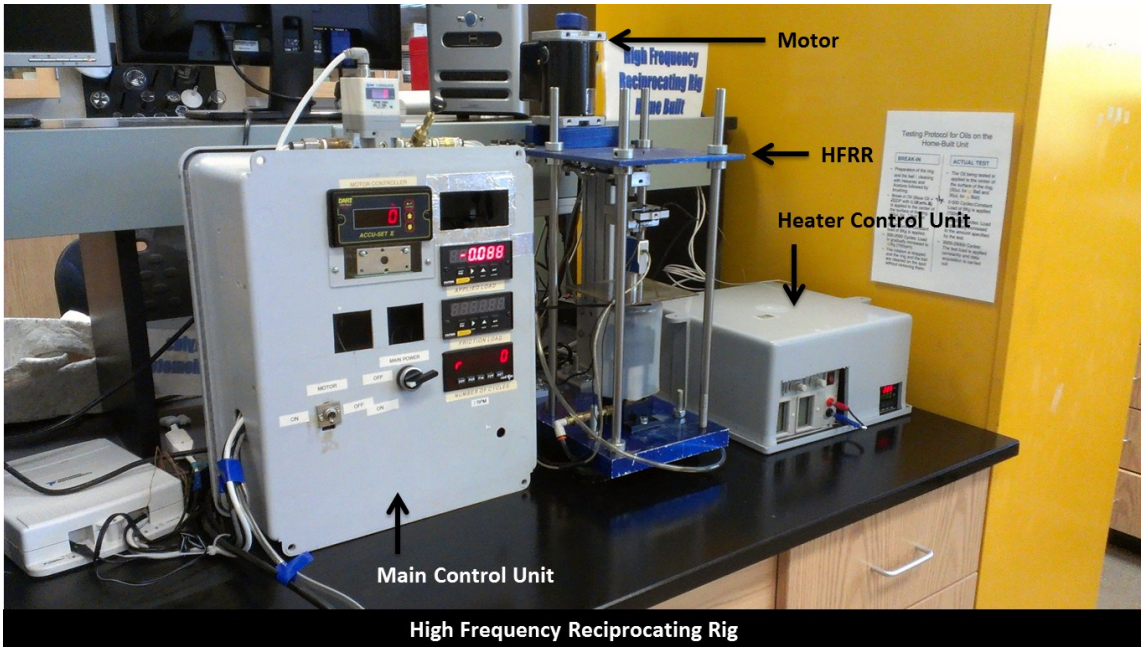


Figure 3.3: High Frequency Reciprocating Rig (HFRR).

The schematic representation of the sample compartment of the High Frequency reciprocating rig is shown in figure below (Figure 3.4).

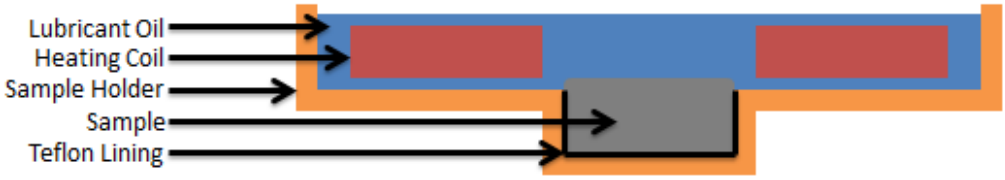


Figure 3.4: Cross Section view of the sample compartment in HFRR.

The sample pellet/coupons are made of ASTM 52100 steel. The coupons are cut to a thickness of 4mm from a half inch diameter (13mm diameter) McMaster ASTM 52100 steel rods using the Leco VariCut Diamond saw at 300rpm. The cut coupons are then hand polished with 320 grit & 600 grit sand papers (Leco Silicon Carbide paper). Final polishing is carried out with 5um alumina slurry and Selvyt Polishing cloth (Metallurgy Systems Inc.). The coupons are then stored in base oil to prevent oxidation and corrosion. The coupons are cleaned with light hydrocarbon solvent (hexane) before mounting onto the HFRR sample holder. The coupon is then lined with Teflon to give air tight fit in the sample holder. Once the sample is mounted, the heating block is placed in the holder and the lubricant is filled (20ml) till the sample and the heating block is immersed completely. The power is supplied to the heating block to heat the oil to a temperature of 100ºC. The heating block also contains a thermocouple which is used to determine the oil temperature. Once the temperature of the oil reaches 100ºC the reciprocating action is initiated. The wear on the coupon is brought about by ASTM E52100 steel ball (6mm in diameter). The steel ball is mounted onto a holder and this holder is then mounted onto the reciprocating arm. The load is applied by a pneumatic press from the bottom (from the sample towards the steel ball). A cross sectional schematic of the sample holder and the reciprocating setup with the steel ball is shown in Figure 3.5.

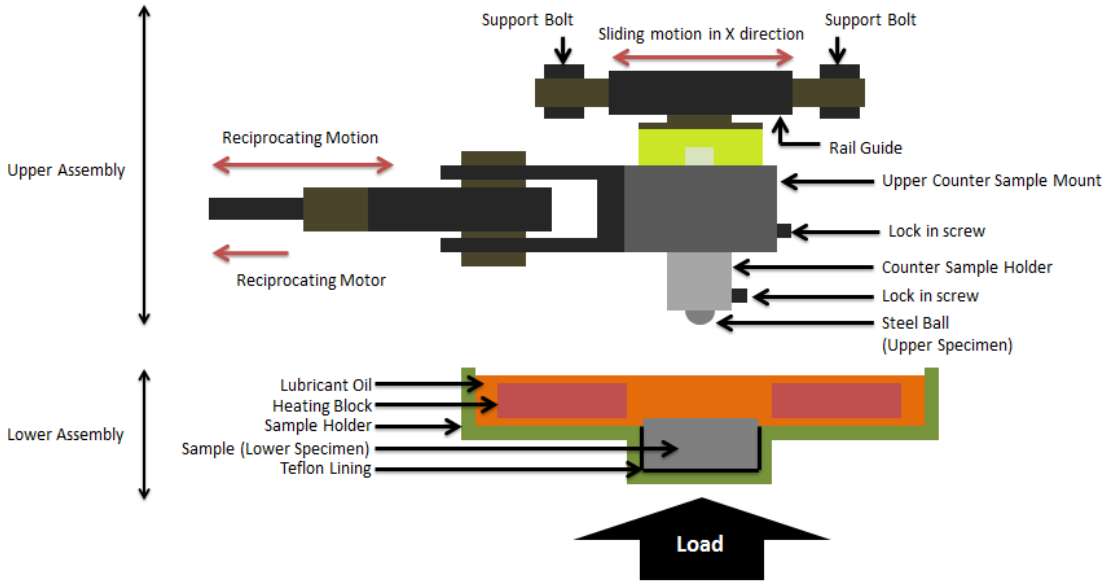


Figure 3.5: Cross Sectional schematic of HFRR (High Frequency Reciprocating Rig).

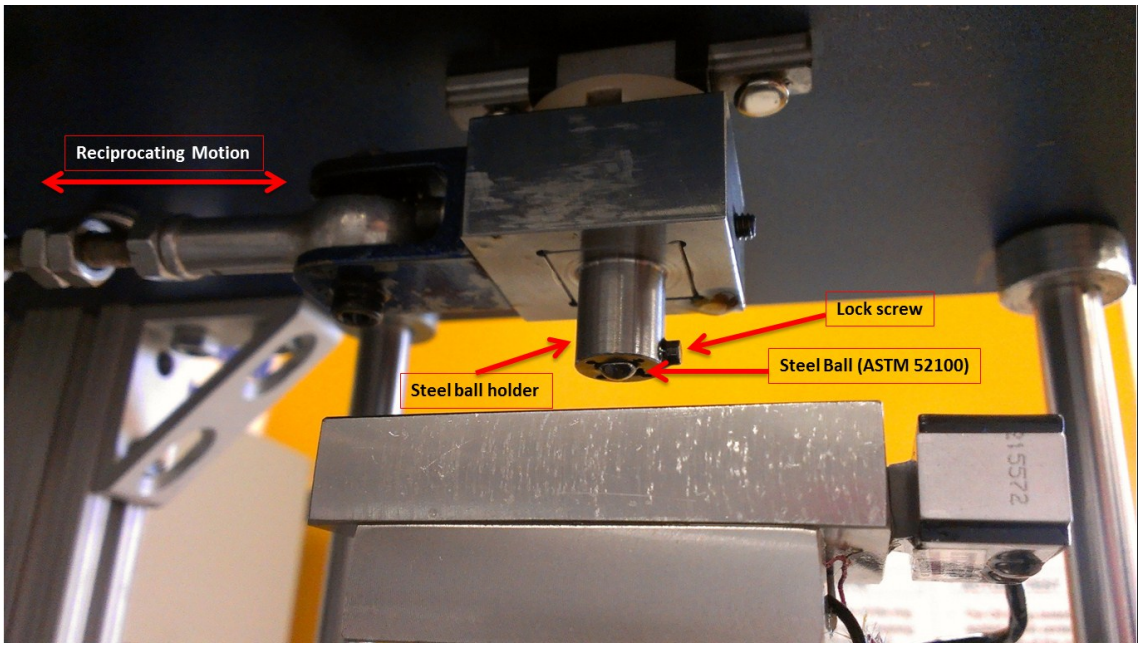


Figure 3.6: HFRR Setup

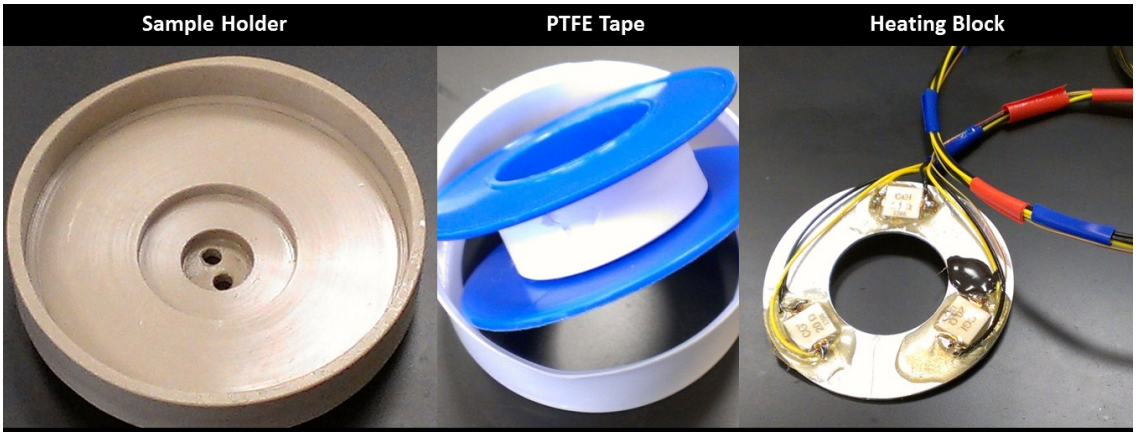


Figure 3.7: Images of sample holder, PTFE Tape & heating block

The load of 1 Kg is applied from the bottom (from the lower specimen to the upper specimen). The test is carried out for 1 hour at 100ºC. The wear produced is about 2.3 to 2.5 mm in length. The speed of the motor during the test is 3000rpm. The home built HFRR's test parameters, controls and interfaces are controlled through LabView software. Before each test, the holder for the steel ball, steel ball, sample holder and the heating block are washed with hexane ultrasonically and thoroughly air-dried. After the test, the sample is removed from the holder and the PTFE coating is removed. The sample is then cleaned with hexane and stored in sample holders with a film of base oil to prevent oxidation and corrosion. The wear volume is determined by the optical profiler. SEM (Scanning Electron Microscopy) images of the wear scar are taken. The wear scar is divided into three regions (Spot 1, Spot 2 & Spot 3) for convenience. Figure 3.8 shows the different regions of the wear scar.

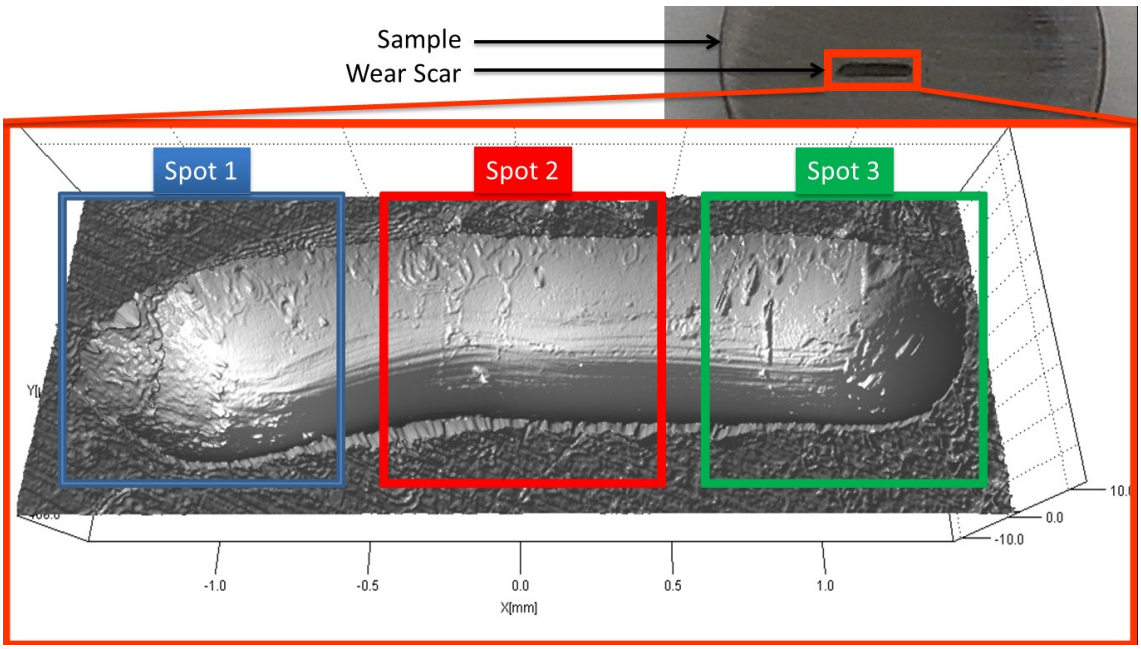


Figure 3.8: Different regions of the wear scar

The wear scar is slightly offset from the center of the metal coupon; hence the corner that is close to the edge of the metal coupon is Spot 1 and the other opposite corner is Spot 3. The region in the middle is Spot 2. The depth profile of the wear scar is obtained from the laser profiler. The chemical composition and makeup of the Tribofilm is obtained by X-Ray Absorption near Edge Spectroscopy (XANES). Nano indentation is performed on Spot 2 to understand the mechanical properties of the Tribofilm. The table below summarizes the analysis carried out on the wear scar of all the samples according to the different spots.

Table 3.3: Analysis performed on different spots of the wear scar.

| Analysis | Spot 1 | Spot 2 | Spot 3 |
|---|---|---|---|
| SEM images | Yes | Yes | Yes |
| Nano indentation | | Yes | |
| XANES | | Yes | |
| Optical Surface Profiler | Yes | Yes | Yes |

# CHAPTER 4

# MECHANISM OF WEAR AND TRIBOFILM FORMATION WITH ASHLESS ANTIWEAR ADDITIVES

## 4.1 Introduction

Traffic congestion is one of the most challenging problems in our today's cities. This is obvious from the number of vehicles on the roads and the amount of pollution they cause. To control the effects of pollution, governing bodies created clean-air laws that restrict the amount of pollution that vehicles produce. Modern day engine exhaust system contains a small device called the catalytic converters that reduce the harmful effects of engine exhaust gases. Latest catalytic converters contain Three-way catalysts (TWCs) formulation that would aid improved poison tolerance and thermal stability. Thermal stability is necessary to maintain prolonged catalytic activity during its lifecycle. During its lifetime, catalytic converters are exposed continuously to the engine exhausts that gradually change its structural and morphological aspects. This leads to deterioration of their catalytic performance [108,109]. The surfaces of catalytic converters are poisoned or deactivated by the deposits of P & S as well as metallic and organometallic compounds. Recent approaches have included developing formulations lower in phosphorous and sulfur as well as using ashless antiwear agents. The poisoning of TWCs is the result of the chemisorption of impurities on the active catalytic sites. There are two mechanisms by which chemical deactivation may occur [109]:

1. Selective Poisoning: This is caused by irreversible strong chemisorption of the impurities present in the exhaust gas stream. The adsorbed poisoning species deactivates the catalytic activity partially or completely by the modification of the electronic environment of the noble metal atoms near the poisoning species.

2. Non-selective poisoning: This kind of poisoning involves deposition of foreign chemical substances on the outer catalytic surface. The contaminants block the pore's mouth also known as fowling or masking, thereby blocking access to the rest of the catalyst in the converter region.

The poisoning of three way catalysts have been extensively studied [110]. The main sources of TWC poisoning include fuel, lubrication oil, and wear of engine oil and exhaust of tailpipe parts.

## 4.2 Mechanism of Catalytic poisoning

The phosphorus in engine oil antiwear additive (such as ZDDP – zinc Dialkyldithiophosphate) is one of the key species that causes catalytic poisoning. Phosphorus is found in the converters as $P_2O_5$ in the largest amount, followed by Ca and Zn. Ca and Zn are present in engine oil detergent additives [111,112]. The effect of phosphorus poisoning on the oxygen storage and release capacity of $CeO_2$ and Ce-Zr-O have been extensively studied by Larese et al. [113,114] and Granados et al. [115,116]. The formation of $CePO_4$ results in the unavailability of $Ce^{3+}$ and $Ce^{4+}$ redox pair. $Ce^{3+}$ and $Ce^{4+}$ redox pair are required for the efficient functioning of TWCs [113,115].

In this study, antiwear properties of Ashless additives (Fluorothiphosphates PFC18 & Dialkyldithiophosphate SSC18) in base oil are compared with ZDDP in base oil. The antiwear additives are added to base oil at a nominal composition of 0.1wt% P. The wear performance was examined using the High Frequency Reciprocating Rig (HFRR) where a limited quantity of oil (~12 ml) was used and a contact load of 1 kg was used. The wear surface was examined with Scanning Electron Microscope (SEM) and the profile of the sample was obtained using Veeco Surface Profiler. Nanoindentation was carried out in the middle of the wear scar to determine the thickness, hardness and modulus of the tribofilm.

## 4.3 Chemistry

### *4.3.1 Octadecylphosphorofluoridothioate (PFC18)*

Engine oil contains additives to facilitate in the lubrication and protection of moving parts in the engine. The presence of phosphorus in lubricant additives hinders the performance of catalytic converters. Automotive industries eventually would have to completely do away with phosphorus containing additives due to stringent Anti-pollution laws. In addition, ZDDP produces ash due to the presence of zinc. Ashless additive such as alkylphosphorofluoridothioates developed by Chen et al [117] exhibit superior wear protection compared to zinc dialkyldithiophosphates. PFC18 being more active compared to ZDDP can be used at lower levels of P compared to ZDDP, thus resulting in less fouling of the catalytic converters. The chemical structure of PFC18 is given below in Figure 4.1.

Octadecylphosphorofluoridithioate

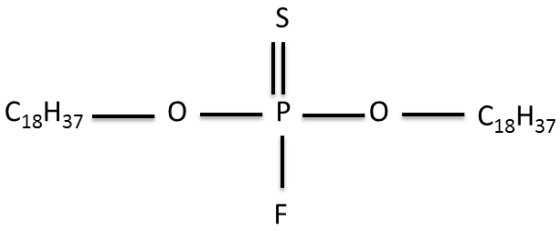


Figure 4.1: Octadecylphosphorofluoridithioate (PFC18) [117].

Physical Properties:

- Colorless solid
- Melting point: 36-37º C

PFC18 contain 50% lower sulfur concentration than ZDDP because alkylphosphorofluoridothioates have only one sulfur atom for every one phosphorus atom while ZDDP have two sulfur atoms for each phosphorus atom in the structure. The amount of alkylphosphorofluoridothioates in lubricant oil depends on the wt% of phosphorus content

required in the lubricant. In this study, 0.1 wt% phosphorus PFC18 content in base oil is prepared.

*4.3.2 Octadecylthioperoxydiphosphate (SSC18)*

Octadecylthioperoxydithiophosphate is prepared in stages. O, O' dialkyl dithiophosphoric acid was obtained by mixing phosphorus pentasulfide with alcohols at elevated temperature in toluene. This is followed by the oxidation of O, O' dialkyl dithiophosphoric acid by the addition of $H_2O_2$ solution (37%) into a vigourously stirred O, O' dialkyl dithiophosphoric acid/ice mixture held in an ice bath [118]. The general structure is given Figure 4.3 & chemical structure of Octadecylthioperoxydithiophosphate is mentioned below in Figure 4.4 [118].

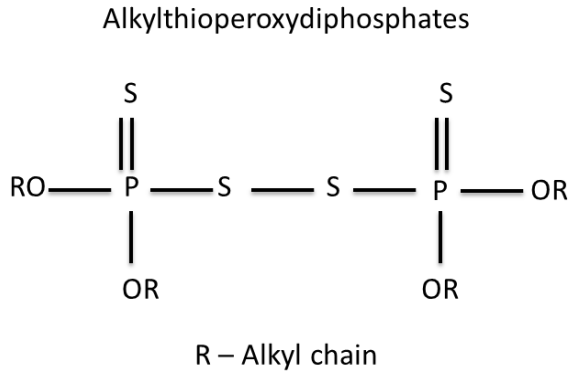


Figure 4.2: Chemical Structure of Alkylthioperoxydiphosphates [118].

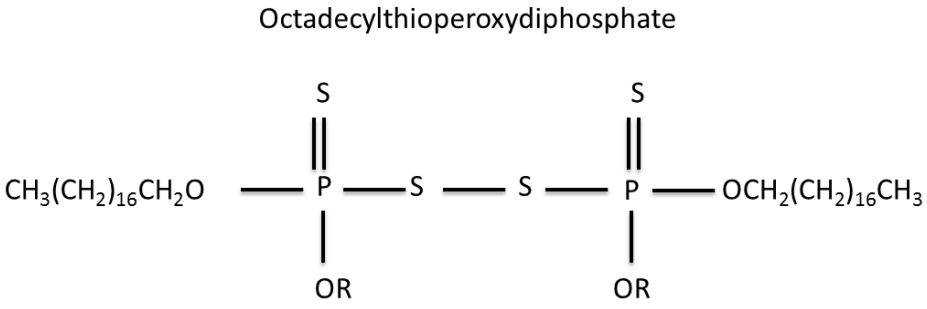


Figure 4.3: Chemical Structure of Octadecylthioperoxydiphosphate [118].

*4.3.3 Zinc Dialkyldithiophosphate (ZDDP)*

Metal dialkyldithiophosphates are prepared by the reaction of phosphorus pentasulfide with alcohols to form dithio-phosphoric acid, which is then followed by the neutralization of the acids with an appropriate metal compound. Many types of alcohols have been used to bring about this reaction such as aliphatic, cyclic [58], and phenolic derivatives. High molecular weight alcohols are preferred because they bring about sufficient thermal stability to the final products while rendering sufficient solubility in oils. For the neutralization of the acids, zinc, molybdenum, or calcium oxides are usually chosen. For many years, zinc salts of dialkyldithiophosphates have been used because of its superior antioxidant capability. It is also cost effective antioxidant to be produced and therefore have been included as a key component in many oxidation inhibitor packages for engine oils and transmission fluids. ZDDP functions as an antioxidant and an antiwear additive. Its antiwear properties are attributed to the fact that ZDDP decomposes to form sulfide and phosphate films in the valve train area through corrosive reactions on the metal surface.

## 4.4 Experimental Procedure

The tribological performance of Ashless additives was evaluated using High Frequency Reciprocating Rig (HFRR) (shown in figure 3.3). The synergism on combining two Ashless additives (PFC18 & SSC18) was also analyzed. The various lubricant formulation evaluated is outlined in Table 4.1.

Table 4.1: Lubricant Formulation

| Mixture in Base Oil |
|---|
| 1. 100ZDDP |
| 2. 100PFC18 |
| 3. 100SSC18 |
| 4. 80PFC18-20SSC18 |
| 5. 60PFC18-40SSC18 |
| 6. 40PFC18-60SSC18 |
| 7. 20PFC18-80SSC18 |

The cross sectional schematic of HFRR is shown in Figure 4.5. The wear on steel coupon (ASTM E52100) is produced by the reciprocating action of steel ball (ASTM E52100) on a metal coupon. The performance of the lubricant oil is analyzed by adding it as a medium in between the steel ball and the coupon. The wear was produced by application of 1 kg load on steel coupons (dimension 0.5 inch Ø and 4 mm thick). The steel coupons were polished with 320 and 600 grit silicon carbide papers. The final polish was carried out with 5μm alumina slurry. The reciprocating action of steel ball on the metal coupon was carried out for a period of 1 hour at 100º C. The lubricant formulation was added in the oil bath that houses the metal coupon (shown in Figure 4.4). The oil bath houses the steel coupon, lubricant oil and the heating block. The heating block facilitates in rising the temperature of the lubricant oil to 100º C. The test conditions used is summarized below in Table 4.2. Thermocouple is attached to the heating block that determines the oil temperature. The steel coupon was placed in the oil bath/sample holder by lining it with Teflon tape to give it a tight seal and fit. Steel coupon, steel ball and all other components were thoroughly cleaned with hexane to remove contaminants, debris and residue oil before the start of the test. About 12 ml of lubricant oil is used for every test.

Table 4.2 HFRR Test condition

| | |
|---|---|
| Test duration (in minutes) | 60 |
| Load | 1 kg (9.8N) |
| Stroke length (in mm) | 2.5 |
| Stroke frequency (in Hz) | 50 |
| Temperature (in ºC) | 100 |
| Ball | 52100 steel (6.25mm diameter) |
| Coupon | 52100 steel |

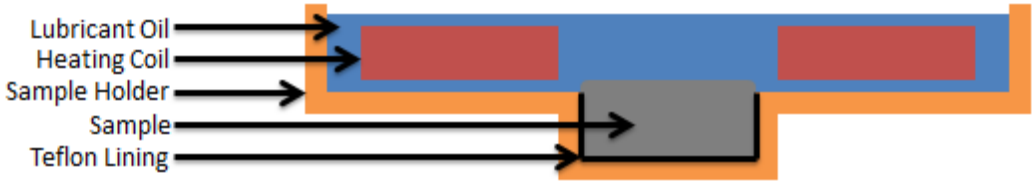


Figure 4.4: HFRR sample holder

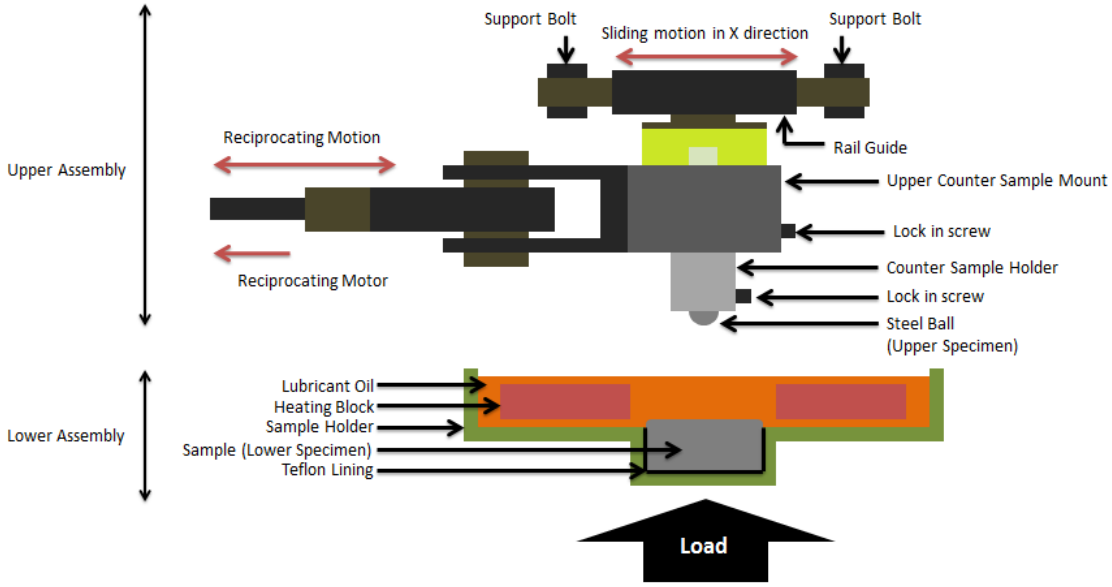


Figure 4.5: Cross sectional Schematic of HFRR

After completion of a test, the steel coupon was removed, washed with hexane to remove debris and residue oil. Hexane was used to clean the coupons because it does not wash away the Tribofilm that is formed in the wear scar. The steel coupon was then soaked in base oil before storage to prevent corrosion. The wear scar profile was obtained using Veeco Wyko NT9100 Optical profiler to understand the extent of wear produced. Effective Tribofilm formation results in lower wear depth while formulations that do not form homogenous Tribofilm, results in greater wear depth. The topography of the wear was studied using the Scanning

Electron Microscope (SEM) and the thickness, hardness and modulus of the Tribofilm formed was obtained using the Hysitron Nanoindenter.

## 4.5 Tribological Test Results

### *4.5.1 Wear Data*

Topography of the wear scar was obtained using Veeco Wyko NT 9100 Optical Profiler. The data obtained was then post processed with Image Metrology SPIP 6.0.6 software. The post processing details are summarized in Table 4.3.

Table 4.3 SPIP 6.0.6 Post Processing Details

| | |
|---|---|
| Fill Void Pixels | Sets void pixel to values found by interpolation |
| Particle and Pore Analysis | To obtain the wear volume |
| Cross Section Profile | To obtain the depth of the wear |

The typical wear scars obtained for the three lubricant formulations (100ZDDP, 100PFC18 & 100SSC18) are shown below (Figure 4.6).

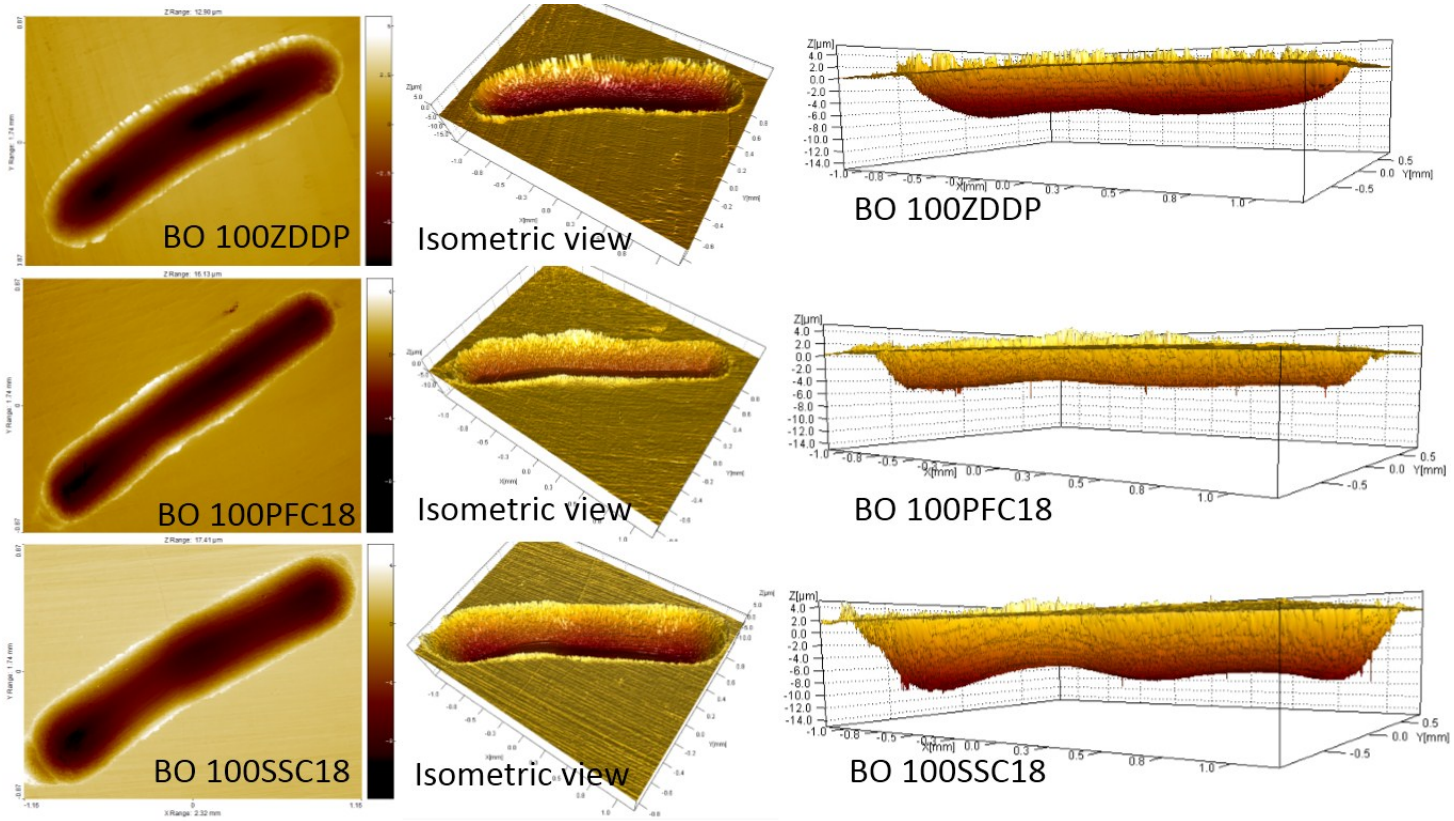


Figure 4.6: Wear Scar of HFRR test with 100ZDDP, 100PFC18, 100SSC18 in Base oil

A number of studies have shown that initial surface roughness of the metal sample influences the friction and wear process in tribological testing [119,120]. Higher the initial surface roughness of the contacting surfaces, higher is the wear rate [121]. The coefficient of smoother surface is higher than a rough unpolished surface and decreases with increase in surface roughness [119]. During the run of the experiment, initial surface roughness plays a significant role in determining the sliding conditions at the interface. During the wear process, the geometrical state of the interface is modified which influences the sliding conditions and can lead to change in sliding regime from partial slip to gross slip [122]. The samples are hence, mirror polished to mitigate the influence of initial surface roughness. The metal coupons are polished with 320 grit & 600 grit Silicon Carbide papers, followed by 5um Alumina slurry polish for the final finish. The wear developed on the steel coupon is greater than 5 μm in depth and the surface roughness is in terms of nanometers. Hence in this study, initial surface fineness does not play a deciding factor in the wear propagation. The surface roughness of the steel coupons is shown & summarized below in Figure 4.7 and Table 4.4.

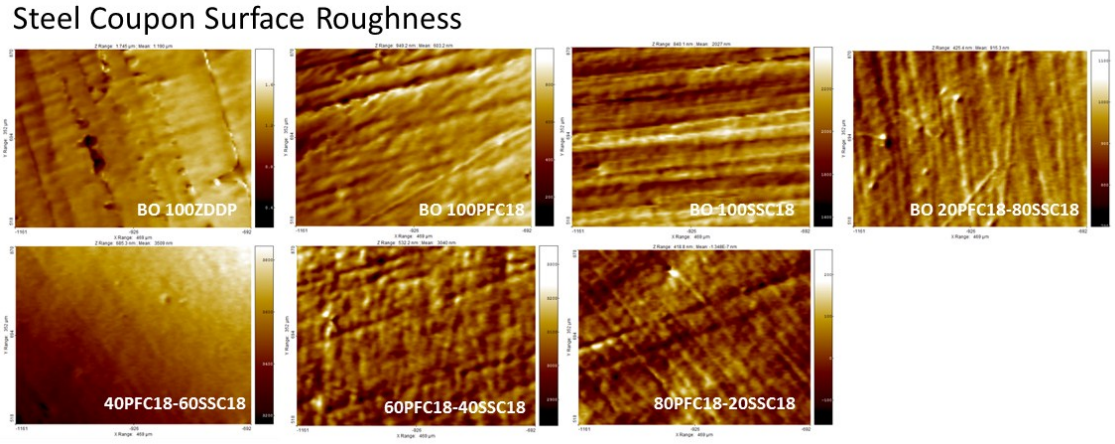


Figure 4.7: Surface roughness of Steel coupons

Table 4.4 Surface roughness data

| Sample Name | Sa (nm) | Sq (nm) | Sy (nm) | Sv (nm) | Sp (nm) | Smean (nm) | Sdr (%) | S2A ($nm^2$) | S3A ($nm^2$) |
|---|---|---|---|---|---|---|---|---|---|
| **100ZDDP** | 69.68 | 99.04 | 1548.57 | 921.2 | 627.36 | 1.23E-07 | 0.022 | 1.65E+11 | 1.65E+11 |
| **100PFC** | 70.1 | 92.86 | 949.51 | 475.54 | 473.97 | 1.25E-06 | 0.02 | 1.65E+11 | 1.65E+11 |
| **100SSC** | 85.89 | 106.63 | 810.73 | 421.66 | 389.07 | 5.46E-07 | 0.023 | 1.65E+11 | 1.65E+11 |
| **2080** | 28.98 | 37.62 | 427.64 | 198.18 | 229.45 | -5.77E-08 | 0.004 | 1.65E+11 | 1.65E+11 |
| **4060** | 14.44 | 18.8 | 215.35 | 105.57 | 109.78 | -3.95E-09 | 0.001 | 1.65E+11 | 1.65E+11 |
| **6040** | 40.87 | 52.17 | 547.42 | 245.74 | 301.68 | -2.94E-07 | 0.006 | 1.65E+11 | 1.65E+11 |
| **8020** | 35.81 | 45.81 | 418.82 | 160.29 | 258.53 | -1.71E-09 | 0.003 | 1.65E+11 | 1.65E+11 |

Sa – Roughness average

Sq – Root Mean Square

Sy – Peak-Peak height (Peak to Valley)

Sv – Maximum valley depth

Sp – Maximum peak height

Smean – Mean Height

Sdr – Surface area ratio

S2A – Scanning area

S3A – Surface area

2080 – BO 20PFC18-80SSC18

4060 – BO 40PFC18-60SSC18

6040 – BO 60PFC18-40SSC18

8020 – BO 80PFC18-20SSC18

The wear test for every lubricant formulation was carried out twice (2 batches viz. B1 & B2) to obtain a statistical wear data. The wear volume of the scar was obtained using SPIP 6.0.6 and the depth of the wear scar was taken from three regions. The wear scar is divided into three regions (Spot 1, Spot 2 & Spot 3) for convenience. Figure 4.8 shows the different regions of the wear scar.

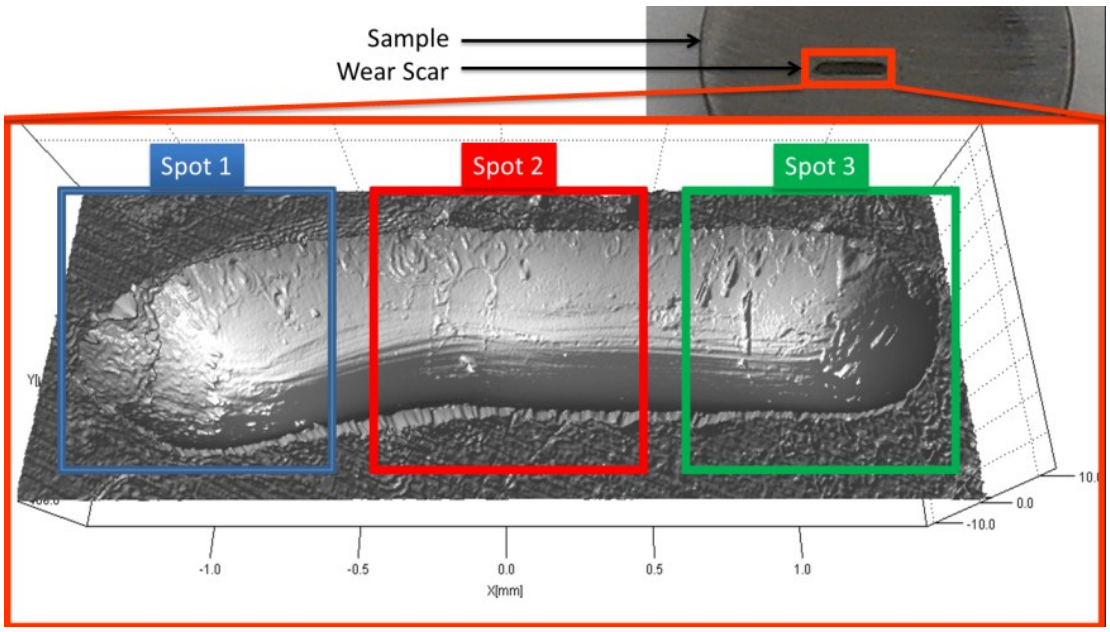


Figure 4.8: Three regions of the wear scar

The wear scar is slightly offset from the center of the metal coupon; hence the corner that is close to the edge of the metal coupon is Spot 1 and the other opposite corner is Spot 3. The wear volume from the two batches for the various ashless formulations is shown below (Figure 4.9).

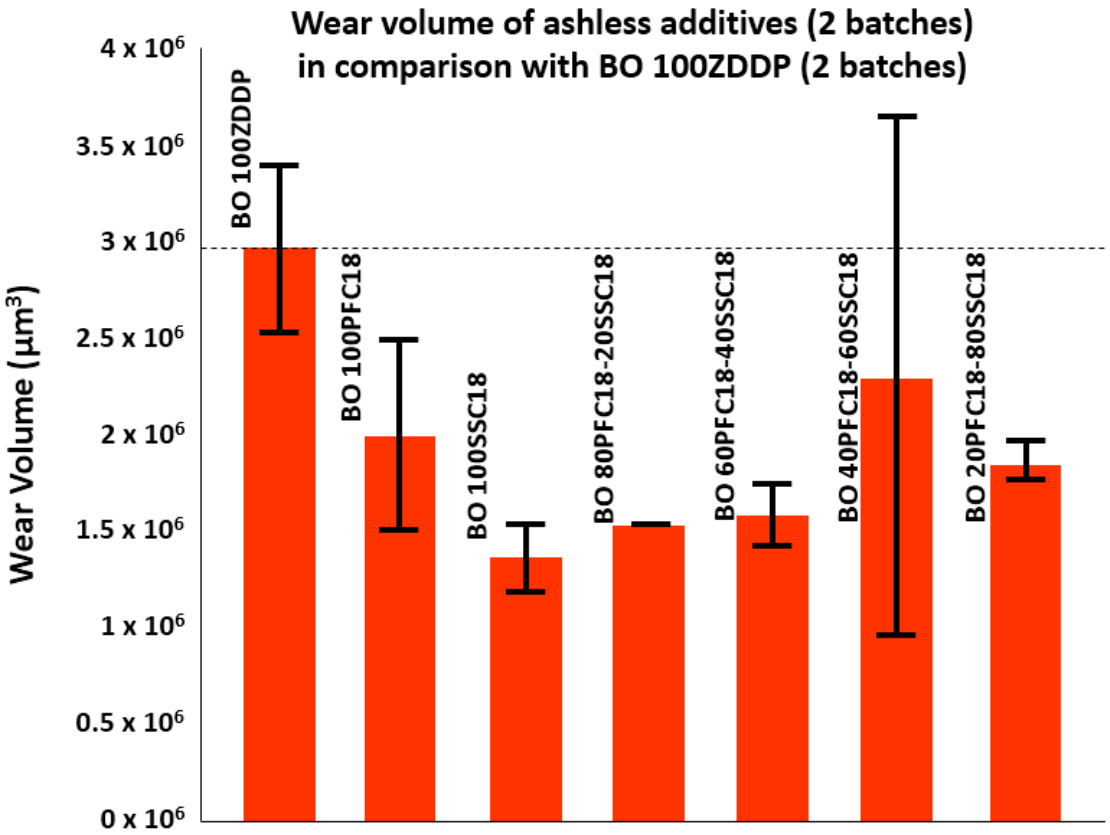


Figure 4.9: Wear scar volume of various lubricant additives in base oil

The volume of the wear scar is determined using the Veeco Wyko NT9100 Optical profiler to determine the additive's antiwear performance. The volume of wear is indicative of the efficiency of the lubricant in facilitating the formation of antiwear film (boundary lubrication) between the interacting surfaces. In general, lower the wear volume better is the antiwear performance of that ashless chemistry. Figure 4.9 is a comparative study of wear volume of the various ashless chemistries in base oil with ZDDP in base oil. In order to obtain accurate & statistical information on the wear volume, 2 batches were developed for each lubricant formulation. A large variation in the wear volume is observed in BO 40PFC18-60SSC18. The

dotted line in Figure 4.9 indicates the mean value of BO 100ZDDP. The results indicate that all ashless formulations have better or equivalent antiwear performance in comparison to 100ZDDP in base oil. BO 100SSC18 shows the least variation in wear volume among the ashless chemistries and ZDDP. The two batches of each lubricant formulation show similar values to each other. The wear volume observed is summarized in the table below (Table 4.5)

Table 4.5 Wear volume of 2 batches

| Sample | Batch 1 ($\mu m^3$) | Batch 2 ($\mu m^3$) |
|---|---|---|
| BO 100ZDDP | $2.55 \times 10^6$ | $3.41 \times 10^6$ |
| BO 100PFC18 | $1.52 \times 10^6$ | $2.5 \times 10^6$ |
| BO 100SSC18 | $1.55 \times 10^6$ | $1.2 \times 10^6$ |
| BO 80PFC18-20SSC18 | $1.55 \times 10^6$ | $1.55 \times 10^6$ |
| BO 60PFC18-40SSC18 | $1.44 \times 10^6$ | $1.76 \times 10^6$ |
| BO 40PFC18-60SSC18 | $0.97 \times 10^6$ | $3.66 \times 10^6$ |
| BO 20PFC18-80SSC18 | $1.78 \times 10^6$ | $1.98 \times 10^6$ |

20PFC18-80SSC18 < 100ZDDP < 80PFC18-20SSC18 < 100SSC18 < 60PFC18-40SSC18 < 40PFC18-60SSC18 < 100PFC18

The difference between the 2 batches for all lubricant formulation is mentioned below (Table 4.6)

Table 4.6 Wear volume difference

| | |
|---|---|
| BO 100ZDDP | $8.6 \times 10^5$ |
| BO 100PFC18 | $9.8 \times 10^5$ |
| BO 100SSC18 | $3.5 \times 10^5$ |
| BO 80PFC18-20SSC18 | 0 |
| BO 60PFC18-40SSC18 | $3.2 \times 10^5$ |
| BO 40PFC18-60SSC18 | $2.69 \times 10^5$ |
| BO 20PFC18-80SSC18 | $2 \times 10^5$ |

Table 4.7 Wear depth at Spot 1

| Sample | Batch 1 (μm) | Batch 2 (μm) |
|---|---|---|
| BO 100ZDDP | 8.11 | 5.07 |
| BO 100PFC18 | 5.97 | 1.94 |
| BO 100SSC18 | 5.29 | 4.87 |
| BO 80PFC18-20SSC18 | 5.71 | 2.51 |
| BO 60PFC18-40SSC18 | 5.72 | 5.94 |
| BO 40PFC18-60SSC18 | 4.01 | 9.69 |
| BO 20PFC18-80SSC18 | 5.99 | 6.24 |

Table 4.8 Wear depth at Spot 2

| Sample | Batch 1 (μm) | Batch 2 (μm) |
|---|---|---|
| BO 100ZDDP | 8.67 | 10.7 |
| BO 100PFC18 | 5.8 | 1.14 |
| BO 100SSC18 | 4.04 | 3.99 |
| BO 80PFC18-20SSC18 | 4.62 | 4.29 |
| BO 60PFC18-40SSC18 | 5 | 5.97 |
| BO 40PFC18-60SSC18 | 3.32 | 9.32 |
| BO 20PFC18-80SSC18 | 5.49 | 6.83 |

Table 4.9 Wear depth at Spot 3

| Sample | Batch 1 (μm) | Batch 2 (μm) |
|---|---|---|
| BO 100ZDDP | 8 | 13 |
| BO 100PFC18 | 5.23 | 1.50 |
| BO 100SSC18 | 5.87 | 3.56 |
| BO 80PFC18-20SSC18 | 5.67 | 7.72 |
| BO 60PFC18-40SSC18 | 5 | 5.64 |
| BO 40PFC18-60SSC18 | 2.83 | 9.76 |
| BO 20PFC18-80SSC18 | 7.35 | 6.95 |

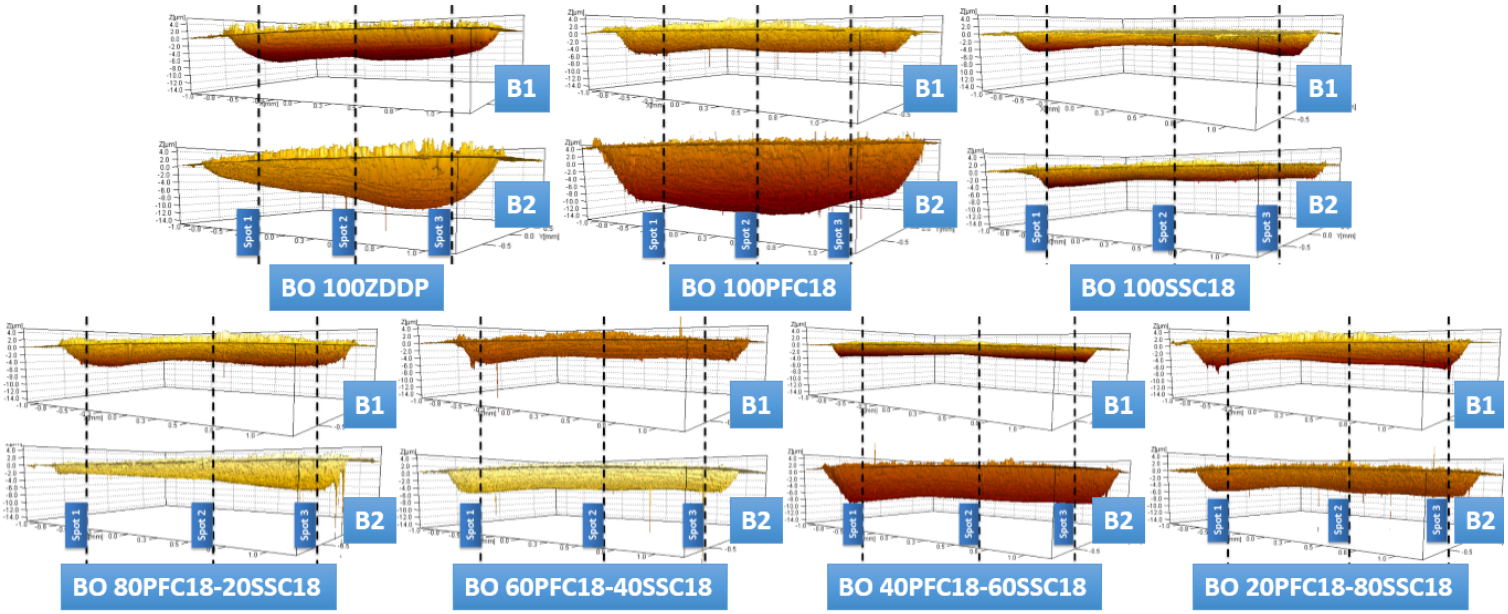


Figure 4.10: Wear depth comparison between the 2 batches

The topographical image of the wear scar derived from SPIP 6.0.6 shown in figure 4.10 illustrates the variation in the depth of the wear in the three regions (Spot 1, 2 & 3). The wear depth is not uniform along the length of the scar. The region in between spot 1 & 2 and spot 2 & 3 is shallow & has lower wear depth. The elevation or kink observed in the region between spot 1 & 2 is prominent compared to the region in between spot 2 & 3. The edge of the wear track corresponding to the shallow region has a large debris buildup compared to the other regions in the wear scar. BO 100ZDDP has a high amount of debris pileup along the sides of the wear track and BO 100SSC18 shows the least debris pileup.

## 4.6 Tribofilm Analysis

### *4.6.1 Scanning Electron Microscopy*

Scanning electron microscopy using secondary electrons was used to examine the local morphology of wear scar (Spot 2) in all the lubricant compositions. Figure 4.11 shows typical wear scars for the different ashless lubricant formulations in comparison to ZDDP. The morphology and characteristics of the wear track provide significant information about the wear behavior of the various chemistries. The images shown in figure 4.11 are from the batch that showed the least wear volume in each ashless formulation. The image of BO 100PFC18 & BO 100SSC18 are smooth compared to ZDDP & other Ashless additives indicating that the Tribofilm formed by these Ashless chemistries are continuous. Continuous Tribofilm provide better antiwear protection than the patchy films and this statement is supported by the low wear volume numbers of BO 100PFC18 & BO 100SSC18. BO 20PFC18-80SSC18 shows a smooth surface with a number of divots which is indicative of incomplete integration of Tribofilm pads. Tribofilms nucleates at various sites and it grows in size till the pads come in contact with each other. Incomplete integration of the Tribofilm leaves divot like marking. These markings could also be due to the Tribofilm pullout. This statement cannot be ruled out since the markings are

along the direction of wear. The antiwear film formed by BO 40PFC18-60SSC18 is very patchy and discontinuous. The top and bottom region of BO 40PFC18-60SSC18 image appear to have large Tribofilm patches while the center appears to have smaller patches, indicating that the center region is either in the film growth stage or it is subjected to higher wear rate compared to the other regions along the length of the wear track. BO 60PFC18-40SSC18 has discontinuous antiwear pads and there are a number of horizontal lines running along the length of the wear track which is indicative of extensive wear and BO 80PFC18-20SSC18 shows a high amount of Tribofilm pullout and this is indicative of abrasive wear of the additive. BO 100ZDDP also exhibits patchy films and has the highest wear volume among the chemistries under study, which indicates that, the ashless chemistries have better antiwear performance.

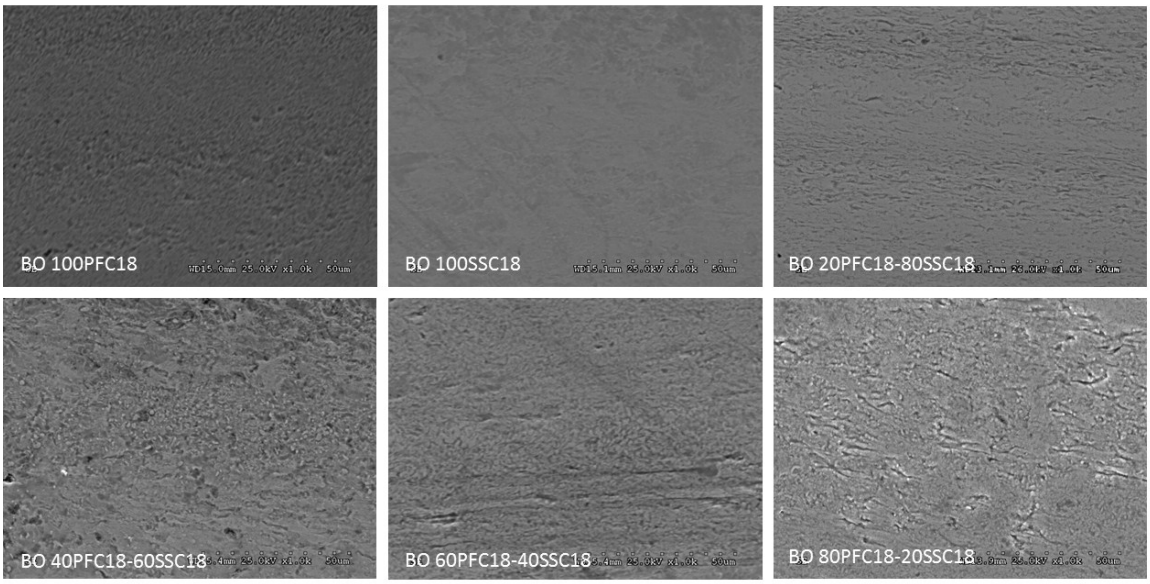


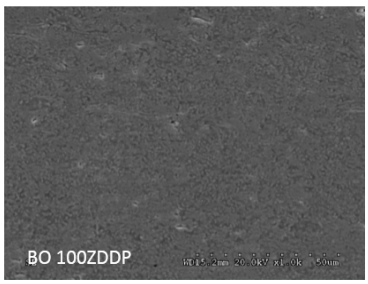


| SAMPLE | BATCH | WEAR VOLUME |
|---|---|---|
| BO 100PFC18 | BATCH 2 | 0.25 X $10^6$ µm$^3$ |
| BO 100SSC18 | BATCH 2 | 1.20 X $10^6$ µm$^3$ |
| BO 20PFC18-80SSC18 | BATCH 1 | 1.78 X $10^6$ µm$^3$ |
| BO 40PFC18-60SSC18 | BATCH 2 | 0.97 X $10^6$ µm$^3$ |
| BO 60PFC18-40SSC18 | BATCH 2 | 1.44 X $10^6$ µm$^3$ |
| BO 80PFC18-20SSC18 | BATCH 1 | 1.55 X $10^6$ µm$^3$ |
| BO 100ZDDP | BATCH 1 | 2.55 X $10^6$ µm$^3$ |

Figure 4.11: Secondary electron micrographs of wear scars (Spot 2).

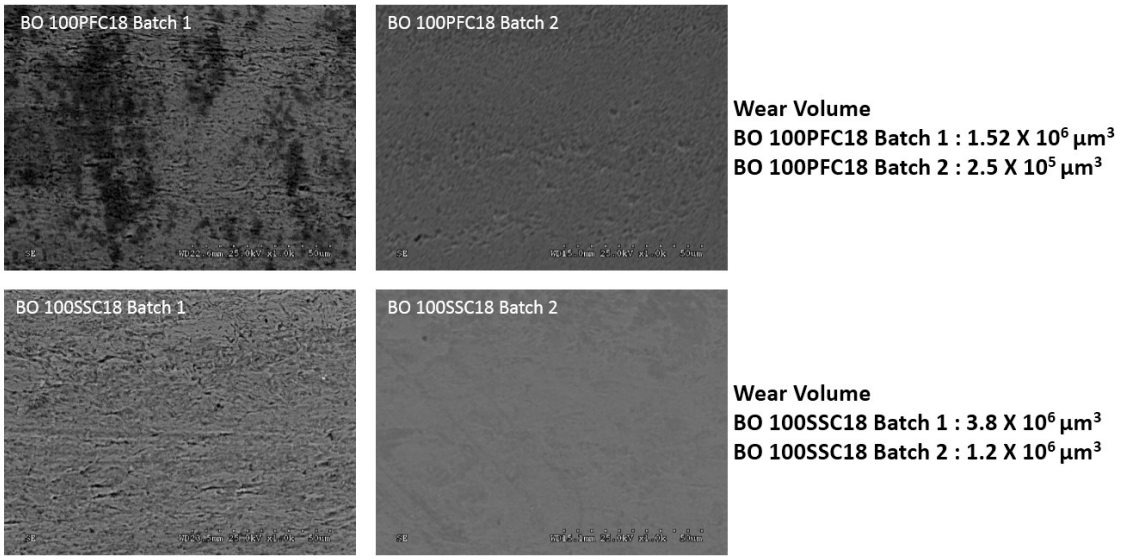


Figure 4.12: SEM Comparative study between the 2 batches

Figure 4.12 gives a comparative study between batch 1 samples and batch 2 having the least wear volume. BO 100PFC18 Batch 1 show signs of abrasive wear and tribofilm pullout along the wear track.

*4.6.2 Scanning Probe Microscopy and Nanoindentation*

In recent years, the development of scanning probe microscopy (SPM) has brought intense interest not only in directly obtaining three-dimensional morphology of the surface under study, but also in obtaining various physical properties on a nanometer scale. The physical properties of the surface correspond to the interaction force between the sample surface and the probing tip. The interaction force is greatly influenced by the proximity of the probe tip to the surface of the sample. Nanoindetation with topographical imaging is a powerful method of determining the mechanical properties of the surface of interest. It is especially useful in the cases where the surface is not homogenous and is made of multiple materials. It is useful in determining the tribofilm's mechanical properties (hardness and stiffness) which is likely to determine the film's longevity [7,123]. Nano indentation was carried out on spot 2 of all the

samples in batch 1. The indentation conditions used are summarized in the tables given below (Table 4.10 & Table 4.11).

Table 4.10 Imaging Controls

| | |
|---|---|
| Scan rate | 0.2 Hz |
| Tip velocity | 12 µm/sec |
| Scan size | 30 µm x 30 µm |
| Scan load | 2 µN |
| Post Processing Software | SPIP 6.0.6 (Image Metrology) |
| ▪ Global Leveling<br>▪ Global Bow Removal | |
| Z axis scaling | |
| Minimum | -100 nm |
| Maximum | 100 nm |
| Aspect Ratio (x,y,z) | 1,1,30 |

Table 4.11 Indentation Controls

| Tip used | Berkovich |
|---|---|
| Indentation | Array 4 x 4 |
| Spacing between indents in X | 7 µm |
| Spacing between indents in Y | 7 µm |
| Load Function | Trapezoidal |
| Begin Force | 0.00 µN |
| End Force | 500 µN |
| Segment time | 5 sec |
| Number of segments | 3 |

An array of 4 x 4 (16) indents were carried out in spot 2 to understand the mechanical properties of the tribofilms. The average of 16 indents for each sample is calculated. The indents which do not exhibit accurate data (outliers) are ruled out and the average of the remaining data is considered. The surface roughness is determined from the SPM image of the sample using SPIP 6.0.6 image processing software. The standard deviation for the indentations are shown in figure 4.13. Table 4.12 below summarizes the average contact depth, modulus & hardness values.

Table 4.12 Properties of tribofilm from various chemistries

| | 100ZDDP | 100PFC | 100SSC | 8020 | 6040 | 4060 | 2080 |
|---|---|---|---|---|---|---|---|
| **Contact Depth (nm)** | 47.55 | 33.75 | 39.43 | 25.51 | 42.02 | 36.72 | 31.33 |
| **Er (GPa)** | 126.06 | 149.19 | 138.61 | 174.06 | 147.39 | 158.4 | 169.05 |
| **H (GPa)** | 3.96 | 6.33 | 5.15 | 9.45 | 4.88 | 5.72 | 7.05 |
| **Sa (nm)** | 18.75 | 10.74 | 19.13 | 5.1 | 18.63 | 17.28 | 7.2 |
| **Sq (nm)** | 24.22 | 13.48 | 29.66 | 6.71 | 28.23 | 22.99 | 10.36 |
| **Sy (nm)** | 245.85 | 118 | 519.45 | 115.28 | 344.37 | 200.91 | 173.22 |
| **Sv (nm)** | 162.05 | 46.05 | 296.03 | 65.02 | 212.71 | 95.87 | 79.74 |
| **Sp (nm)** | 83.81 | 71.96 | 223.41 | 50.26 | 131.66 | 105.04 | 93.49 |
| **Smean (nm)** | 2.60E-10 | 1.23E-09 | 3.88E-09 | -1.85E-08 | -8.38E-10 | -6.03E-09 | -7.94E-10 |
| **Sdr (%)** | 0.14 | 0.0719 | 0.21 | 0.022538 | 0.2 | 0.11 | 0.071 |
| **S2A (nm2)** | 9E+08 | 9E+08 | 9E+08 | 9E+08 | 9E+08 | 9E+08 | 9E+08 |
| **S3A (nm2)** | 9.01E+08 | 9.01E+08 | 9.02E+08 | 9.00E+08 | 9.02E+08 | 9.01E+08 | 9.01E+08 |

Er – Modulus

H – Hardness

Sa – Roughness Average

Sq – Root Mean Square (RMS)

Sy – Peak-Peak

Sv – Maximum Valley depth

Sp – Maximum peak height

Smean – Mean height

Sdr – Surface area ratio

S2A – Scanning area

S3A – Surface area

100ZDDP – BO 100ZDDP

100PFC – BO 100PFC18

100SSC – BO 100SSC18

8020 – BO 80PFC18-20SSC18

6040 – BO 60PFC18-40SSC18

4060 – BO 40PFC18-60SSC18

2080 – BO 20PFC18-80SSC18

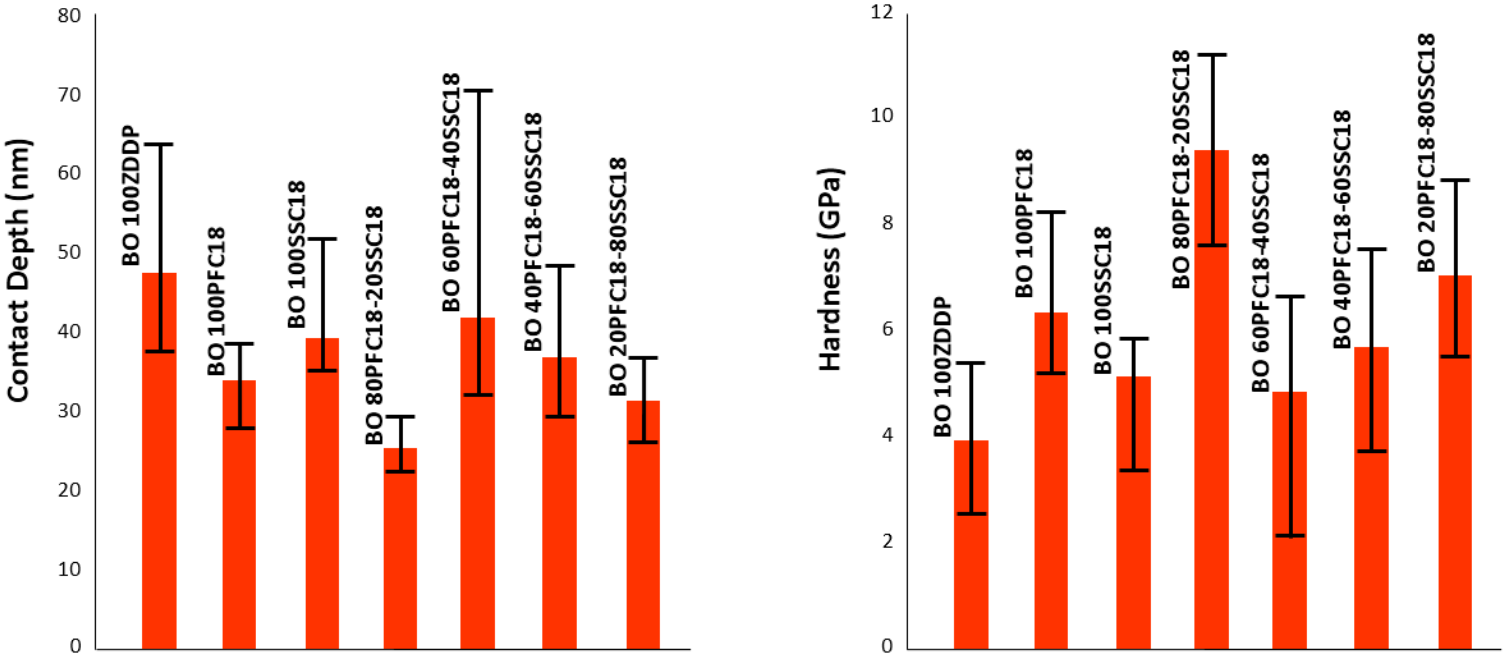


Figure 4.13: Standard deviation of contact depth (in nm) and hardness (in GPa)

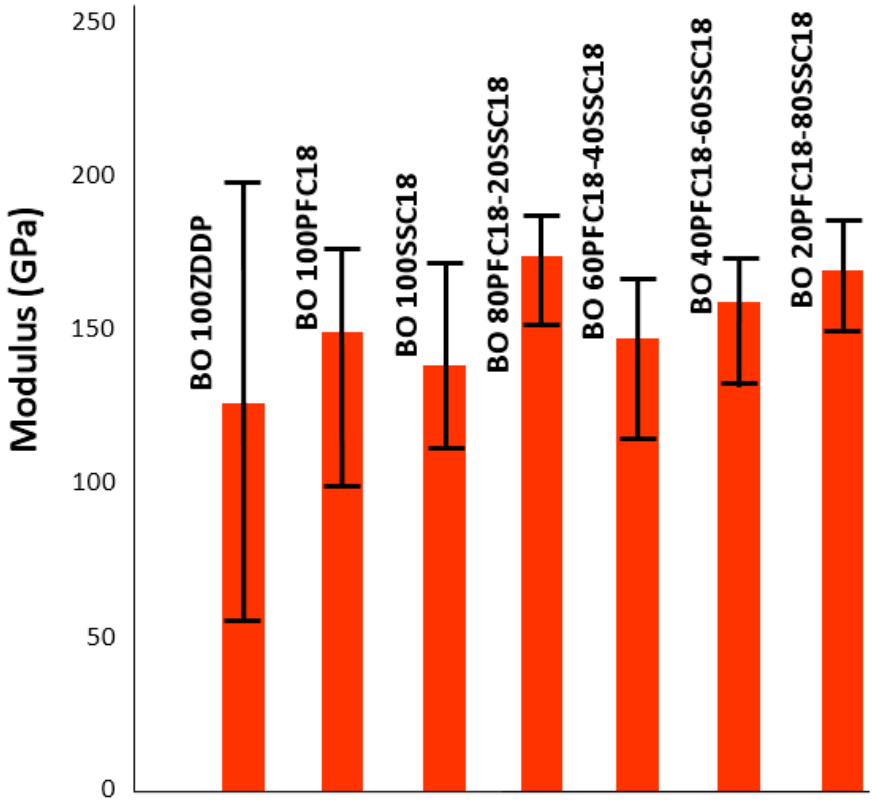


Figure 4.14: Standard deviation of Modulus (in GPa).

A large variation is observed in the contact depth, modulus and hardness values for each lubricant chemistry (figure 4.13 & figure 4.14). This is due to the fact that the tribofilm formed on the wear surface is not uniform and continuous. The indentation data acquired from greater depths (or dark regions of the SPM images shown in figure 4.15 and figure 4.16) have higher hardness & modulus values. This can be explained by the fact that thin or incomplete tribofilms have greater influence of the steel substrate underneath. A direct correlation can be made between the contact depth and hardness from figure 4.13. Higher the contact depth, lower is the hardness and vice-versa. The tribofilm is characterized by chemically adsorbed long chain polyphosphates on the upper layers of the film and short chain phosphates towards the steel surface [124]. Once the indenter penetrates through the upper layers of long chain phosphates of the tribofilm, the hardness drops. The short chain phosphate layer is relatively soft and acts as cushion/shock absorber during wear [124].

The lowest hardness & modulus values were observed for BO 100ZDDP. The average indentation depth is high for ZDDP sample. The hardness of ZDDP at the surface was shown to be higher than at greater depths, thus all things considered; ZDDP tribofilm is hard at the surface and becomes compliant as the depth of the indentation increases. The measured indentation values at higher depths are greatly influenced by the steel substrate underneath the tribofilm and the measured reduced modulus starts to increase to that of steel substrate, i.e. 200 GPa. The indentation data that were close to that of steel substrate values were ruled out when considering the average of the array indents. The modulus and hardness values of the Ashless chemistries are relatively high and the contact depth is low when compared to ZDDP.

The SPM image of spot 2 for each sample is shown in Figure 4.15 and the location of (4X4) array indents for each sample is shown in Figure 4.16.

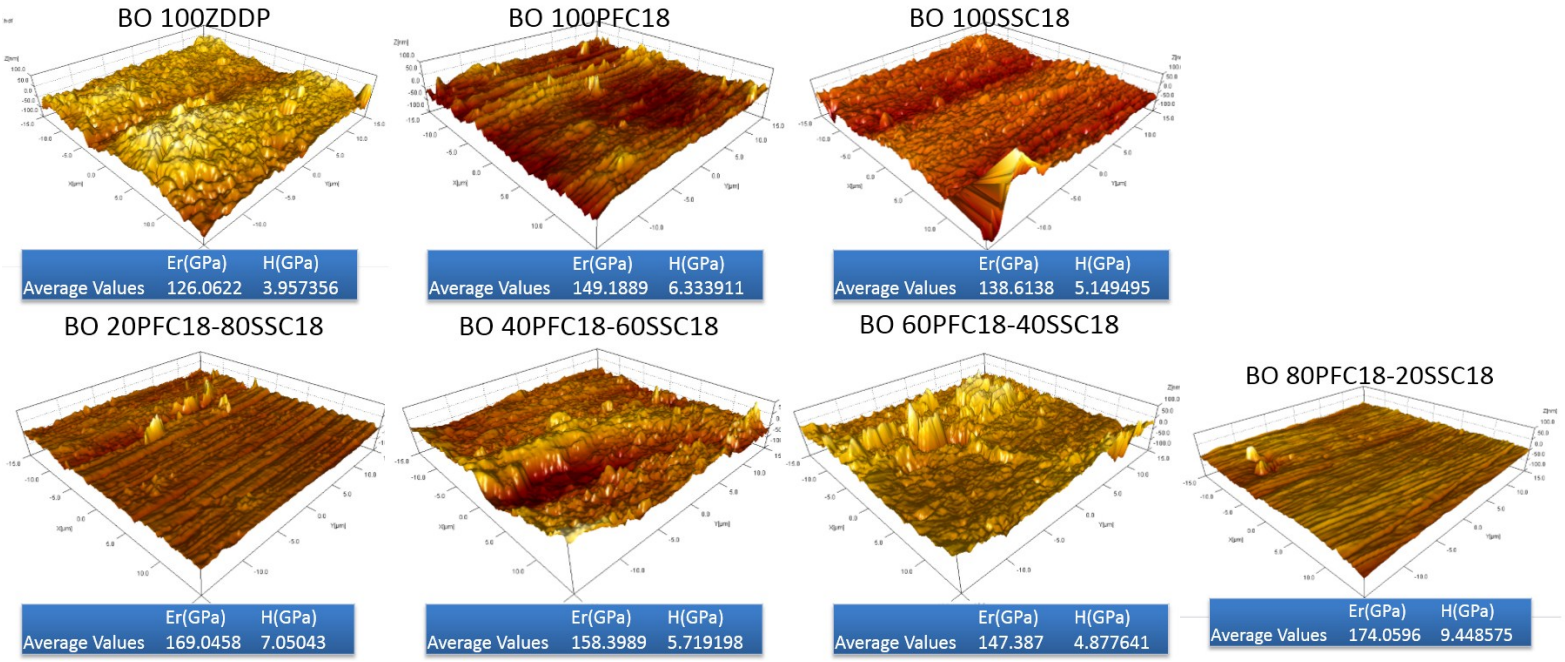


Figure 4.15: SPM and Nanoindentation

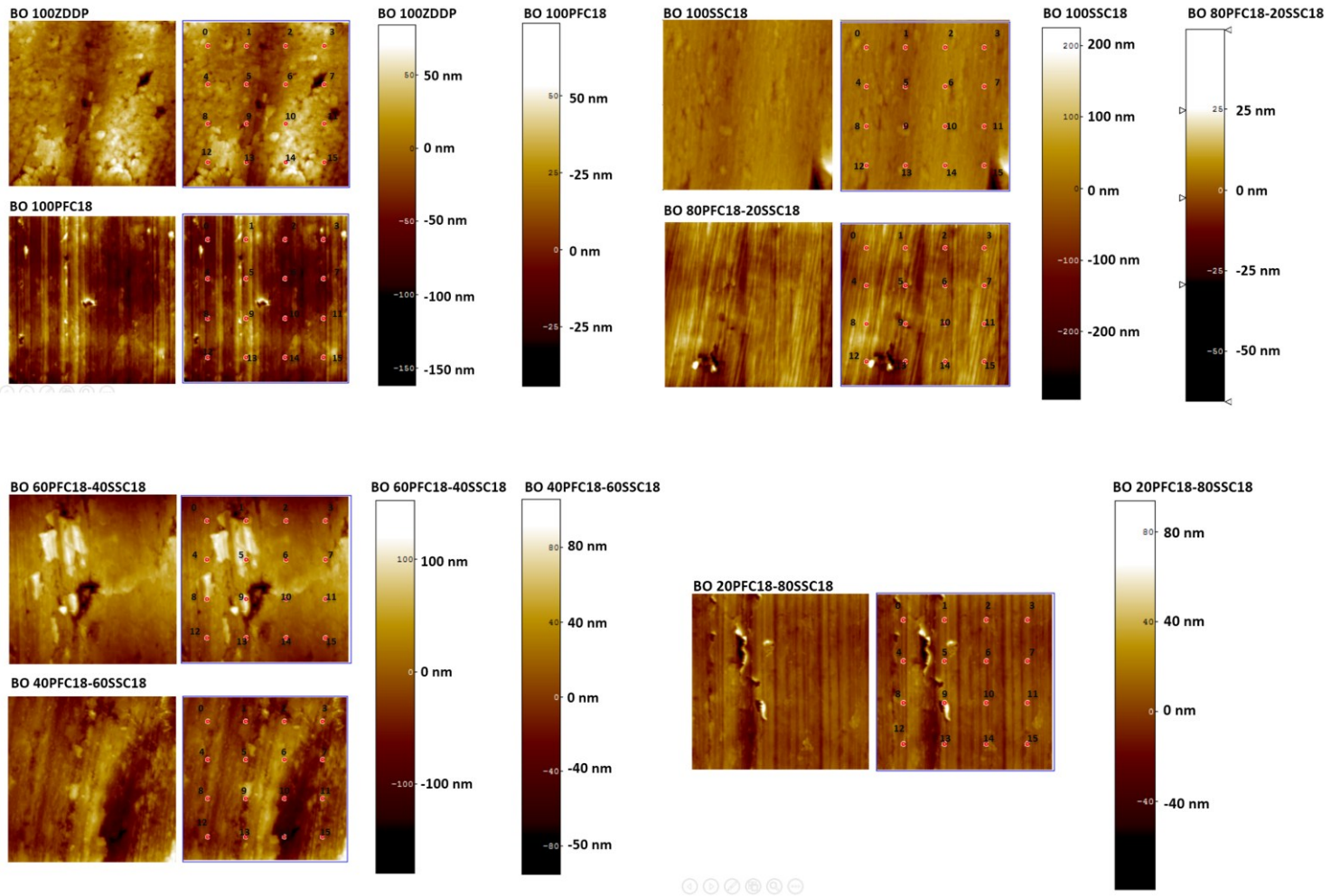


Figure 4.16: (4 X 4) Array Indentation.

4.6.2.1 Analysis of the SPM and Nanoindentation

The scanning probe microscopy image was captured of the surface prior to performing the indentations in order to better understand the change in the properties with change in the topography of the surface. The SPM image and the nanoindentation were performed with the Berkovich tip. The sample was lined up with the length of the wear track in the vertical direction as shown in Figure 4.17.

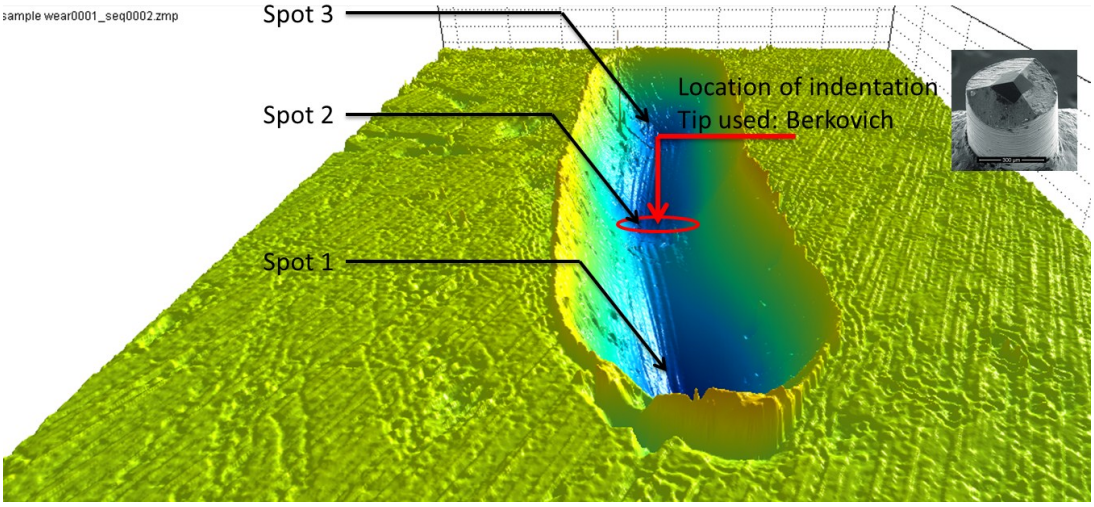


Figure 4.17: Orientation of the sample in Nanoindenter

The 3D isometric view of the SPM images in Figure 4.15 show the contour and the nature of the surface.

1. BO 100ZDDP has a patchy texture on a curved surface. The surface is curved parallel to the length of the wear track. The center of the image dips down forming a valley that is indicated by a dark color. The region that is at a higher elevation is represented by a bright color. The indentations (array) performed were on all the regions. The indentations that were on the elevated regions of the surface showed low hardness and modulus values indicating that the tribofilm is thick and is not influenced by the properties of the steel substrate. Indentations that landed on the valley regions of the

surface showed higher values of hardness and modulus. This could be due to the presence of thinner tribofilm in the valley and the property of the film is masked by the underlying steel substrate. The dark patches in BO 100ZDDP SPM image near the indents 7, 9 & 11 could be deep pits or valleys into which the tip was not able to land completely and this could contribute to the higher values shown by these indentations.

2. BO 100PFC18 surface is relatively flat with vertical lines running along the length of the wear track. The surface is slightly curved perpendicular to the direction of the wear track. The bright regions are very thin and the dark regions are in the form of depressions on the surface. This is observed from the measured indentation values. The hardness values along the bright regions are similar (~6GPa) while the indents in the depressions are noted to have higher hardness value.
3. BO 100SSC18 has a surface that is slightly curved along the length of the wear track. This is also supported by similar indentation values (hardness) across the surface. The indentation at location 15 has low hardness value. This could be due to the presence of a deep trench in the proximity. Pits and trenches on the substrate is covered with lose tribofilm which does not have tightly packed layers. Thus the hardness recorded in these regions is very low.
4. BO 80PFC18-20SSC18 has a very smooth surface with streaks of lines running at a small angle from the vertical length of the wear track. This could be explained by the fact that wear scar is not straight and it bends at the center (Spot 2) as shown in figure 4.18. The hardness values recorded are high (~9 to 11 GPa) but the reduced modulus values are less than 200 GPa which is indicative of the presence of thin tribofilm. BO 20PFC18-80SSC18 has similar surface smoothness with high hardness values with low reduced modulus.

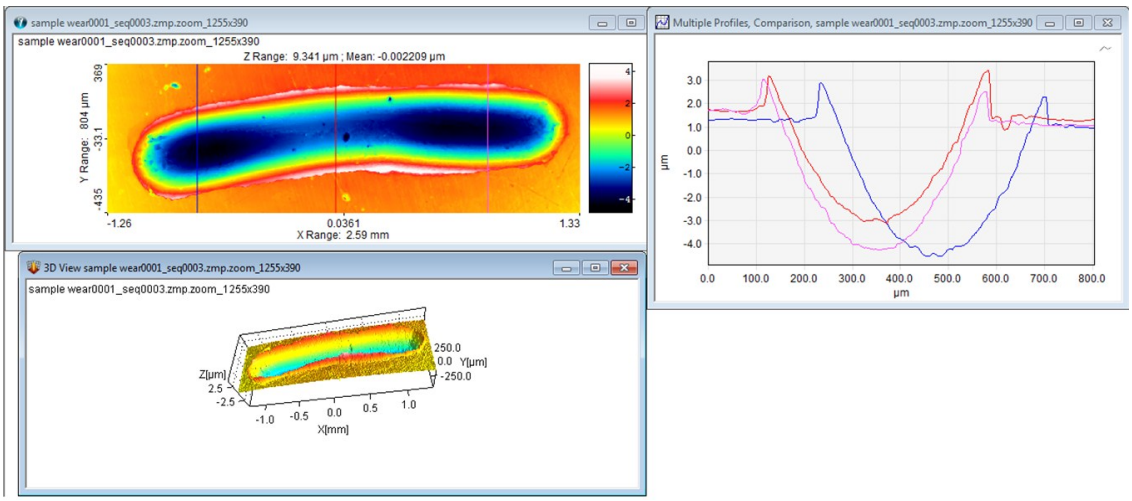


Figure 4.18: BO 80PFC18-20SSC18 wear scar

5. BO 60PFC18-40SSC18 & BO 40PFC18-60SSC18 have uneven surface with a number of patchy elevation and deep pits/trenches. The hardness values noted for both the chemistries were in between 4 to 5 GPa and reduced modulus close to 150 GPa.

*4.6.3 XANES study of tribofilms*

X-ray absorption near edge spectroscopy (XANES) analysis has been frequently used to understand the chemical interactions between the additives in the engine oil and the metallic surfaces of the engine. This discipline of tribology is known as tribochemistry. This field explains the interaction between the rubbing contacts, the morphology of the interacting surfaces, the antiwear film formation process and the strength reduction during wear. Initiation of tribofilm formation occurs between the interacting surfaces at high temperatures and pressure. Engine oil contains a number of additives that influence its antiwear performance. The decomposition rate, thickness & the chemical makeup of the antiwear film is dependent on the chemical makeup and the type of additives used in the engine oil. Thus XANES study of tribofilm is a direct correlation to the additives types present in the engine oil. The characterization of the tribofilm is carried out by examining the model compounds. The comparison of antiwear film

curves with the model compounds provides a brief understanding of the chemical makeup & the synergistic & antagonist interaction of various additives in the engine oil.

The ashless additives on base oil and ZDDP in base oil were analyzed under boundary conditions. All XANES spectra were acquired in two modes, the Total Electron Yield (TEY) mode and Fluorescent Yield mode (FY) with the goal of understanding the structure and bonding environment around the phosphorus and sulfur atoms in the tribofilms. The concentration of fluorine being very low, was not detected by XANES and hence not reported here. The TEY mode gives the chemical information of sample's surface or the near sample surface regions. The fluorescent yield (FY) gives information of the bulk of the tribofilm. The sampling depths of Tribofilm in the TEY mode for phosphorus and sulfur are around 5nm at the L-edge and around 50 nm in the FY mode. The sampling depth in the K edge for phosphorus and sulfur in the TEY mode is around 50nm and FY mode is around 400nm [125].

4.6.3.1 Phosphorus L edge XANES spectral analysis

The phosphorus L edge spectra of the various AW films were collected in both TEY & FY mode. The phosphorus L edge spectra (TEY) of films plotted along with model compounds $FePO_4$ (ferric orthophosphate) and $Zn_3(PO_4)_2$ (zinc phosphate) are shown in figure 4.19 and the FY spectra plotted along with $FePO_4$ (ferric orthophosphate), $Zn_3(PO_4)_2$ (zinc phosphate) & $Fe_4(P_2O_7)_3$ (iron pyrophosphate) is shown in figure 4.22. All the spectral scans were carried out together one after the other at the Canadian Light Source (Saskatoon, Canada). The phosphorus and sulfur L-edge scans were taken together with VLS-PGM (Varied Line Spacing Plane Grating Monochromator) and normalized to the incident beam $I_0$. A comparative study of tribofilms obtained from the various ashless chemistries and ZDDP in base oil is mentioned below as the spectra for each sample were obtained one after the other, maintaining all the settings & parameters consistent. The P L-edge spectra provides richer chemical information

compared to K-edge spectra. The L-edge spectra of phosphorus is characterized by spin-orbit splitting of the phosphorus 2p electrons and excitation to the anti-bonding orbitals. Peaks labelled a and b (shown in figures 4.20 & 4.21) are assigned to the transitions from the 2p3/2 and 2p1/2 to the $a_1$* anti-bonding orbital [126]. Peak c is attributed to the transition of the phosphorus 2p electrons to the $t_2$* molecular orbital. Peak d, known as a shape resonance peak, located at ~146.5 eV, is only present when phosphorus is coordinated to three or more electronegative atoms, such as oxygen [127,128]. The shape resonance peak is characteristic of all phosphates regardless of structure, whether crystalline or glassy [127].

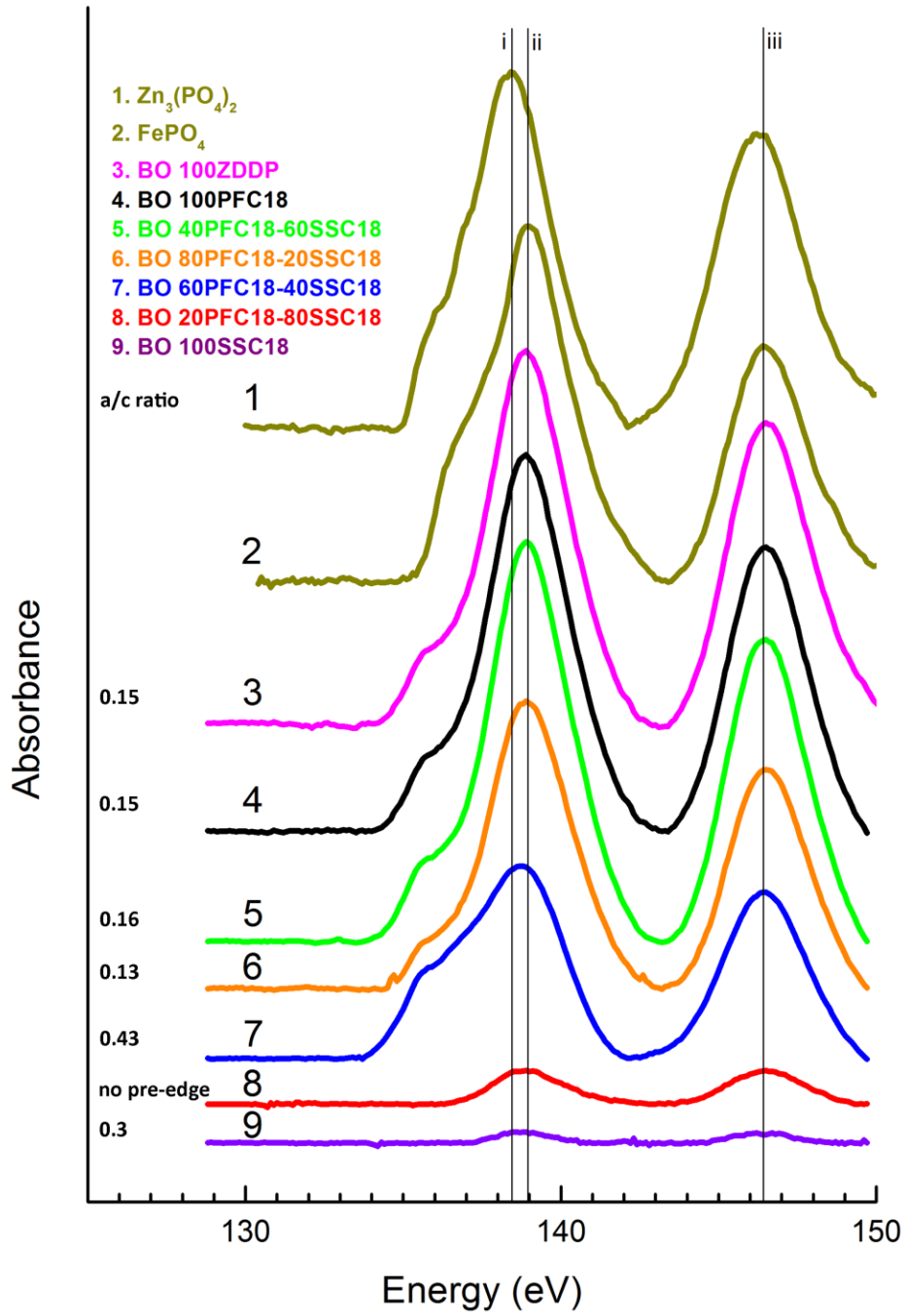


Figure 4.19: XANES Spectra of Phosphorus L-edge. The spectra of model compounds are superimposed: (Total Electron Yield)

The chain length of polyphosphate glass can be determined from the phosphorus L-edge spectra. The ratio of the intensity of the pre-edge peak (peak a) to the white peak (peak c) as shown in figure 4.21 indicates the phosphate chain length. This was shown by Yin et al. [129]. The L-edge XANES spectra of the various lubricant chemistry films show that polyphosphate glass with different chain lengths have formed on the 52100 surface. Table 4.14 summarizes the a/c ratios of the lubricant chemistries under study and table 4.13 shows the chain length corresponding to the various a/c ratio.

Table 4.13 Phosphate chain length for the various a/c ratios [129]

| | |
|---|---|
| 0.2 | Orthophosphate or pyrophosphate |
| 0.3 | Short chain polyphosphate |
| 0.2 – 0.35 | Short chain polyphosphate |
| 0.6 | Long chain polyphosphate |
| 0.35 – 0.55 | Medium chain polyphosphate |

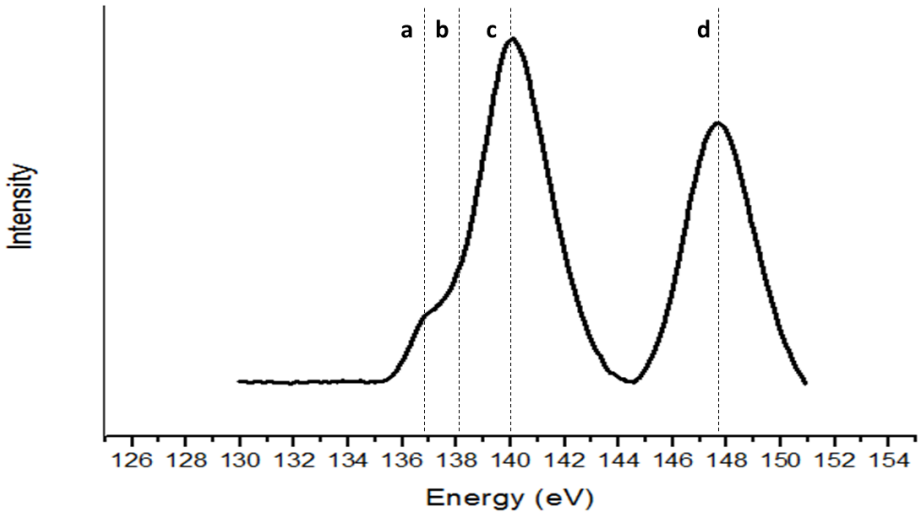


Figure 4.20: Phosphate chain length can be determined from the ratio of peaks a & c.

The a/c ratio determined for BO 60PFC18-40SSC18 is shown below in figure 4.21. The shoulder peak of the white line is peak ‘a’ and the white curve itself is peak ‘c’. Deconvolution process is carried out to determine hidden peaks in the overall curve. In this case, it is used to

determine the ratio a/c. The a/c ratio gives an idea about the type of crosslinking that occurs in the upper layers of the tribofilm.

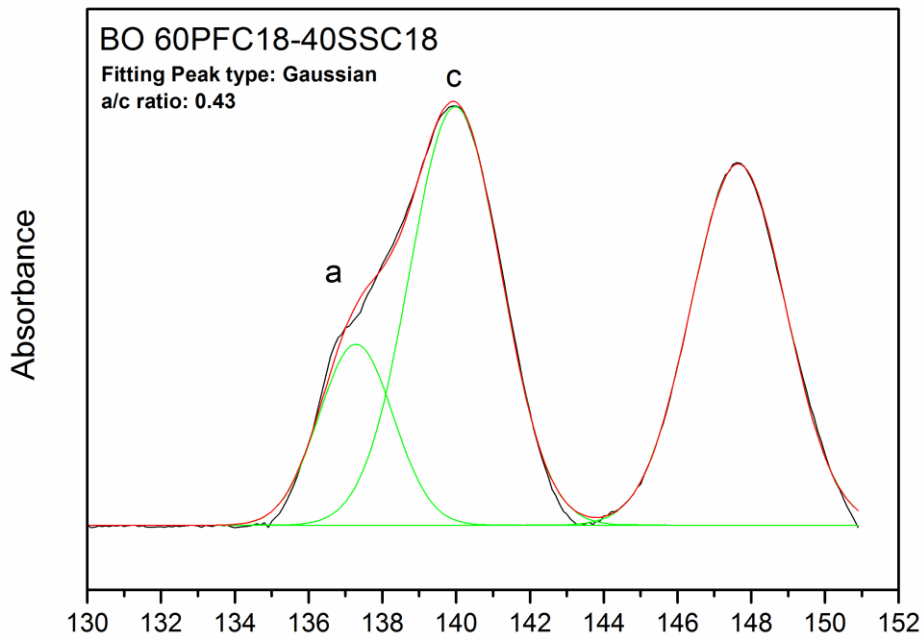


| Peak Index | Peak Type | Area Intg | FWHM | Max Height | Center Grvty | Area IntgP |
|---|---|---|---|---|---|---|
| 1. | Gaussian | 0.70773 | 2.37064 | 0.28046 | 137.28791 | 15.66379 |
| 2. | Gaussian | 2.01497 | 2.918 | 0.64871 | 139.98229 | 44.59646 |
| 3. | Gaussian | 1.79553 | 3.02921 | 0.56006 | 147.6506 | 39.73975 |

Figure 4.21: a/c ratio determined for BO 60PFC18-40SSC18.

The a/c ratios of all ashless chemistries & BO 100ZDDP except BO 60PFC18-40SSC18 is less than 0.3 indicating the film's surface is composed of short chain polyphosphates or orthophosphates. The pre-edges of all the curves lie in the range of 136 eV to 138 eV. BO 60PFC18-40SSC18 showed an a/c ratio of 0.4 indicating its film has a composition of medium chain polyphosphates. BO 20PFC18-80SSC18 did not show the presence of a pre-edge.

Table 4.14: a/c ratio of ashless additives

| Sample | a/c ratio | Phosphate chain length |
|---|---|---|
| BO 100ZDDP | 0.15 | Short chain polyphosphates or orthophosphates |
| BO 100PFC18 | 0.15 | Short chain polyphosphates or orthophosphates |
| BO 100SSC18 | 0.3 | Short chain polyphosphates |
| BO 80PFC18-20SSC18 | 0.13 | Short chain polyphosphates or orthophosphates |
| BO 60PFC18-40SSC18 | 0.43 | Medium chain polyphosphates |
| BO 40PFC18-60SSC18 | 0.16 | Short chain polyphosphates or orthophosphates |
| BO 20PFC18-80SSC18 | No pre-edge | short chain polyphosphates or orthophosphates |

The TEY spectra of phosphorus shows the white line of $Zn_3(PO_4)_2$ is found in the energy value of ~138.5eV and $FePO_4$ in the range of ~139eV. All ashless chemistry spectra have a pre-edge except for BO 20PFC18-80SSC18. The white line of all the peaks are around ~139eV. This indicates that the composition of the tribofilm on the upper layers is close to $FePO_4$. A notable observation is that with the decrease in the PFC18 content in the ashless chemistries, the phosphate curve intensity decreases except BO 40PFC18-60SSC18. BO 40PFC18-60SSC18 shows higher peak intensity than BO 80PFC18-20SSC18. BO 100SSC18 has negligible phosphate curves. Table 4.15 summarizes the area under the phosphate curve for the various lubricant chemistries under study.

Table 4.15: Area under the phosphate curves

| No | Sample | Total Area |
|---|---|---|
| 1 | BO 100ZDDP | 7.75 |
| 2 | BO 100PFC18 | 7.34 |
| 3 | BO 100SSC18 | 0.15 |
| 4 | BO 80PFC18-20SSC18 | 5.65 |
| 5 | BO 60PFC18-40SSC18 | 4.52 |
| 6 | BO 40PFC18-60SSC18 | 4.78 |
| 7 | BO 20PFC18-80SSC18 | 0.64 |

Table 4.15 shows that with the increase in PFC18 content the area under the curves increases. BO 100ZDDP has the highest phosphate curve intensity and the highest area while BO 100SSC18 has the least.

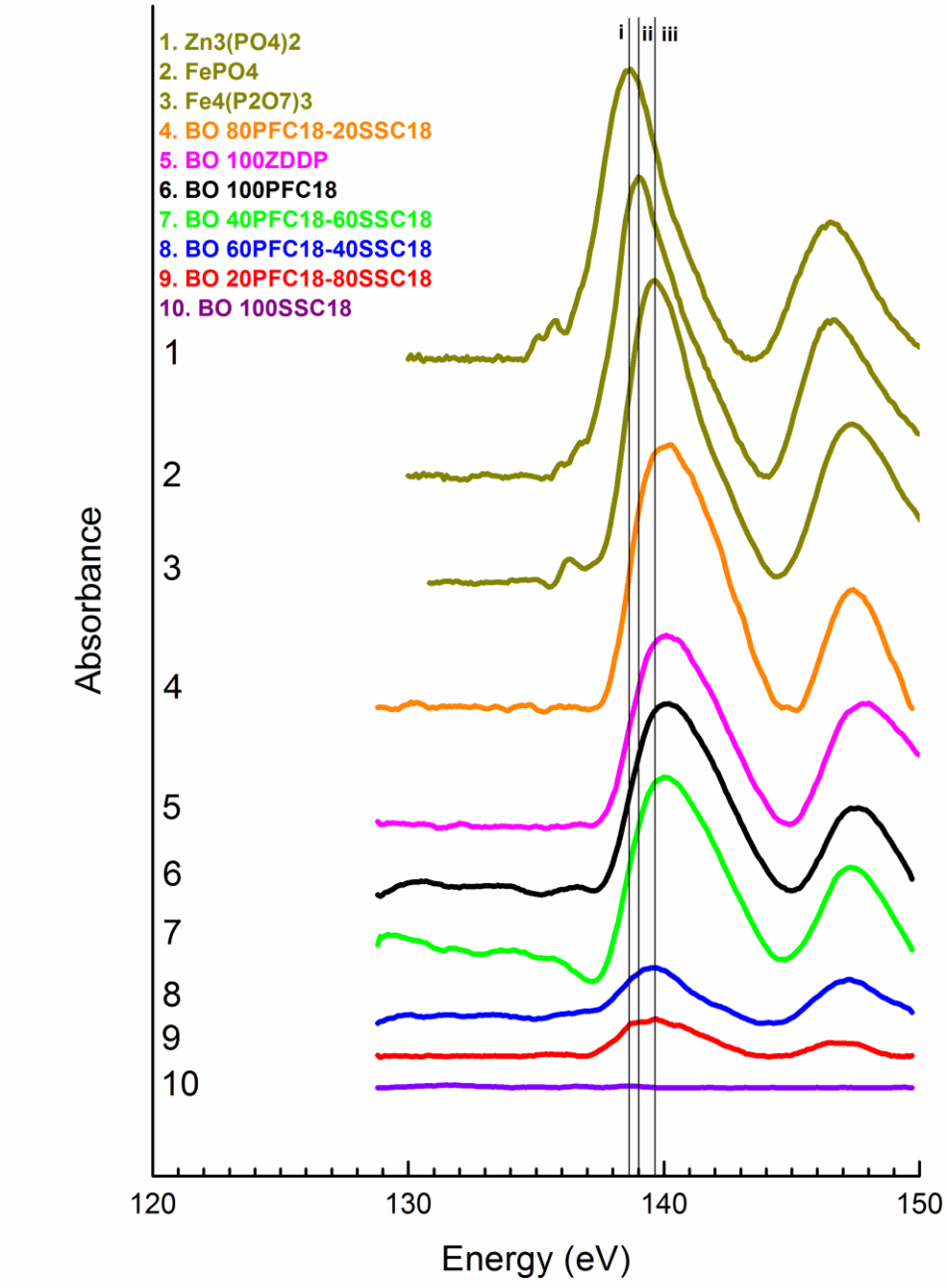


Figure 4.22: XANES Spectra of Phosphorus L-edge. The spectra of model compounds are superimposed: (Fluorescent Yield)

The Fluorescent Yield (FY) curves of P L edge are compared with three model compounds viz. $Zn_3(PO_4)_2$ , $FePO_4$ & $Fe_4(P_2O_7)_3$. The white line of $Zn_3(PO_4)_2$ is at ~138.6eV, $FePO_4$ at ~139eV & $Fe_4(P_2O_7)_3$ at ~139.6eV. The FY spectra provides information from the top 50nm of the tribofilms. The curves from all the lubricant chemistries do not have pre-edges indicating the absence of phosphate chain cross linking in the bulk of the tribofilm. Most of the phosphorus in the bulk of the tribofilm is in the form of phosphates or very short chain polyphosphates. The FY spectra, like the TEY spectra show a similar trend in the intensity of the phosphate peaks. With the increase in SSC18 (or decrease in PFC18) in the lubricant formulation, the intensity of the phosphate peak decreases except BO 80PFC18-20SSC18 & BO 40PFC18-60SSC18. BO 80PFC18-20SSC18 shows the highest intensity of phosphate curves and BO 40PFC18-60SSC18 shows peak intensity higher than BO 60PFC18-40SSC18. All the antiwear film curves under study are to the right of iron pyrophosphate (~139.6eV) indicating the phosphorus presence in the form pyrophosphates. The bulk of the tribofilm has phosphorus content in the form of pyrophosphates and orthophosphates with pyrophosphates being the dominant form.

SSC18 has twice the amount of sulfur compared to PFC18. The fluorine present in PFC18 is polar in nature and the strong P-F bond present is highly unlikely to break in solution but does degrade during the tribofilm formation and is incorporated into the tribofilm bonded with iron from the substrate. The strong P-F bond is attributed to the fact that P-F has a high binding energy (439 KJ/mol) as compared to HS-SH (272 KJ/mol). The highly electronegative fluorine atoms promotes the affinity of the ashless antiwear compounds to the steel substrate during the initial stages of tribofilm formation.

4.6.3.2 Sulfur L edge XANES Spectral Analysis

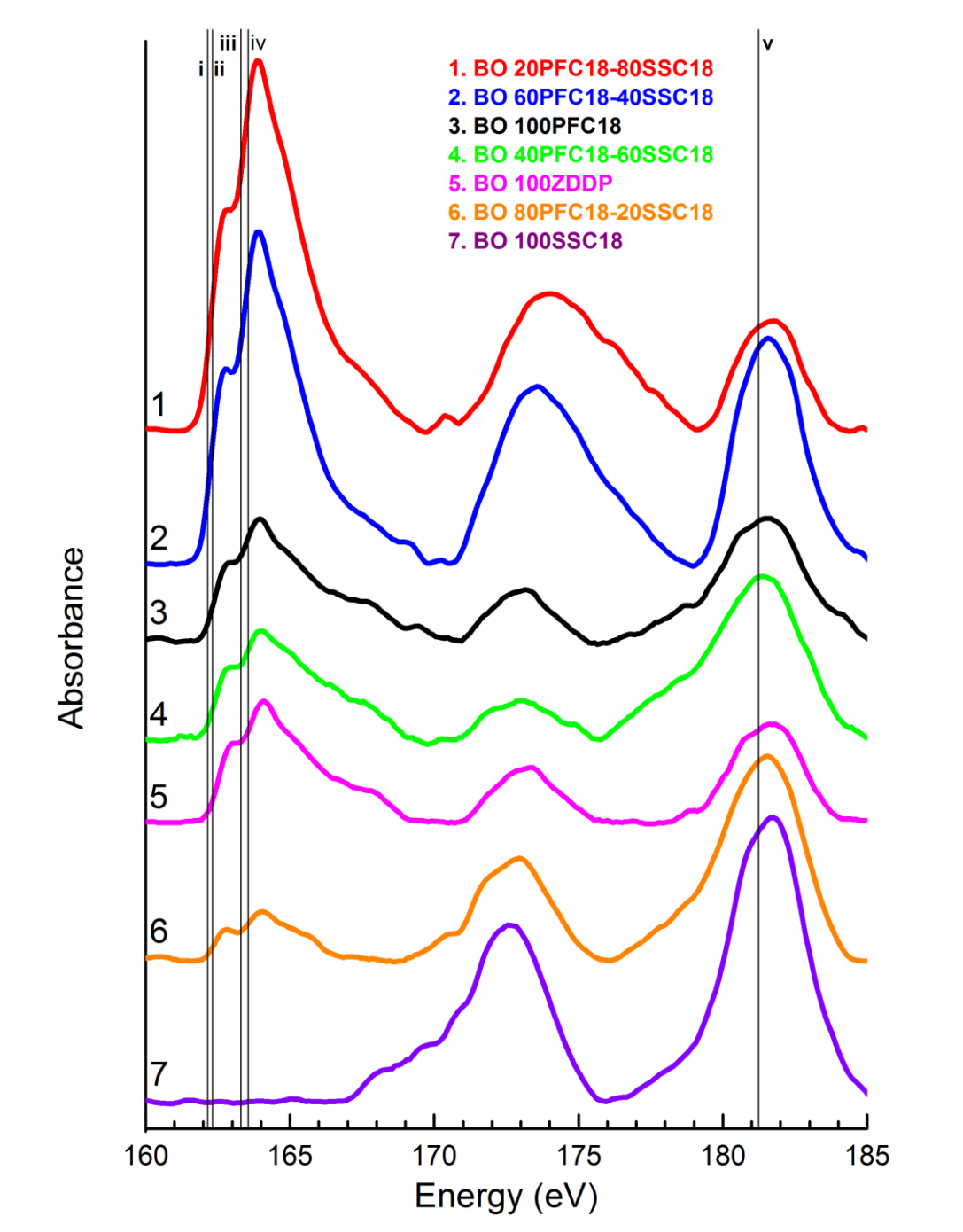


Figure 4.23: XANES Spectra of Sulfur L edge (Total Electron Yield)

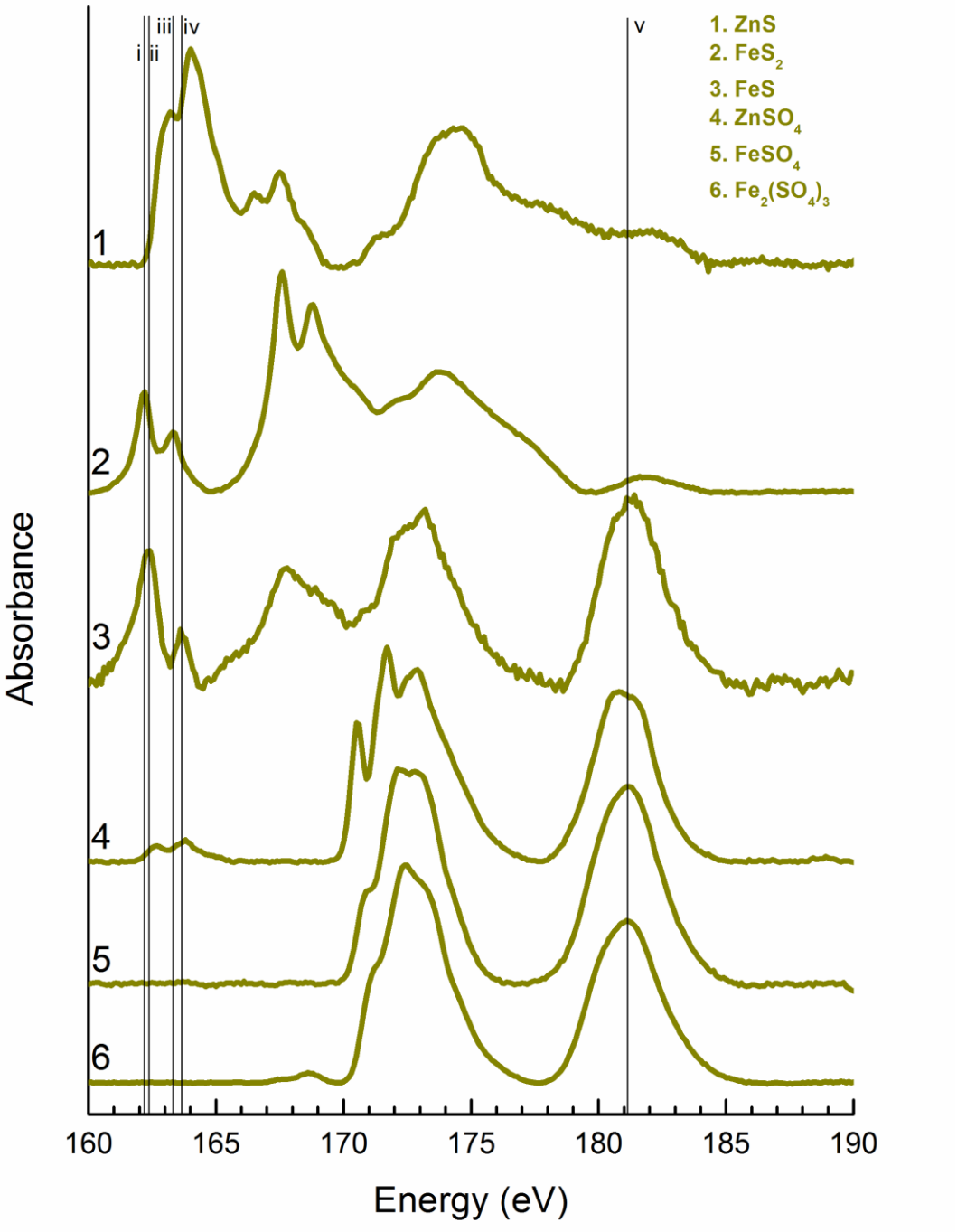


Figure 4.24: XANES Spectra of model compounds.

The sulfur L-edge spectra of the ashless additives and ZDDP in base oil, recorded in TEY mode are shown in figure 4.23 & figure 4.24. The different additive chemistries generated are compared with six different model compounds. The model compounds can be broadly classified into two types; sulfide and sulfate series. The sulfide based model compounds are ZnS, FeS and $FeS_2$ and sulfate based compounds are $ZnSO_4$, $FeSO_4$ & $Fe_2(SO_4)_3$. Model compounds, iron sulfide (FeS) and iron sulfate (FeSO4 or Fe2(SO4)3) have two main peaks, but iron sulfide has a sharp peak at lower energy that is missing in the sulfates. Zinc sulfate has three small peaks at first main peak. All the generated additive chemistry contain sulfur in the combination of sulfates and sulfides. The first peak (i & ii) of the various lubricant chemistries resemble FeS and $FeS_2$. The peaks characteristic of sulfides are in the energy range 162 to 162.5 eV (peak i) and 163.2 to 163.8 eV (peak ii). Zinc sulfide is ruled out as the chemistries under study does not have zinc except for BO 100ZDDP. The position of the peaks i and ii are closer to FeS and hence the tribofilm contains sulfur in the form of FeS and $FeS_2$ with FeS being the dominant form of sulfur species. PFC18 concentration promotes the formation of sulfides although there is no direct correlation between the PFC18 concentration and sulfide content (sulfide concentration does not increase with increase in PFC18). BO 20PFC18-80SSC18 shows the highest concentration of sulfides among the formulations under study and BO 100SSC18 shows complete absence of sulfides. The presence of sulfur in the form of sulfates on the other hand is observed in highest quantity in BO 100SSC18 and least in BO 20PFC18-80SSC18. The peak characteristic of sulfates is in the energy value of ~181.5 eV. The presence of sulfides makes the tribofilm soft and shear-able. The presence of sulfates makes the film hard and rigid, much like the steel substrate underneath, causing further wear. The peak at ~162.7 eV in the ZDDP tribofilm most likely corresponds to the ZnS peak and to a lesser extent the FeS peak. The clear detection of sulfur in the form of sulfides and sulfates in the tribofilm indicates that the layers are not stratified and it is discontinuous. Stratification of

layers leads to poor spectra for sulfur and very low intensity of the peaks, as sulfur will be underneath the phosphate chain cross linking. The curves in the FY mode were noisy and no clear data was obtained from it and hence it is not reported here.

## 4.7 Relative proportions of phosphorus and sulfur

The area under the curve for P & S L-edge TEY is calculated and summarized below (Table 4.16). The ratio of phosphorus to sulfur in the TEY mode for each lubricant formulation is also determined.

Table 4.16: Area under the curve (sulfur) and P:S ratio

| No | Sample | Sulfur (area under curve) | Phosphorus (area under curve) | P:S | Remarks |
|---|---|---|---|---|---|
| 1 | BO 100ZDDP | 2.8 | 7.75 | 2.8 | P content is higher than S |
| 2 | BO 100PFC18 | 3.61 | 7.34 | 2.03 | P content is higher than S |
| 3 | BO 100SSC18 | 5.41 | 0.15 | 0.03 | S content is higher than P |
| 4 | BO 80PFC18-20SSC18 | 3.99 | 5.65 | 1.41 | P content is higher than S |
| 5 | BO 60PFC18-40SSC18 | 7.86 | 4.52 | 0.58 | S content is higher than P |
| 6 | BO 40PFC18-60SSC18 | 4.08 | 4.78 | 1.17 | P content is higher than S |
| 7 | BO 20PFC18-80SSC18 | 6.95 | 0.64 | 0.09 | S content is higher than P |

The phosphorus to sulfur ratio is determined to understand the change in concentration of phosphorus and sulfur according to the change in PFC18 & SSC18 content. BO 100ZDDP has a high P:S value and among the ashless formulations BO 100PFC18 exhibits the highest P:S ratio. This indicates the presence of phosphorus in higher concentrations than sulfur. BO 60PFC18-40SSC18 shows the highest amount of sulfur. The distribution of sulfur in the form of sulfates and sulfides in the antiwear film is determined and is summarized below in table 4.17.

Table 4.17: Sulfides and sulfates distribution

| No | Sample | Sulfides | Sulfates | Sulfides:Sulfates |
|---|---|---|---|---|
| 1 | BO 100ZDDP | 1.39 | 1.42 | 0.98 |
| 2 | BO 100PFC18 | 2.1 | 2.09 | 1 |
| 3 | BO 100SSC18 | - | 5.41 | - |
| 4 | BO 80PFC18-20SSC18 | 0.46 | 3.54 | 0.13 |
| 5 | BO 60PFC18-40SSC18 | 3.31 | 4.55 | 0.73 |
| 6 | BO 40PFC18-60SSC18 | 1.45 | 2.63 | 0.55 |
| 7 | BO 20PFC18-80SSC18 | 3.9 | 3.05 | 1.28 |

BO 100SSC18 does not show three peaks and has only sulfate content. The distribution of sulfides and sulfates is equal in BO 100PFC18 & BO 100ZDDP. BO 20PFC18-80SSC18 has sulfides content higher than the sulfates.

## 4.8 Conclusion

Based on the above mentioned observations, a number of conclusions can be drawn.

The wear scar on all the lubricant formulation samples are not uniformly deep along the length of the wear track. An elevation or kink is observed in between spot 1 & 2 and spot 2 & 3. The debris pileup is found to be higher along the wear length corresponding to the regions of elevation of kink. BO 100ZDDP has the highest amount of debris pileup and BO SSC18 has the least debris pileup.

All ashless chemistries except BO 40PFC18-60SSC18 have lower mean wear volume than BO 100ZDDP. A clear distinction in the surface morphology, hardness and modulus was observed between the samples from batch have the highest wear volume number and the samples from the batch having the lowest wear volume number. Batch 1 of BO 40PFC18-60SSC18 & 60PFC18-40SSC18 exhibits the highest wear among its 3 batches. The surface of BO 40PFC18-60SSC18 & BO 60PFC18-40SSC18 Batch 1 samples are highly irregular with a number of peaks and valleys. The surface of BO 40PFC18-60SSC18 has multiple horizontal scratches along the length of the wear track indicating the presence of very thin tribofilm and extensive abrasive wear. The batch 2 of BO 40PFC18-60SSC18 & BO 60PFC18-40SSC18

exhibits the least wear volume among its three batches and the surface is characterized by patchy and discontinuous tribofilm. The center region has small and multiple pads while the neighboring regions have larger pads. 100PFC18 & 100SSC18 shows uniform and continuous antiwear film formation. BO 80PFC18-20SSC18 has multiple divots along its surface much similar to 100ZDDP. These divots could be due to the incomplete integration of the antiwear film or tribofilm pullout, but the wear volume numbers of BO 80PFC18-20SSC18 are lower than the mean value of BO 100ZDDP suggesting the presence of thick and resistive antiwear film.

All ashless chemistries showed higher modulus and hardness than BO 100ZDDP. This could be explained by the fact that, the tribofilms formed by the ashless lubricants are thinner than the ZDDP film and the hardness and modulus values are influenced by the underlying steel substrate.

The XANES Phosphorus L edge spectral analysis shows that all the ashless chemistries have pre-edges except BO 20PFC18-80SSC18 (in the TEY mode, i.e. upper layers of the tribofilm). The pre-edge is indicative of crosslinking of phosphate chains in the upper layers of the antiwear film. BO 60PFC18-40SSC18 shows higher a/c ratio indicating the top layer of layer of the film to be composed of medium chain polyphosphates. All the other ashless lubricant formulations show short or orthophosphate chain crosslinking. The composition of the tribofilm on the upper layers is close to $FePO_4$ and with the decrease in the PFC18 content in the ashless formulations, the phosphate curve intensity decreases. The presence of PFC18 also promotes the presence of sulfur in the form of sulfides. The sulfides are shearable and ductile thus enabling absorption of shocks and loads. Sulfates were found to be present in high quantities in BO 100SSC18. All ashless lubricant formulations exhibit better or similar antiwear performance as ZDDP in base oil indicating its potential as a replacement in the commercial engine oils.

# CHAPTER 5

# ROLE OF ADDITIVES ON THE MECHANISM OF WEAR WITH ASHLESS ANTIWEAR COMPOUNDS

## 5.1 Introduction

The mechanical efficiency of the engine is dependent on the extent of reduction of friction and wear by the engine oil. In order to cater this requirement, a number of additives are added to the lubricant mixture to enhance its performance. In the boundary lubrication regime, the formation of an antiwear film on the chemically active steel surface of the engine is the determining factor in minimizing friction and wear. The additives present in the lubricant system determine the nature and chemistry of the antiwear film. Zinc dialklydithiophosphate is the most sought after antiwear additive in the lubricant industry. But due to its detrimental effects on the catalytic converters in the exhaust system, additives containing very low concentrations of phosphorus and sulfur with no metal salts are being investigated due to the current environmental antipollution policies. Ashless antiwear additive is a viable replacement for ZDDP. Lubricants used in the engine oil deteriorate after a certain number of cycles in the engine. The deterioration of the lubricants often leads to the buildup of insoluble deposits or sludge. The development of sludge leads to increase in the viscosity of the lubricant. The reduction or delay in the above mentioned effect is brought about by antioxidants present in the lubricants. It is the key additive that protects the lubricant from oxidative degradation. To minimize the change in viscosity, viscosity modifiers are added to the lubricant system and finally detergents are included to prevent the deposition of sludge and formation of varnish on the engine surface

.

In the present study, the synergistic effect of combining ashless antiwear compounds with various other lubricant additives such as detergents, antioxidants & viscosity modifiers in base oil was investigated by tribological tests and characterization of tribofilms with XANES.

## 5.2 Chemistry

Octadecylphosphorofluoridothioate (PFC18) and Octadecylthioperoxydiphosphate (SSC18) are diluted in base oil separately to obtain a phosphorus concentration of 0.1% by weight in base oil. Base oil with PFC18 and base oil with SSC18 are mixed together in the ratio of 2:8 respectively. The chemical structure and the description of PFC18 & SSC18 are mentioned below.

### *5.2.1 Octadecylphosphorofluoridothioate (PFC18)*

Ashless additive such as alkylphosphorofluoridothioates developed by Chen et al [117] exhibit superior wear protection compared to Zinc dialkyldithiophosphates. PFC18 contains low amounts of phosphorus compared to ZDDP, thus less fouling of the catalytic converters in automobiles. The chemical structure of PFC18 is given below in Figure 5.1.

Octadecylphosphorofluoridithioate

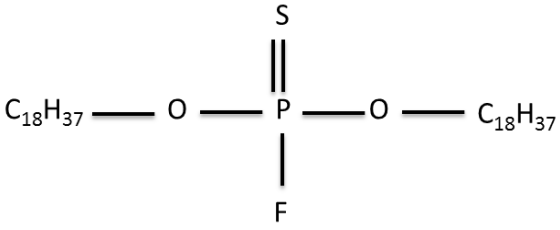


Figure 5.1: Octadecylphosphorofluoridithioate (PFC18) [117].

Physical Properties:

- Colorless solid
- Melting point: 36-37º C

*5.2.2 Octadecylthioperoxydiphosphate (SSC18)*

Octadecylthioperoxydithiophosphate is prepared in stages. O, O' dialkyl dithiophosphoric acid was obtained by mixing phosphorus pentasulfide with alcohols at elevated temperature in toluene. The chemical structure of Octadecylthioperoxydithiophosphate (SSC18) is mentioned below in Figure 5.2 [118].

Octadecylthioperoxydiphosphate

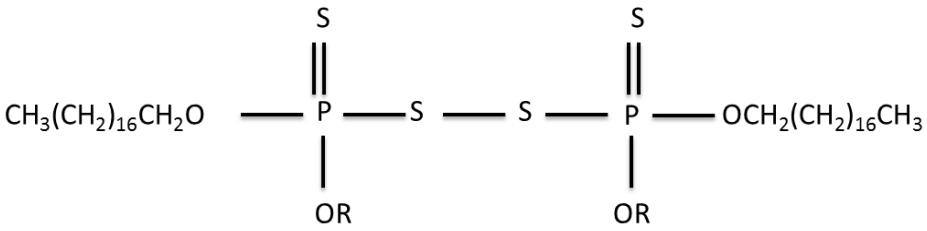


Figure 5.2: Chemical Structure of Octadecylthioperoxydiphosphate [118].

## 5.3 Mechanism of Antioxidant Action

Engine oil is formulated to be effective in all conditions of temperature & pressure inside the internal combustion engine. It also contains a wide variety of additives that prevent the thickening of the oil due to oxidation. The viscosity of the oil is crucial to its performance and has to be maintained low in order to facilitate the lubricant movement in between low clearance regions in the engine. The increase of oil viscosity is mainly due to oil oxidation. The mechanism of oxidation is to introduce oxygen atoms into the base oil molecules, thereby converting the hydrocarbons in the base oil into aldehydes and eventually into acids. The end products of the oxidation process are unstable and they tend to be further attacked. The final end products are in the form of sludge and varnish on the surface of engine parts [130]. This leads to increased engine wear, insufficient lubrication and thereby leading to loss of fuel economy. This also leads to the increase in exhaust-gas emissions, clogging of oil filters and finally results in the deterioration of the engine. In order to prevent this, engine oil comes

equipped with antioxidant additives that prevent the above mentioned catastrophes. Antioxidants minimize and delay the onset of lubricant oxidation. Periodic replacement of the engine oil is crucial to the life of the engine as one of the reasons being, antioxidants get consumed. This will lead to increase in the rate of oxidation. Oxidation of the lubricant system occurs in four stages; initiation, chain propagation, chain branching and chain termination.

*5.3.1 Initiation*

$$R - R \xrightarrow{\text{ENERGY}} R' + R'$$

This reaction is initiated in the presence of heat, UV light or mechanical shear stress and catalyzed by the presence of metal ions from the surface of the engine. The cleavage of R-H bond is determined by the C-H bond strength and the resultant radical stability. The hydrogen in the alpha position to a carbon-carbon double is the most susceptible to cleavage [131].

*5.3.2 Chain Propagation*

$$R' + O_2 \longrightarrow ROO'$$
$$ROO' + RH \longrightarrow ROOH + R'$$

The alkyl radicals produced in the initiation stage reacts with oxygen forming alkyl peroxy radicals. This is followed by the hydrogen abstraction from a hydrocarbon molecule by an alkyl peroxy radical to form hydroperoxide and another alkyl radical.

*5.3.3 Chain branching*

5.3.3.1 Radical Formation

$$ROOH \longrightarrow RO' + HO'$$
$$RO' + RH \rightarrow ROH + R'$$
$$HO' + RH \rightarrow H_2O + R'$$

5.3.3.2 Aldehyde or Ketone formation

$$RRaHCO' \rightarrow RCHO + R_a'$$
$$RR_aR_bCO \longrightarrow RR_aCO + R_b'$$

This process begins with the cleavage of hydroperoxide into alkoxy and hydroxyl radicals. This reaction becomes significant only at temperatures above 150º C. The alkoxy and hydroxyl radicals then can react with hydrocarbons to form more alkyl radicals, alcohols and water. Secondary and tertiary alkoxy radicals will readily form aldehydes and ketones, respectively. These aldehydes and ketones condense via acid catalyzed aldol reactions. These condensates can lead to polymeric degradation products that eventually manifest themselves as sludge and varnish deposits in engines [131].

*5.3.4 Chain termination*

$$R' + Ra' \longrightarrow R\text{-}R_a$$
$$R' + R_aOO' \longrightarrow ROOR_a$$

The termination of the chains occurs by the combination of radicals. Two alkyl radicals can combine to form a hydrocarbon molecule. Alternatively, an alkyl radical can combine with an alkyl peroxy radical to form peroxide, or two alkyl peroxy radicals can combine to form

peroxide with evolution of oxygen. However, peroxides easily break down and generate more alkyl peroxy radicals [131].

## 5.4 Detergents

Detergents are classified under the class of deposit control agents along with oxidation inhibitors & dispersants. Detergents are additives added to the engine oil to neutralize strong acids that are produced in the engine during combustion. Detergents prevent the formation of varnish lacquer and other sludge deposits on the hot metal surfaces in the engine. It also functions to remove neutralization products derived from partial oxidation either by inhibiting the oxidative breakdown of the lubricant or by suspending the harmful products already formed in the bulk lubricant. Detergents are metal salts of organic acids that are enclosed by excess base particles in the form of either carbonate or sulfonate. These colloidal dispersions of metal hydroxides, carbonates or borates are stabilized by metallic soaps such as phenates, salicylates or sulfonates.

Over based detergents (OD) are composed of inorganic/organic hybrid nanoparticles (~2 to 5 nm in diameter) [48,49]. Over based detergents contain an inorganic core surrounded by a surfactant shell. The inorganic core is typically calcium carbonate. Figure 5.3 shows a schematic of a sulfonate OD particle. The most commonly used surfactant shells commercially are alkyl sulfonates, sulfurized alkyl phenates, salicylates and calixarates [132].

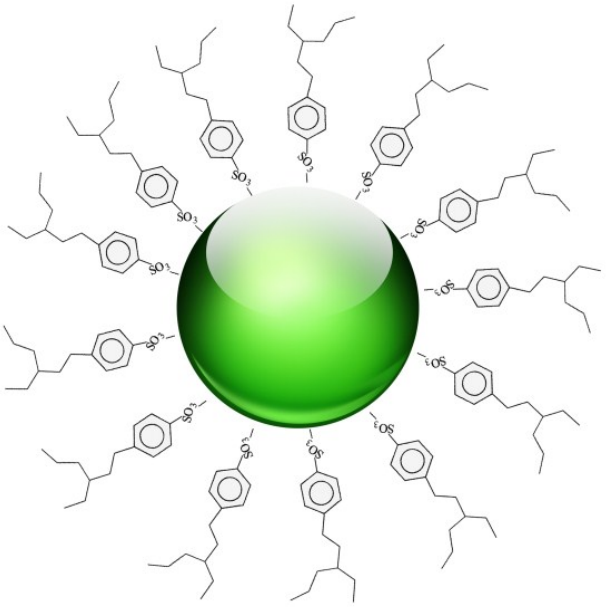

Figure 5.3: Structure of Calcium Sulfonate detergent. The center core is made up of Calcium Carbonate surrounded by sulfonate surfactants [133].

The surfactant polar group is located near the polar mineral core while the hydrocarbon tail of the surfactant is unfolded to the organic solvent, thereby keeping the metal salt (calcium) in solution.

*5.4.1 Neutralization of acidic combustion products*

Neutralization of acidic and oxidative products minimizes the probability of rust and deposit formation on surfaces in engine. The mechanism of acid neutralization involves base transfer from detergent to the acid containing droplet [134,135] This mechanism is illustrated in the figure 5.4. The organic portion of the detergent enables the suspension of neutralized salt in the lubricant medium. The surplus base contained in the detergent aids in the formation of surface film that isolates the metal surfaces from corrosive agents [133,136].

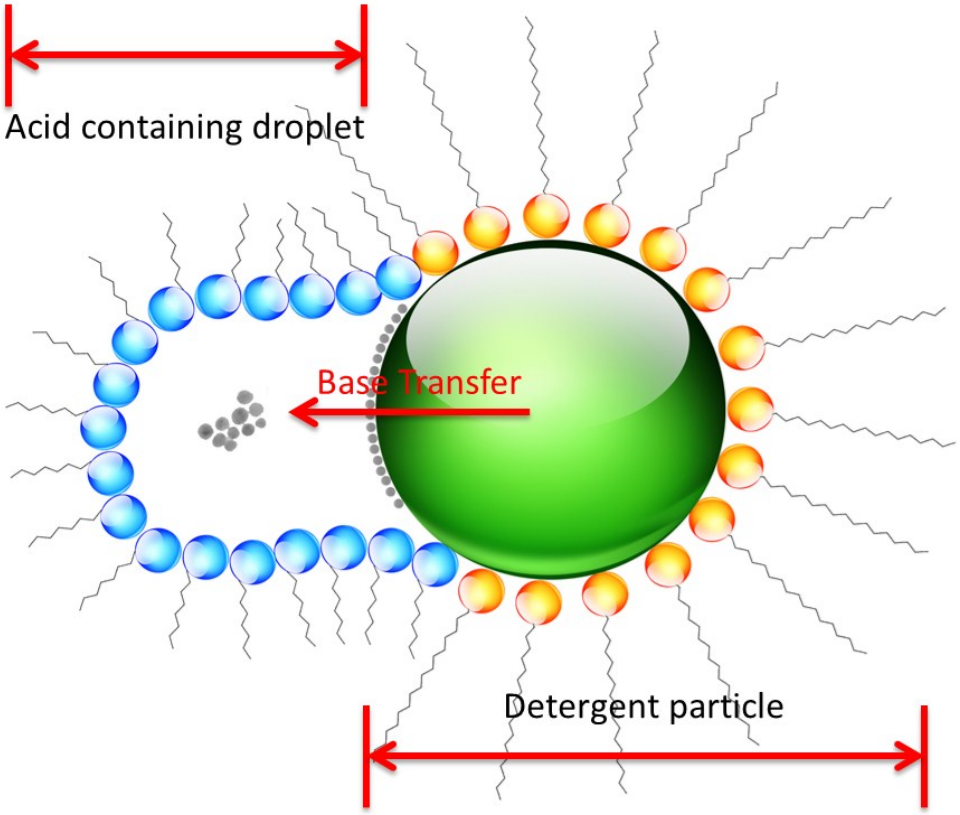


Figure 5.4: Process of transfer of base from a detergent particle to an acid containing droplet. This mechanism of neutralization was proposed by Hone et.al [133].

## 5.5 Viscosity Modifiers

Viscosity modifiers are polymeric additives added to the engine oil in order to maintain the viscosity of the lubricant medium irrespective of the operating conditions. Viscosity modifiers contain polymeric molecules that decrease in volume when cold and increase in volume at elevated temperatures. Lubricant systems without viscosity modifiers will lose viscosity more quickly.

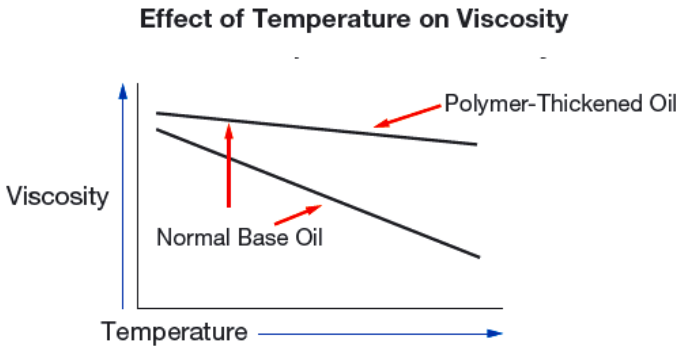


Figure 5.5: Effect of temperature on viscosity.

A number of different types of viscosity modifiers are available commercially for combination in the lubricant mixture. The most commonly used are polyolefins such as polyisobutylene and polyalphaolefins, polyalkylmethacrylates, polyesters and olefin copolymers. The appropriate polymeric compound for a lubricant system is considered based on the chemistry of the lubricant system.

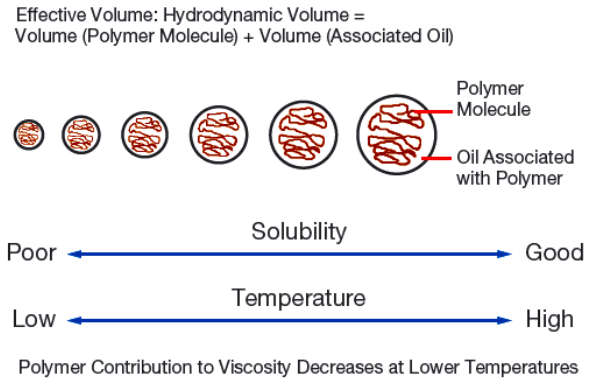


Figure 5.6: Viscosity modifier mechanism

The hydrocarbon chains present in the lubricant system are small and on decomposition breaks down further, thus losing its viscosity. The viscosity modifiers contain polymeric chains much longer compared to the base oil. When the moving surfaces interact; the

oil gets sheared, leading to the breakdown of polymeric molecules. Thus, this results in the drop in viscosity of the lubricant oil.

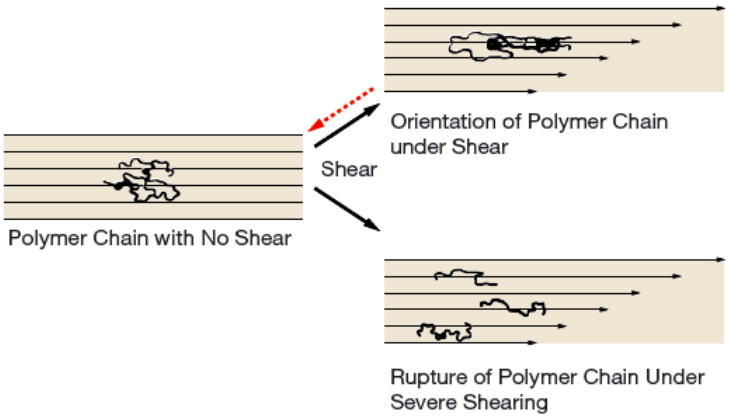


Figure 5.7 Viscosity loss from shear.

In this study detergents, viscosity modifiers & antioxidants are added to base oil containing Octadecylphosphorofluoridithioate (PFC18) & Octadecylthioperoxydiphosphate (SSC18) in the ratio of 2:8. The quantity of PFC18 & SSC18 in base oil is determined by the amount of phosphorus concentration required in the final lubricant oil mixture. Table 5.1 summarizes the various additives present in the chemistries under study.

**Table 5.1 Lubricant formulation**

| | | |
|---|---|---|
| 1 | BO 20PFC18-80SSC18 | AW |
| 2 | BO 20PFC18-80SSC18 Calcium Sulfonate | AW + Detergent |
| 3 | BO 20PFC18-80SSC18 Diphenylamine (DPA) | AW + Antioxidant |
| 4 | BO 20PFC18-80SSC18 Phenolic | AW + Antioxidant |
| 5 | BO 20PFC18-80SSC18 Straight chain OCP | AW + Viscosity Modifier |

The phosphorus content in the lubricant mixture is 0.1% by weight. The amount of phosphorus in PFC18 is about 4.99% by weight and in SSC18, is about 4.88%. PFC18 & SSC18 additives are diluted in base oil to obtain 0.1% phosphorus by weight in the mixture. Both the additive mixture (BO PFC18 & BO 100SSC18) are combined together in the ratio of

20:80. The amount of additive (Antioxidants, detergent or viscosity modifier) added to the mixture is 2% by weight.

## 5.6 Experimental Details

The tribological performance of Ashless compounds with other essential additives was evaluated using High Frequency Reciprocating Rig (HFRR).

The cross sectional schematic of HFRR is shown in Figure 5.9. The wear on steel coupon (ASTM E52100) is produced by the reciprocating action of steel ball (ASTM E52100) on a metal coupon. The metal coupons are of thickness 4mm and about 12.5 mm in diameter. The coupons are polished with 400 grit and 600 grit Silicon carbide paper. The final polish is carried out with 5μm alumina slurry in selvyt cloth. The performance of the lubricant oil is analyzed by adding it as a medium in between the steel ball and the coupon. The wear is produced by application of 1 kg load on steel coupons (dimension 0.5 inch Ø and 4 mm thick). The reciprocating action of steel ball on the metal coupon is carried out for a period of 1 hour at 100º C. The lubricant formulation is added in the oil bath that houses the metal coupon (shown in Figure 4.5). The oil bath houses the steel coupon, lubricant oil and the heating block. The heating block facilitates in rising the temperature of the lubricant oil to 100º C. The test conditions used is summarized below in Table 5.2. Thermocouple is attached to the heating block that determines the oil temperature. The steel coupon is placed in the oil bath/sample holder by lining it with Teflon tape to give it a tight seal and fit. Steel coupon, steel ball and all other components are thoroughly cleaned with hexane to remove contaminants, debris and residue oil before the start of the test. About 12 ml of lubricant oil is used for every test.

Table 5.2 HFRR Test condition

| | |
|---|---|
| Test duration (in minutes) | 60 |
| Load | 1 kg (9.8N) |
| Stroke length (in mm) | 2.5 |
| Stroke frequency (in Hz) | 50 |
| Temperature (in ºC) | 100 |
| Ball | 52100 steel (6.25mm diameter) |
| Coupon | 52100 steel |

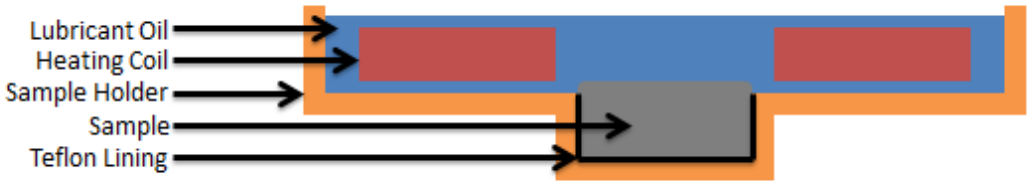


Figure 5.8: HFRR sample holder

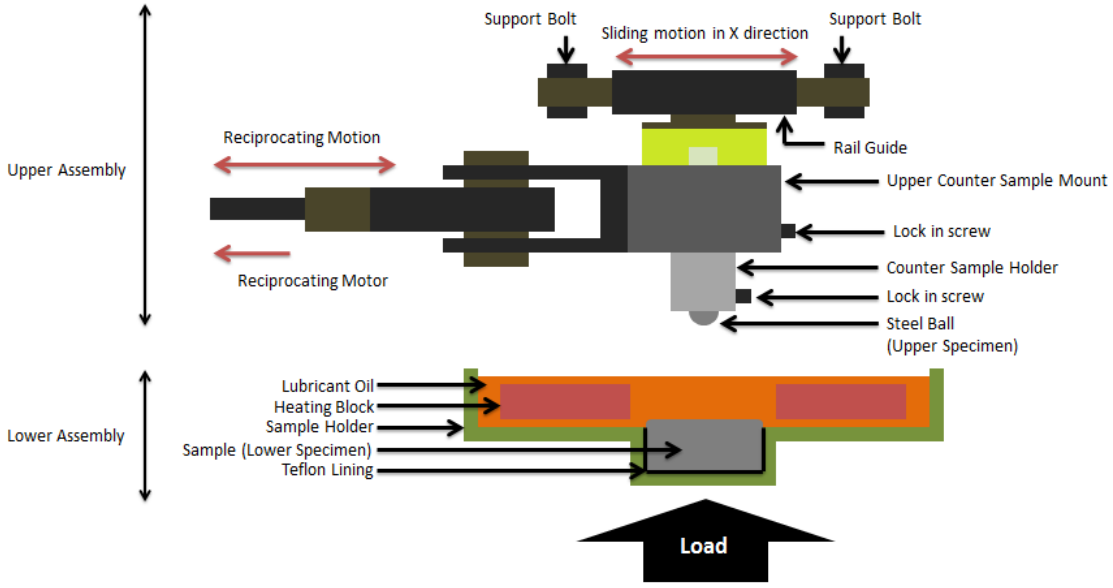


Figure 5.9: Cross sectional Schematic of HFRR

After completion of a test, the steel coupon is removed, washed with hexane to remove debris and residue oil. Hexane is used to clean the coupons because it does not wash away the Tribofilm that is formed in the wear scar. The steel coupon is then soaked in base oil before storage to prevent corrosion. The wear profile & surface roughness was obtained using Veeco Wyko NT 9100 Optical profiler. The surface morphology was determined using the Scanning Electron Microscope. The composition of the Tribofilm was understood with the X-ray Absorption near Edge Spectroscopy (XANES).

## 5.7 Tribological Test Results

### *5.7.1 Wear Data*

Topography of the wear scar is obtained using Veeco Wyko NT 9100 Optical Profiler. The data obtained is then post processed with Image Metrology SPIP 6.0.6 software. The post processing details are summarized in Table 5.3.

Table 5.3 SPIP 6.0.6 Post Processing Details

| | |
|---|---|
| Fill Void Pixels | Sets void pixel to values found by interpolation |
| Particle and Pore Analysis | To obtain the wear volume |
| Cross Section Profile | To obtain the depth of the wear |

The intial surface roughness of the steel sample coupon is recorded as the wear process is influenced by the initial surface roughness of the sample [119,120]. Higher the initial surface roughness of the contacting surfaces, higher is the wear rate [121]. The surface roughness of the steel coupons is shown & summarized below in Figure 5.10 and Tables 5.4, 5.5 & 5.6.

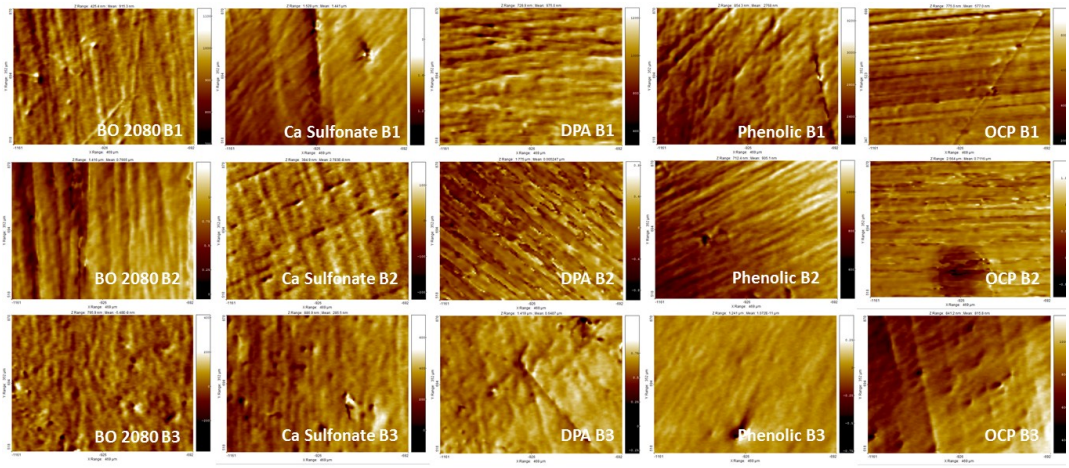


Figure 5.10: Initial surface roughness of the steel coupons.

Table 5.4: Initial surface roughness of steel coupons (Batch 1)

| | BO 2080 | BO 2080 Ca Sulfonate | BO 2080 DPA | BO 2080 Phenolic | BO 2080 OCP |
|---|---|---|---|---|---|
| Sa (nm) | 28.98 | 56.96 | 52.87 | 56.15 | 56.73 |
| Sq (nm) | 37.62 | 82.66 | 68.44 | 73.39 | 74.50 |
| Sy (nm) | 427.64 | 1492.83 | 707.37 | 838.58 | 767.39 |
| Sv (nm) | 198.18 | 672.81 | 420.60 | 385.93 | 422.72 |
| Sp (nm) | 229.45 | 820.02 | 286.76 | 452.66 | 344.67 |
| Smean (nm) | -5.77E-08 | -6.19E-07 | -3.48E-08 | 6.15E-07 | -7.53E-07 |
| Sdr (nm) | 0.003 | 0.011 | 0.014 | 0.012 | 0.020 |
| S2A (nm2) | 1.65E+11 | 1.65E+11 | 1.65E+11 | 1.65E+11 | 1.65E+11 |
| S3A (nm2) | 1.65E+11 | 1.65E+11 | 1.65E+11 | 1.65E+11 | 1.65E+11 |

Table 5.5: Initial surface roughness of steel coupons (Batch 2)

| | BO 2080 | BO 2080 Ca Sulfonate | BO 2080 DPA | BO 2080 Phenolic | BO 2080 OCP |
|---|---|---|---|---|---|
| Sa (nm) | 114.109 | 26.8844 | 127.693 | 33.5611 | 159.939 |
| Sq (nm) | 144.125 | 34.5671 | 166.827 | 44.3654 | 215.493 |
| Sy (nm) | 1143.33 | 384.877 | 1745.82 | 613.175 | 2505.26 |
| Sv (nm) | 662.529 | 221.211 | 845.84 | 389.357 | 1428.5 |
| Sp (nm) | 480.798 | 163.665 | 899.976 | 223.819 | 1076.76 |
| Smean (nm) | -4.00E-07 | 2.63E-08 | -1.71E-07 | 3.45E-07 | 1.82E-06 |
| Sdr (%) | 0.0306931 | 0.0032007 | 0.183962 | 0.00645504 | 0.130618 |
| S2A (nm2) | 1.65E+11 | 1.65E+11 | 1.65E+11 | 1.65E+11 | 1.65E+11 |
| S3A (nm2) | 1.65E+11 | 1.65E+11 | 1.65E+11 | 1.65E+11 | 1.65E+11 |

Table 5.6: Initial surface roughness of steel coupons (Batch 3)

| | BO 2080 | BO 2080 Ca Sulfonate | BO 2080 DPA | BO 2080 Phenolic | BO 2080 OCP |
|---|---|---|---|---|---|
| | Value | Value | Value | Value | Value |
| Sa (nm) | 36.0753 | 36.962 | 50.8589 | 30.0083 | 41.3268 |
| Sq (nm) | 47.4847 | 50.7936 | 69.8794 | 48.2998 | 55.9689 |
| Sy (nm) | 795.947 | 882.296 | 1391.12 | 1240.51 | 652.385 |
| Sv (nm) | 380.221 | 454.73 | 939.455 | 771.701 | 413.237 |
| Sp (nm) | 415.726 | 427.565 | 451.669 | 468.808 | 239.149 |
| Smean (nm) | -4.95E-08 | -1.45E-08 | 1.16E-07 | 1.02E-08 | 3.48E-07 |
| Sdr (%) | 0.00619862 | 0.00577266 | 0.0104371 | 0.00398551 | 0.00525254 |
| S2A (nm2) | 1.65E+11 | 1.65E+11 | 1.65E+11 | 1.65E+11 | 1.65E+11 |
| S3A (nm2) | 1.65E+11 | 1.65E+11 | 1.65E+11 | 1.65E+11 | 1.65E+11 |

The wear tests were done thrice (3 batches viz. B1, B2, B3) for each additive chemistry to obtain a statistical wear data. The wear volume of the scar was obtained using SPIP 6.0.6 and the depth of the wear scar was taken from three regions. The wear scar is divided into three regions (Spot 1, Spot 2 & Spot 3) for convenience. Figure 5.11 shows the different regions of the wear scar.

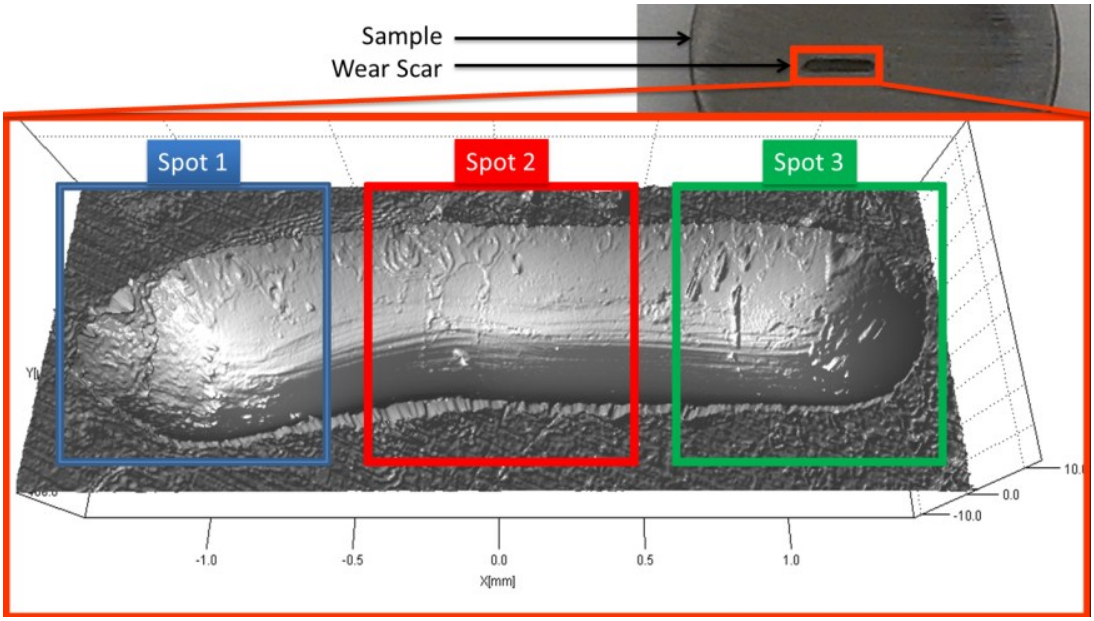


Figure 5.11: Three regions of the wear scar

The wear scar is slightly offset from the center of the metal coupon; hence the corner that is close to the edge of the metal coupon is Spot 1 and the other opposite corner is Spot 3. The wear volume of the three batches for the various chemistries is summarized below (Figure 5.12).

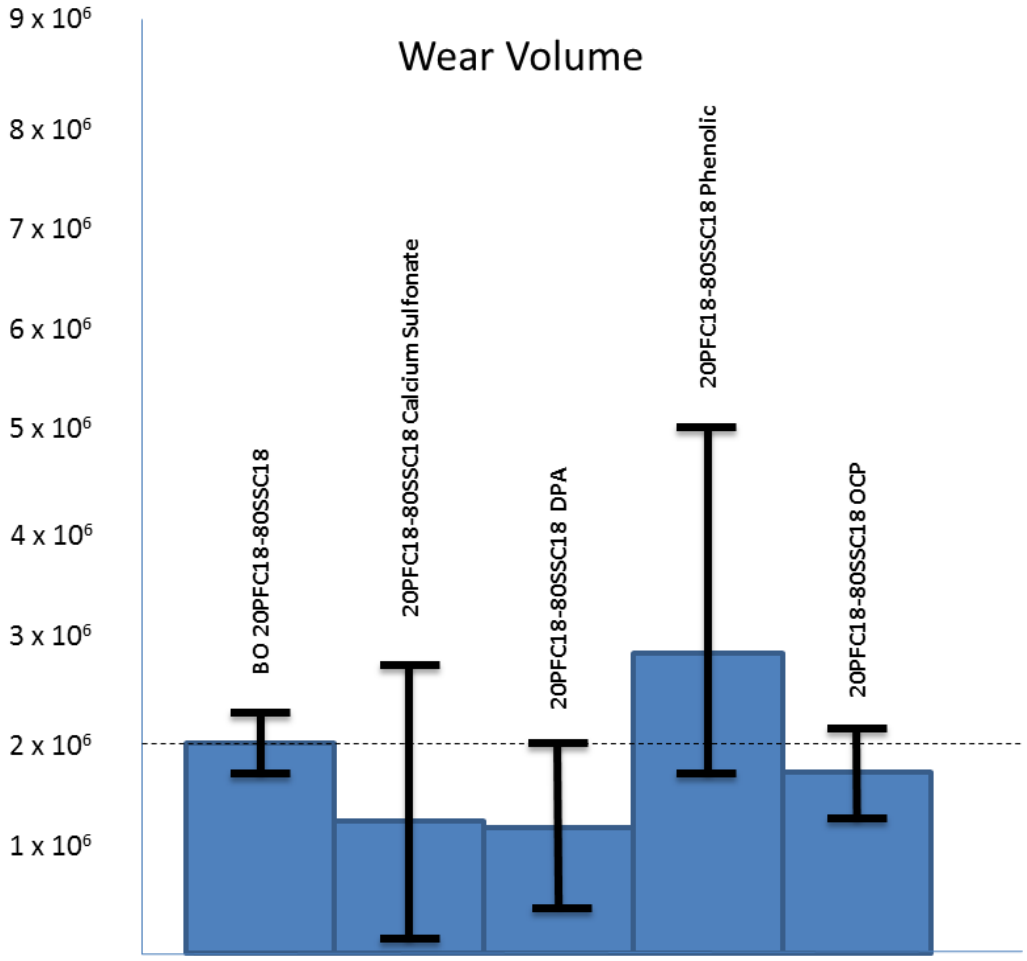


Figure 5.12: Wear Volume

Table 5.7: Wear Volume Data

| **Sample** | **Batch 1 ($\mu m^3$)** | **Batch 2 ($\mu m^3$)** | **Batch 3 ($\mu m^3$)** |
|---|---|---|---|
| BO 20PFC18-80SSC18 | $1.78 \times 10^6$ | $1.98 \times 10^6$ | $2.3 \times 10^6$ |
| BO 20PFC18-80SSC18 Calcium Sulfonate | $2.8 \times 10^6$ | $0.025 \times 10^6$ | $0.768 \times 10^6$ |
| BO 20PFC18-80SSC18 DPA | $1.96 \times 10^6$ | $0.422 \times 10^6$ | $1.11 \times 10^6$ |
| BO 20PFC18-80SSC18 Phenolic | $5.04 \times 10^6$ | $1.93 \times 10^6$ | $1.76 \times 10^6$ |
| BO 20PFC18-80SSC18 St. chain OCP | $1.28 \times 10^6$ | $1.86 \times 10^6$ | $2.09 \times 10^6$ |

The mean wear volume values of all the additives chemistries are less than the mean of BO 20PFC18-80SSC18 (indicated by the dotted line) except for the formulation with Phenolic, indicating that the antiwear properties are improved on addition of DPA, Calcium Sulfonate & straight chain OCP. This was also noticed in the individual wear depths taken in Spots 1, 2 & 3. The volume of wear is indicative of the efficiency of the lubricant in facilitating the formation of antiwear film (boundary lubrication) between the interacting surfaces. The variation in the wear volume among the three batches for each formulation was the least for BO 20PFC18-80SSC18 and highest for BO 20PFC18-80SSC18 Phenolic.

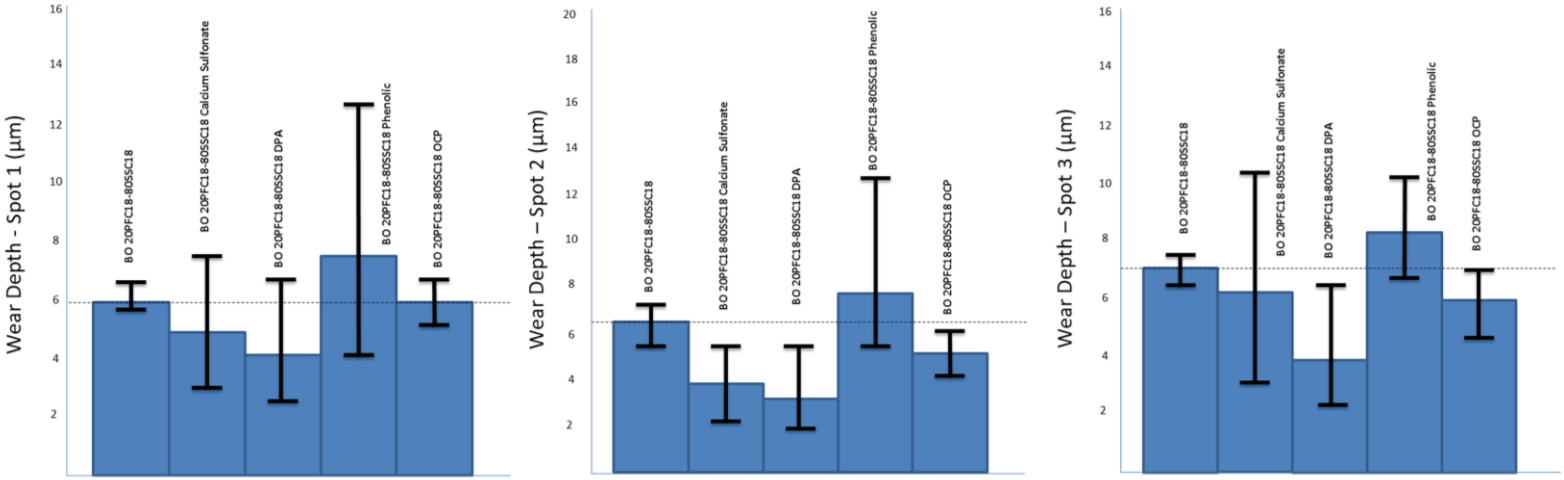


Figure 5.13: Wear Depths in Spot 1, 2 & 3.

All the lubricant blends are arranged in the increasing order of mean wear volume.

(BO 2080 DPA) < (BO 2080 calcium sulfonate) < (BO 2080 OCP) < (BO 20PFC18-80SSC18) < (BO 2080 Phenolic)

The topographical image of the wear scar derived from SPIP 6.0.6 shown in figure 5.14 illustrates the variation in the depth of the wear in the three regions (Spot 1, 2 & 3). The wear depth is not uniform along the length of the scar. The region in between spot 1 & 2 and spot 2 & 3 is shallow & has lower wear depth. The elevation or kink observed in the region between spot 1 & 2 is prominent compared to the region in between spot 2 & 3. The edge of the wear track corresponding to the shallow region has a large debris buildup compared to the other regions in the wear scar.

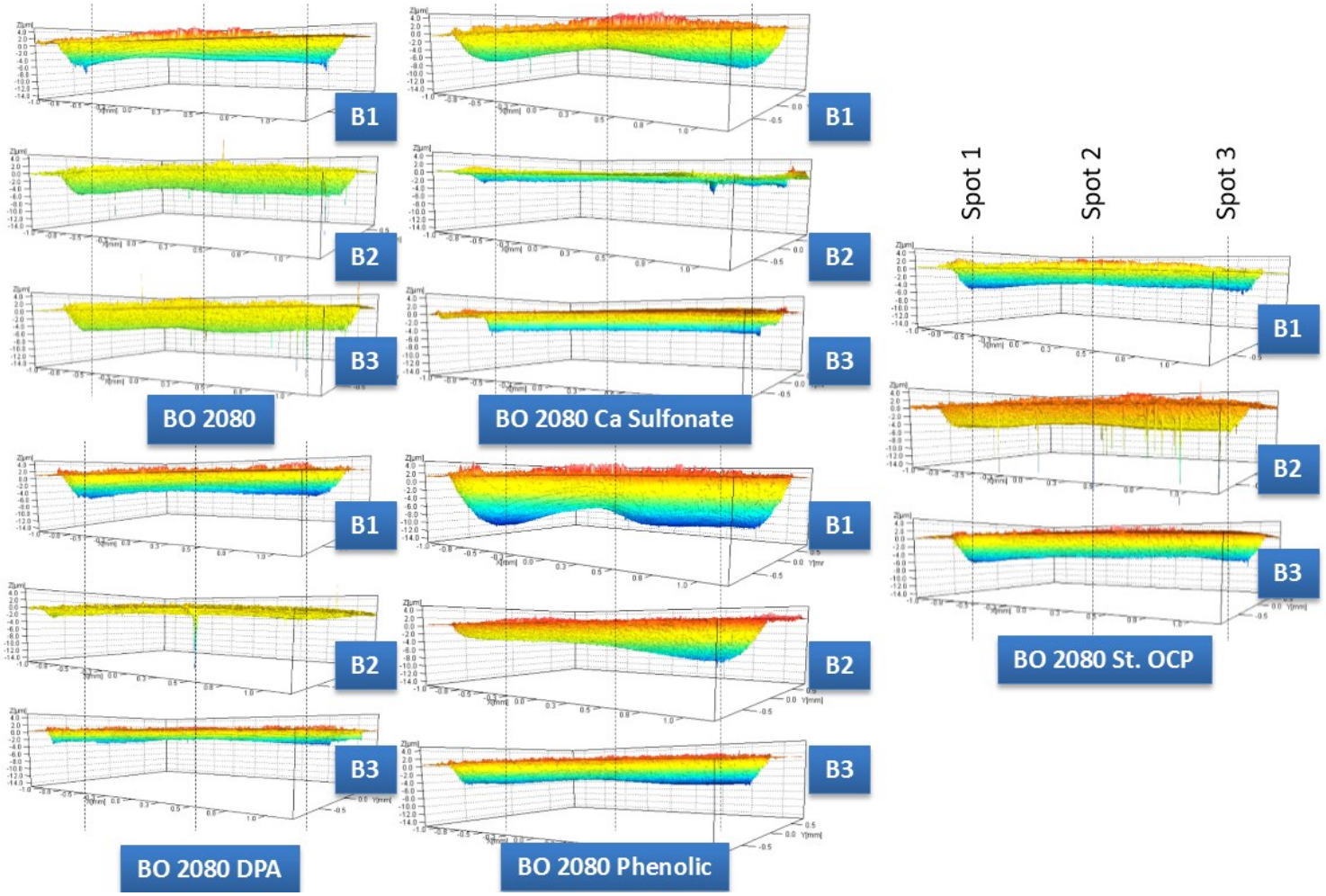


Figure 5.14: Wear depth comparison between the three batches.

## 5.8 Tribofilm Analysis

### *5.8.1 Scanning Electron Microscopy*

Scanning electron microscopy using secondary electrons was used to examine the local morphology of wear scar (Spot 2) in all the lubricant compositions. Figure 5.15 shows typical wear scars for the ashless lubricant formulation BO 20PFC18-80SSC18 with antioxidants (Diphenylamine, Phenolic), viscosity modifier (Straight chain Olefin copolymer) & detergent (Calcium Sulfonate). The morphology is compared with BO 20PFC18-80SSC18. The morphology and characteristics of the wear track provide significant information about the wear behavior of the various chemistries. Chemistries with calcium sulfonate and DPA show streaks of tribofilm patches that run along the length of the wear scar. The streaks are close to each other and uniformly spaced. The wear volumes of both the mentioned chemistries are significantly low, supporting the presence of a good antiwear film. The topography of spot 2 of Phenolic chemistry is characterized by a number of deep gorges indicating the sign of abrasive wear of the additive. The antiwear nature of a lubricant chemistry begins by the development of initiation points on the worn surface (at the appropriate conditions of temperature and pressure) from which the antiwear film starts growing. When the patches of films come in contact with each other, it begins to integrate into a continuous film. Incomplete integration of the Tribofilm leaves divot like marking. These markings could also be due to the Tribofilm pullout. This statement cannot be ruled out since the markings are along the direction of wear. The surface is also characterized by a number of scratches, indicative of thin antiwear film and extensive wear. The wear volume of phenolic chemistry is the highest in batch 1 ($5.04 \times 10^6$ $\mu m^3$). The image of straight chain OCP shows patchy film formation. . BO 20PFC18-80SSC18 shows a smooth surface with a number of divots which is indicative of incomplete integration of tribofilm pads.

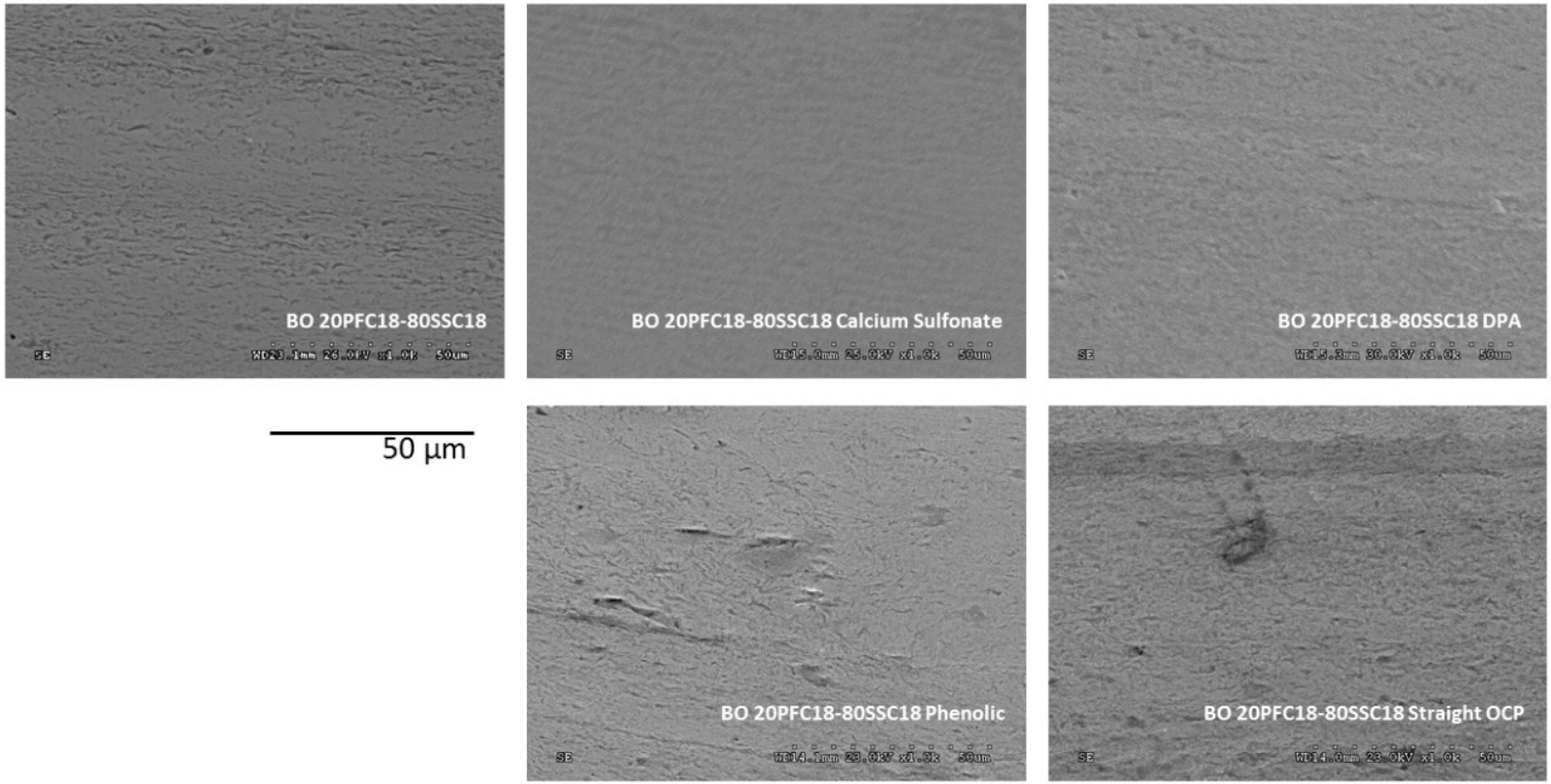


Figure 5.15: SEM Comparative study between different lubricant chemistries

*5.8.2 XANES analysis of tribofilms*

X-ray absorption near edge spectroscopy analysis has been routinely used in the study of tribofilms. It elucidates the complex chemical interactions that occurs between additives in engine oil and metallic surfaces during high temperature and pressure reciprocating wear conditions. It provides a detailed chemical and structural information on the resultant antiwear and tribofilms formed on metallic surfaces [13]. All the XANES spectra included in this study were all acquired at the same time one after another with the same parameters and insturment settings. All XANES spectra were acquired in two modes, the total electron yield (TEY) mode for chemical information of surface or near surface regions and the fluorescence yield (FLY) mode for chemical property of bulk of tribofilm. TEY is used to obtain the surface properties and its sampling depth is around 5nm. The FY mode is to understand the compostion of the bulk of the tribofilm and its sampling depth is around 50nm.

5.8.2.1 Phosphorus L-edge spectral analysis

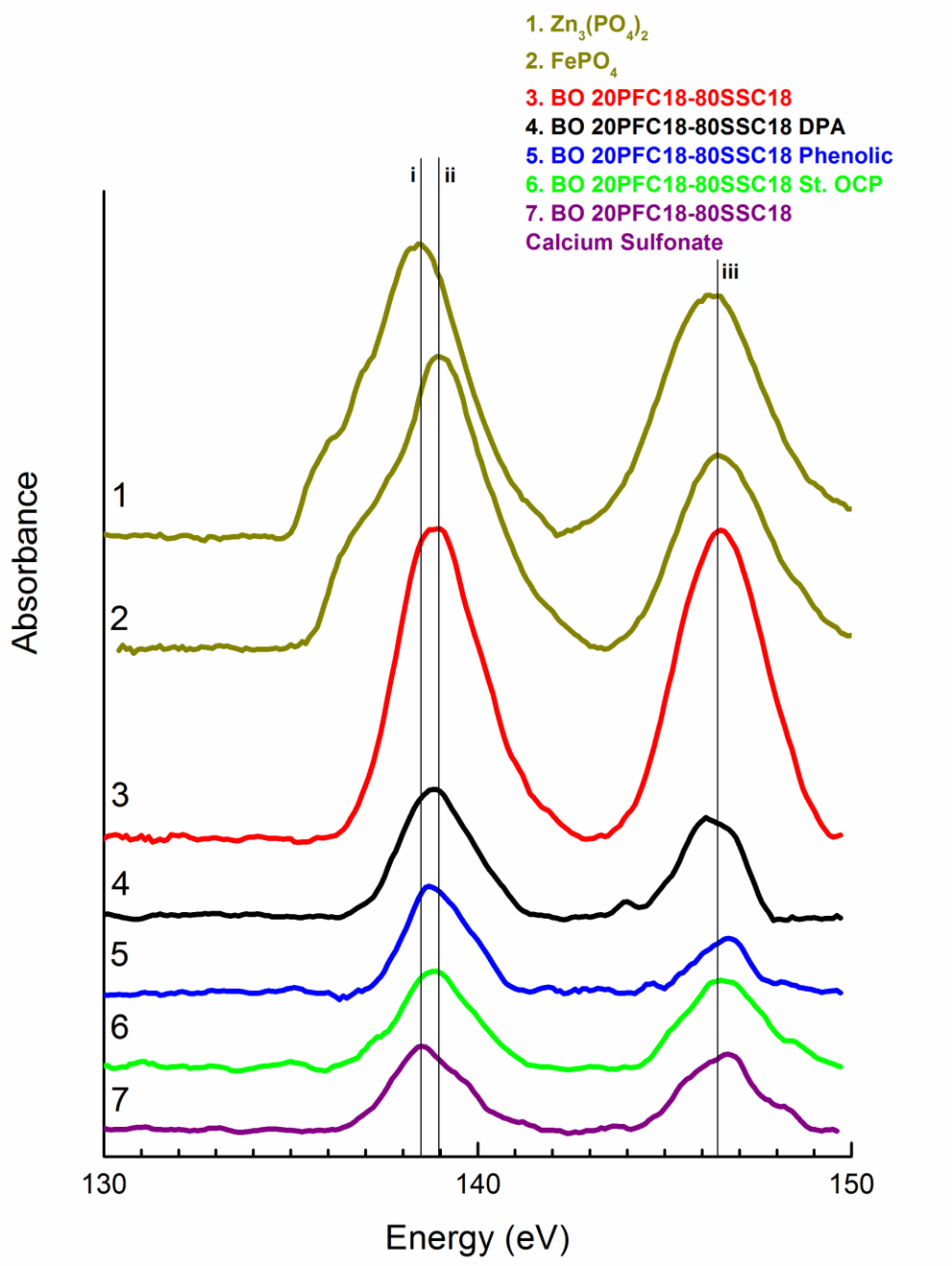


Figure 5.16: P L Edge - Total Electron Yield spectra for model compounds and the various tribofilms.

The phosphorus L edge spectra of the various AW films were collected in both TEY & FY mode. The phosphorus L edge spectra (TEY) of films plotted along with model compounds $FePO_4$ (ferric orthophosphate) and $Zn_3(PO_4)_2$ (zinc phosphate) are shown in figure 5.16 and the FY spectra plotted along with $FePO_4$ (ferric orthophosphate), $Zn_3(PO_4)_2$ (zinc phosphate) & $Fe_4(P_2O_7)_3$ (iron pyrophosphate) is shown in figure 5.18. All the spectral scans were carried out together one after the other at the Canadian Light Source (Saskatoon, Canada). The phosphorus and sulfur L-edge scans were acquired in a single scan in the VLS-PGM (Varied Line Spacing Plane Grating Monochromator) and normalized to the incident beam $I_0$. A comparative study of tribofilms obtained from the various ashless chemistries with additives such as detergents, antioxidants & viscosity modifiers are presented. The P L-edge spectra provides richer chemical information compared to K-edge spectra. The L-edge spectra of phosphorus is characterized by spin-orbit splitting of the phosphorus 2p electrons and excitation to the anti-bonding orbitals [127]. Peaks labelled a and b (shown in figure 5.17) are assigned to the transitions from the 2p3/2 and 2p1/2 to the $a_1$* anti-bonding orbital [126]. Peak c is attributed to the transition of the phosphorus 2p electrons to the $t_2$* molecular orbital. Peak d, known as a shape resonance peak, located at ~146.5 eV, is only present when phosphorus is coordinated to three or more electronegative atoms, such as oxygen [127,128]. The shape resonance peak is characteristic of all phosphates regardless of structure, whether crystalline or glassy [127].

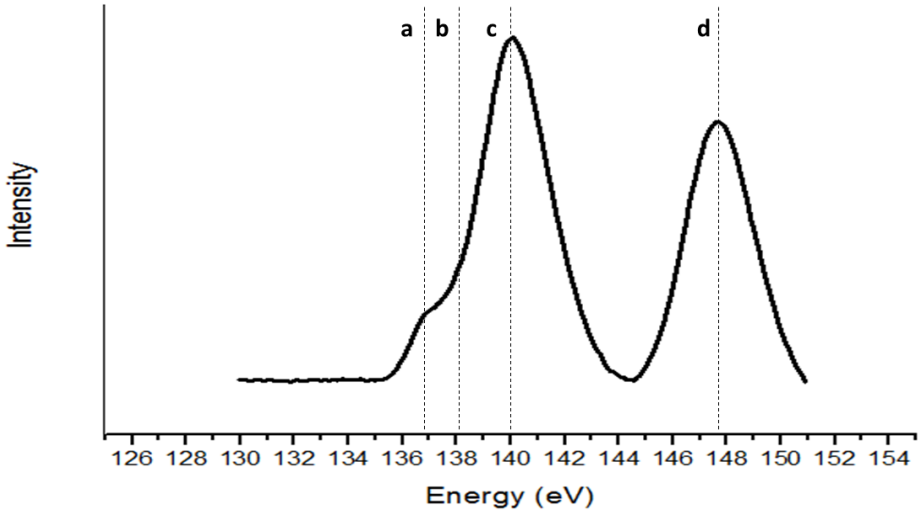


Figure 5.17: Typical P L-edge curve

The ashless chemistries with various additives are compared with the model compounds $Zn_3(PO_4)_2$ and $FePO_4$ in figure 5.16. The TEY spectra of phopshorus is obtained for all the ashless chemistries under study. The white line of $Zn_3(PO_4)_2$ is found in the energy value ~138.5 eV and $FePO_4$ in the range of ~139 eV. All the white lines of the ashless additives do not show pre-edges indicating the nonoccurence of long chain phosphate linking and the layers contain only orthophosphates. BO 20PFC18-80SSC18 shows the highest intensity curves while other chemistries have low intensity peaks indicating that the phosphate concentration is affected on addition of additives (antioxidants, detergents & viscosity modifiers). The white peaks of all the lubricant chemistries are close to the white line of $FePO_4$ indicating the phosphates are in the form of iron orthophosphates in the upper layers of the tribofilm.

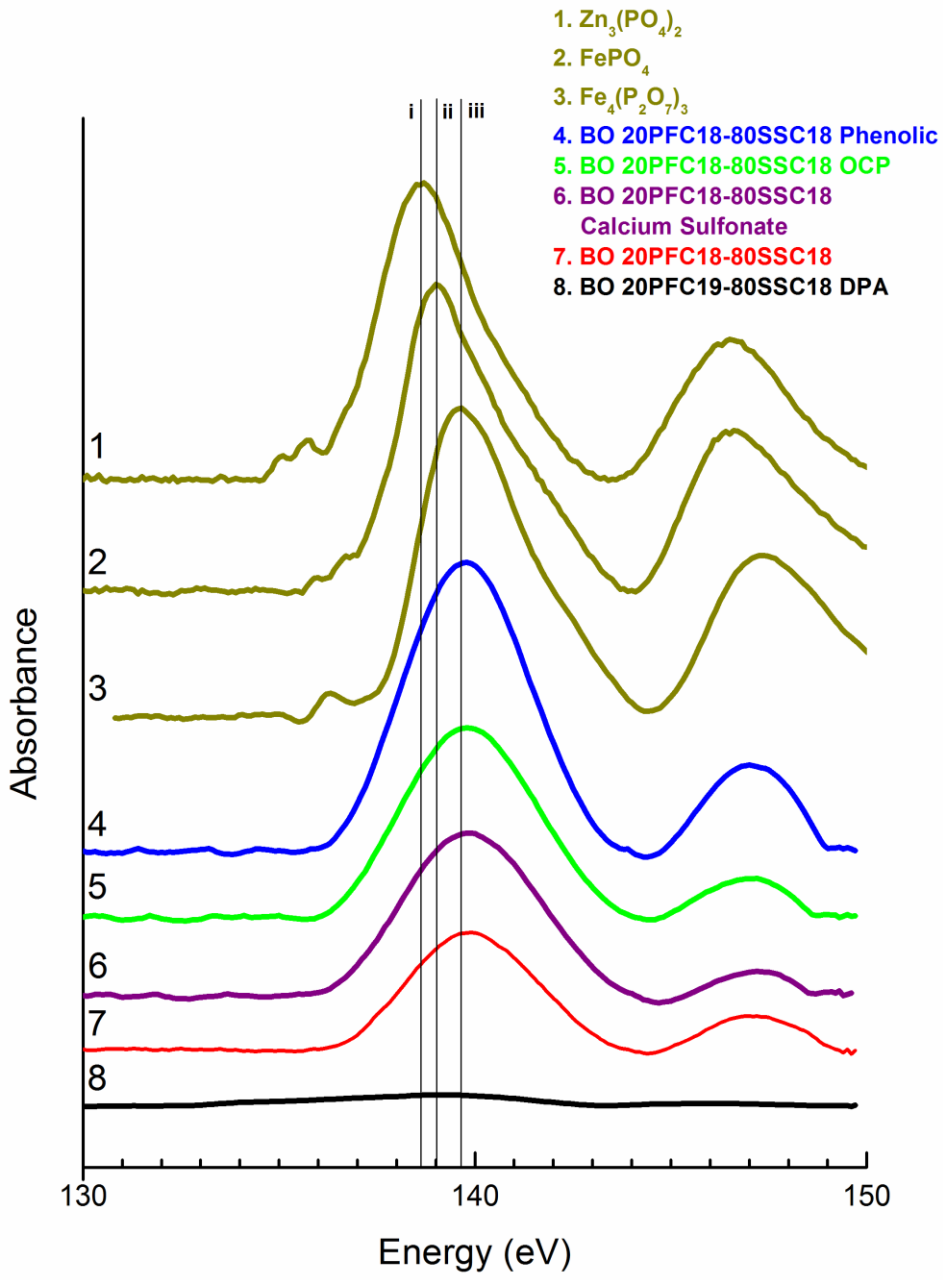


Figure 5.18: P L Edge – Fluorescent Yield

The fluorescent yield (FY) of all the ashless chemistries are compared with three model compounds viz. $Zn_3(PO_4)_2$, $FePO_4$ & $Fe_4(P_2O_7)_3$. The white lines of $Zn_3(PO_4)_2$ is at ~138.5 eV, $FePO_4$ is at ~139 eV & $Fe_4(P_2O_7)_3$ at ~139.6 eV. The white peaks of the ashless chemistries are located at very close proximity to the pyrophosphate model curve indicating the bulk of the tribofilm contains phosphorus in the form of phosphates and pyrophosphates of iron with pyrophosphates in higher concentrations. The possibility of phosphorus in the form of zinc phosphate in the tribofilms is ruled out as there is no zinc present in the lubricant chemistries under study. The peak intensity of formulations with additives such as phenolic, OCP and calcium sulfonate are higher than BO 20PFC18-80SSC18 indicating the bulk of the tribofilm contains iron orthophosphate and iron pyrophosphate. The additives promote the phosphate chain development. BO 20PFC18-80SSC18 with diphenylamine is a straight line indicating the tribofilm formed from this formulation does not promote the phosphate formation and does not contain phosphorus in high concentrations.

5.8.2.2 Sulfur L edge spectral analysis

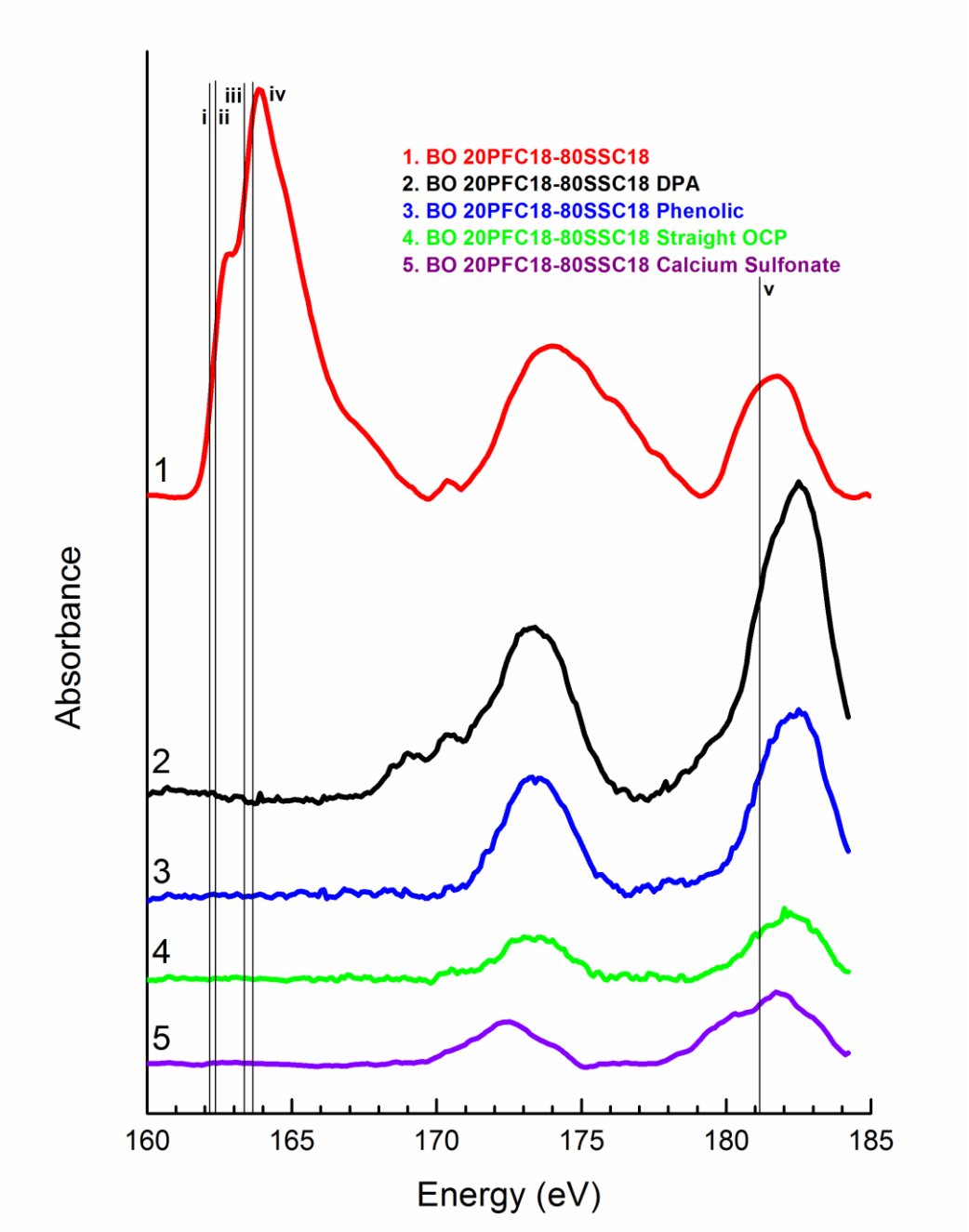


Figure 5.19: Sulfur L edge spectral analysis - Total Electron Yield.

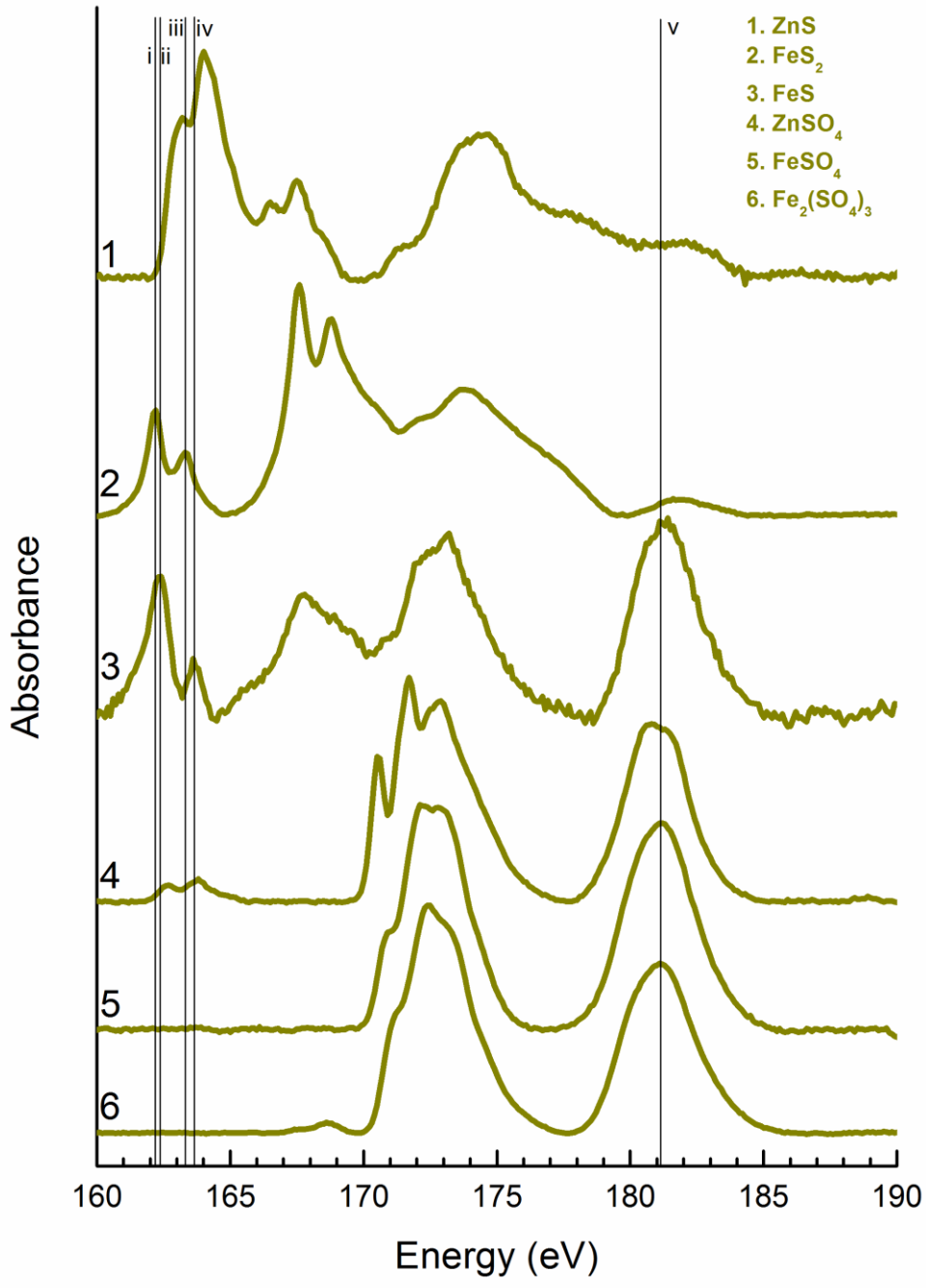


Figure 5.20: Sulfur L edge spectral analysis - model compounds.

The sulfur edge of the lubricant chemistry under study is compared with model compounds viz. ZnS, $ZnSO_4$, $FeSO_4$, FeS, $FeS_2$ & $Fe_2(SO_4)_3$. The TEY spectra of the sample chemistries indicates the composition of the tribofilm in the top layers (5nm). Model compounds iron sulfate ($FeSO_4$ or $Fe_2(SO_4)_3$) have two main peaks (~172.5 eV & ~181 eV). the model compounds containing sulfates have two characteristic peaks and model compounds containing sulfides are characterized by multiple complex peaks as shown in figure 5.20. The first two peaks (i & ii) of BO 20PFC18-80SSC18 resemble FeS and $FeS_2$. The peaks characteristic of sulfides are in the energy range 162 to 162.5 eV (peak i) and 163.2 to 163.8 eV (peak ii). The lubricant chemistries with additives (calcium sulfonate, DPA, Phenolic and OCP) do not exhibit these peaks. This indicates that the additives suppress the formation of sulfides. The tribofilms with additives show only characteristic high intensity sulfate peaks. BO 20PFC18-80SSC18 shows the high sulfate peak intensity (peak v). The peak v of all the formulations with additives are to the right of 181 eV. Zinc sulfide is ruled out as the chemistries under study does not have zinc. The position of the peaks i and ii of BO 20PFC18-80SSC18 are closer to FeS and hence the tribofilm contains sulfur in the form of FeS and $FeS_2$ with FeS being the dominant form of sulfur species. The width of the second peak (peak in between iv & v) in the lubricant formulations containing phenolic, OCP & calcium sulfonate are not broad and resemble the $FeSO_4$ or $Fe_2(SO_4)_3$ indicating the sulfate presence in the mentioned model compound forms. BO 20PFC18-80SSC18 & BO 20PFC18-80SSC18 have broader peak (peak in between peak iv & v) FeS, thus the sulfur could be present in the combination of sulfides (iron sulfide – FeS) and sulfates ($FeSO_4$ or $Fe_2(SO_4)_3$).

## 5.9 Relative proportions of phosphorus and sulfur

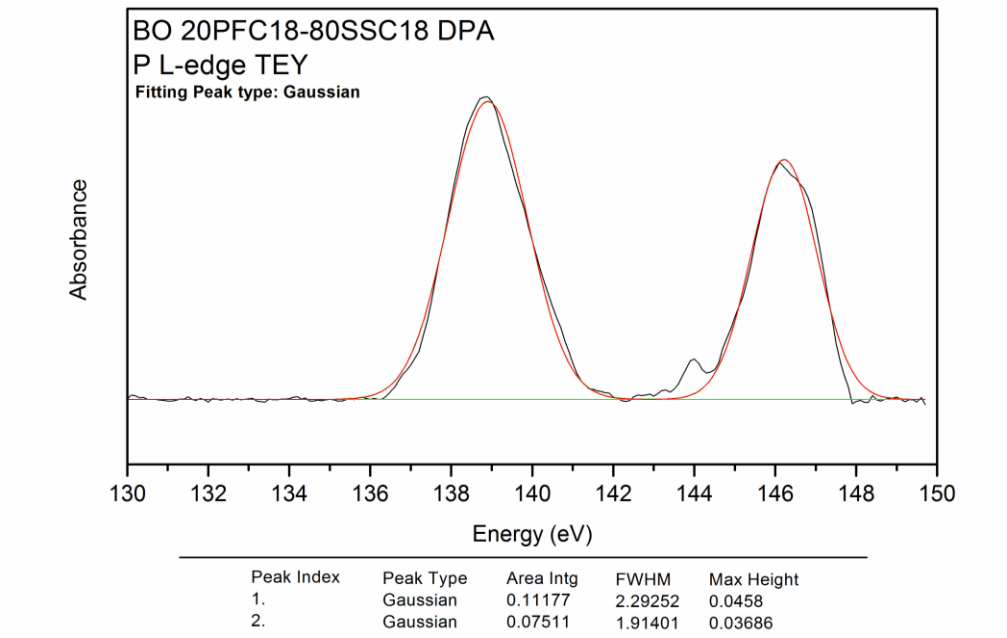


| Peak Index | Peak Type | Area Intg | FWHM | Max Height |
|---|---|---|---|---|
| 1. | Gaussian | 0.11177 | 2.29252 | 0.0458 |
| 2. | Gaussian | 0.07511 | 1.91401 | 0.03686 |

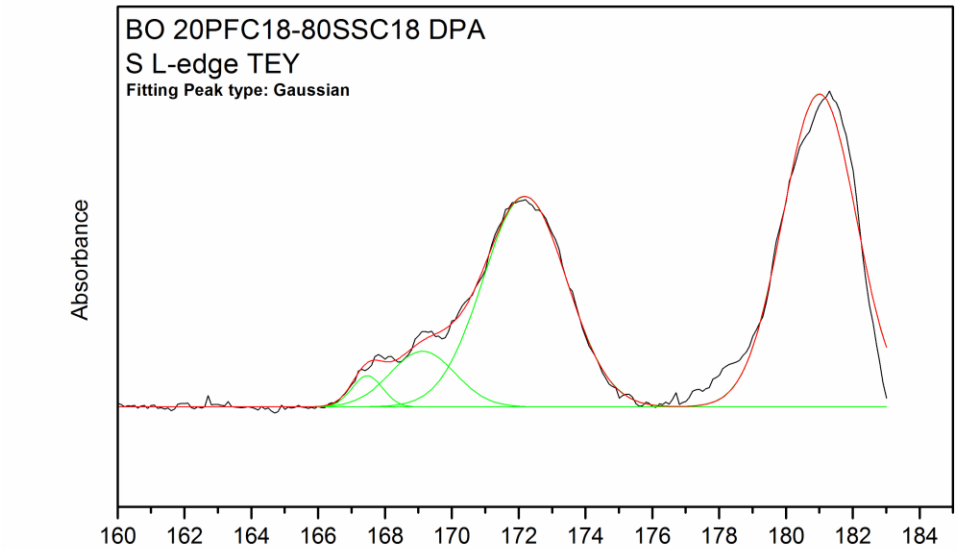


| Peak Index | Peak Type | Area Intg | FWHM | Max Height |
|---|---|---|---|---|
| 1. | Gaussian | 0.33849 | 2.28939 | 0.1389 |
| 2. | Gaussian | 1.64593 | 2.94377 | 0.52526 |
| 3. | Gaussian | 2.08093 | 2.58896 | 0.78193 |
| 4. | Gaussian | 0.08901 | 1.07721 | 0.07762 |

Figure 5.21: Relative proportions of phosphorus and sulfur.

Figure 5.21 shows phosphorus & sulfur L-edge TEY spectra of BO 20PFC18-80SSC18 DPA. The area under the curve is found out to determine the amount of phosphorus & sulfur present in the tribofilm for each lubricant chemistry. The area under the curve for P & S L-edge TEY is calculated and summarized below (Table 5.8).

Table 5.8: Area under the curve & P:S ratio

| No | Sample | Phosphorus (area under curve) | Sulfides (area under curve) | Sulfates (area under curve) | P:S ratio |
|---|---|---|---|---|---|
| 1 | BO 20PFC18-80SSC18 | 0.64 | 3.9 | 3.05 | 0.09 |
| 2 | BO 20PFC18-80SSC18 Calcium Sulfonate | 0.14 | - | 1.07 | 0.14 |
| 3 | BO 20PFC18-80SSC18 DPA | 0.19 | - | 2.17 | 0.09 |
| 4 | BO 20PFC18-80SSC18 Phenolic | 0.06 | - | 2.23 | 0.03 |
| 5 | BO 20PFC18-80SSC18 OCP | 0.17 | - | 0.87 | 0.20 |

The area under the curve is found out using OriginPro 8.5 graphing software and the Gaussian type peak fitting is done. The amount of phosphates observed for all the ashless compounds are less than their corresponding sulfur contents in their tribofilms. Sulfur in the form of sulfides was observed only in BO 20PFC18-80SSC18 while all the other lubricant chemistries contained sulfur in the form of sulfates. The ratio of phosphorus to sulfur in the tribofilms was found to be the least in BO 20PFC18-80SSC18 Phenolic and highest in BO 20PFC18-80SSC18 OCP.

## 5.10 Conclusion

BO 20PFC18-80SSC18 is a combination of two ashless additives viz. Octadecylphosphorofluoridithioate (PFC18) & Octadecylthioperoxydiphosphate (SSC18) in base oil. BO 20PFC18-80SSC18 is compared with BO 20PFC18-80SSC18 containing other additives such as antioxidants (phenolic & diphenylamine), viscosity modifier (Olefinic copolymer) and detergent (calcium sulfonate).

Based on the topography and XANES analysis of the various lubricant chemistries, the following conclusions are drawn.

Olefinic copolymer (OCP) aids in the formation of tribofilm. Olefinic copolymer is combination from ethylene and propylene with non-conjugated diene monomers. OCP along with the phosphorus and sulfur components of the lubricant mixture, form a surface protective tribofilm during the interaction of the rubbing surfaces. The extreme temperature and pressure at the interacting points provides an ideal condition for the copolymers in the lubricant mixture to react with the interacting surfaces thereby mitigating further wear. Lubricant containing Calcium sulfonate also exhibits lower wear than BO 20PFC18-80SSC18. The antioxidant Diphenylamine exhibits good synergism with the ashless additives but phenolic additive has the highest mean wear volume and the largest variation between the highest and least wear volume number. Ashless additives exhibit a good synergism with other additives that impart required properties to the lubricant mixture and as well as aid in the antiwear properties.

The P L-edge TEY XANES spectra of the lubricant chemistries reveal that on addition of additives to the BO 20PFC18-80SSC18, the intensity of phosphate peaks drop indicating the hindrance by the additives (OCP, phenolic, DPA & calcium sulfonate) to the development of phosphates in the upper layers of the tribofilm. On the other hand the FY phosphate peak intensity spikes for BO20PFC18-80SSC18 with calcium sulfonate, OCP and phenolic compared to BO 20PFC18-80SSC18, thus indicating that the bulk of the film contains higher phosphorus concentrations than the surface. Both TEY and FY do not show the presence of pre-edge peaks in the white line curve and hence the phosphorus is present in the form of orthophosphates throughout the tribofilm.

The S L-edge XANES spectra shows with the addition of additives (DPA, OCP, phenolic & calcium sulfonate) to BO 20PFC18-80SSC18, the sulfide formation is completely hindered and only sulfates are observed. BO 20PFC18-80SSC18 shows the presence of both

sulfides and sulfates. BO 20PFC18-80SSC18 DPA's sulfate peaks are the highest and also its wear volume mean is the least.

# CHAPTER 6

# CONCLUSIONS

The objective of this research was to develop a fundamental understanding of the tribological performance of ashless additives, their synergism in combination in base oil and their performance comparison with ZDDP in base oil.

- Alkylthioperoxydiphosphates (SSC18) and Alkylphosphorofluoridothioates (PFC18) additives decompose and react with the underlying substrate to form tribofilms and provide wear resistance superior to ZDDP.

  The XANES Phosphorus L edge spectral analysis showed that all the ashless chemistries have pre-edges except BO 20PFC18-80SSC18. The pre-edge is indicative of crosslinking of phosphate chains in the upper layers of the antiwear film. BO 60PFC18-40SSC18 showed higher a/c ratio indicating the top layer of layer of the film to be composed of medium chain polyphosphates. All the other ashless lubricant formulations show short or orthophosphate chain crosslinking. All Ashless lubricant formulations exhibit better or similar antiwear performance as ZDDP in base oil indicating its potential as a replacement in the commercial engine oils.

  BO20PFC18-80SSC18 with additives such as calcium sulfonate, diphenylamine, phenolic and olefinic copolymers did not exhibit pre-edges in the white line peak indicating the phosphorus presence in the form of orthophosphates. The intensity of the phosphate peaks in the TEY mode for BO 20PFC18-80SSC18 with additives dropped compared to BO 20PFC18-80SSC18, showing the hindrance by the additives could be a possibility.

- Blends of SSC18 and PFC18 are compatible and result in tribofilms with phosphates and sulfides/sulfates.

  All lubricant formulations with ashless additives in various proportions exhibit lower or similar wear volume numbers as BO 100ZDDP. BO 20PFC18-80SSC18 showed the least wear and the formulations with additives (BO 20PFC18-80SSC18 with calcium sulfonate, DPA, phenolic, OCP) exhibited lesser wear volume numbers than BO 20PFC18-80SSC18.

- PFC18 compounds favor the formation of phosphates while the SSC18 compounds favor the formation of sulfides/sulphites/sulfates.

  Lubricant chemistries with high concentrations of PFC18 showed distinct and large phosphate peaks. The intensity of the phosphate peaks in the phosphorus spectra was observed to increase with the increase in PFC18 content except for BO 40PFC18-60SSC18. The intensity of phosphorus white peak for BO 40PFC18-60SSC18 was observed to be higher than 80PFC18-20SSC18 & 60PFC18-40SSC18.

- All neat chemistries and blends with AO, Dispersants, and Detergents retain their antiwear properties.

  OCP along with the phosphorus and sulfur components of the lubricant mixture, form a surface protective tribofilm during the interaction of the rubbing surfaces. The extreme temperature and pressure at the interacting points provides an ideal condition for the copolymers in the lubricant mixture to react with the interacting surfaces thereby mitigating further wear. Lubricant containing calcium sulfonate also exhibits lower wear than BO 20PFC18-80SSC18. The antioxidant Diphenylamine exhibits good synergism with the ashless additives but phenolic additive has the highest mean wear volume and the largest variation between the highest and least wear volume number but is mean wear volume is still lower than BO 100ZDDP. Ashless additives exhibit a good

synergism with other additives that impart required properties to the lubricant mixture and as well as aid in the antiwear properties.

# APPENDIX A

# NANOINDENTATION DATA

1. BO 100ZDDP

Number of Data Points = 16

| File | hc(nm) | Er(GPa) | H(GPa) |
|---|---|---|---|
| 100 ZDDP BO_000.hys | 41.73568 | 190.0876 | 4.642042 |
| 100 ZDDP BO_001.hys | 50.9439 | 109.2605 | 3.500141 |
| 100 ZDDP BO_002.hys | 44.09215 | 134.8791 | 4.297157 |
| 100 ZDDP BO_003.hys | 41.71827 | 117.9019 | 4.643958 |
| 100 ZDDP BO_004.hys | 47.51299 | 113.5712 | 3.862285 |
| 100 ZDDP BO_005.hys | 42.29874 | 143.6577 | 4.556078 |
| 100 ZDDP BO_006.hys | 52.70551 | 129.8096 | 3.336217 |
| 100 ZDDP BO_007.hys | 44.72315 | 131.9107 | 4.211029 |
| 100 ZDDP BO_008.hys | 55.40214 | 92.44373 | 3.098934 |
| 100 ZDDP BO_009.hys | 37.44269 | 165.8395 | 5.402112 |
| 100 ZDDP BO_010.hys | 48.69594 | 98.17305 | 3.731506 |
| 100 ZDDP BO_011.hys | 45.1485 | 198.5783 | 4.161477 |
| 100 ZDDP BO_012.hys | 63.80777 | 82.70477 | 2.515213 |
| 100 ZDDP BO_013.hys | 48.60797 | 121.9603 | 3.742868 |
| 100 ZDDP BO_014.hys | 48.01889 | 56.0088 | 3.795499 |
| 100 ZDDP BO_015.hys | 47.92528 | 130.2085 | 3.821176 |

2. BO 100PFC18

Number of Data Points = 15

| File | hc(nm) | Er(GPa) | H(GPa) |
|---|---|---|---|
| Indent_Data_001.hys | 31.5045 | 176.7582 | 6.892906 |
| Indent_Data_002.hys | 37.63068 | 137.1149 | 5.375328 |
| Indent_Data_003.hys | 22.12432 | 205.4852 | 11.59409 |
| Indent_Data_004.hys | 33.984 | 168.577 | 6.189775 |
| Indent_Data_005.hys | 33.03366 | 143.2652 | 6.435967 |
| Indent_Data_006.hys | 31.68634 | 143.0821 | 6.8197 |
| Indent_Data_007.hys | 35.17218 | 157.9588 | 5.899226 |
| Indent_Data_008.hys | 32.60462 | 173.1113 | 6.557594 |
| Indent_Data_009.hys | 34.02536 | 147.6153 | 6.175564 |
| Indent_Data_010.hys | 32.55865 | 205.3182 | 6.571431 |
| Indent_Data_011.hys | 30.39817 | 172.5468 | 7.233843 |
| Indent_Data_012.hys | 27.67668 | 151.2802 | 8.260353 |
| Indent_Data_013.hys | 37.09064 | 137.5774 | 5.47389 |

| | | | |
|---|---|---|---|
| Indent_Data_014.hys | 35.57392 | 131.6718 | 5.799179 |
| Indent_Data_015.hys | 38.30407 | 98.89665 | 5.227516 |

3. BO 100SSC18

Number of Data Points = 16

| File | hc(nm) | Er(GPa) | H(GPa) |
|---|---|---|---|
| Indent_Data_000.hys | 42.80364 | 127.4601 | 4.475905 |
| Indent_Data_001.hys | 37.32737 | 131.9625 | 5.420503 |
| Indent_Data_002.hys | 39.52725 | 135.2477 | 5.004752 |
| Indent_Data_003.hys | 25.64999 | 194.4707 | 9.233864 |
| Indent_Data_004.hys | 36.09071 | 137.0909 | 5.687657 |
| Indent_Data_005.hys | 25.28484 | 228.3424 | 9.442214 |
| Indent_Data_006.hys | 35.23888 | 171.9329 | 5.879864 |
| Indent_Data_007.hys | 29.06761 | 169.4438 | 7.698868 |
| Indent_Data_008.hys | 34.71239 | 174.7239 | 6.012522 |
| Indent_Data_009.hys | 36.06296 | 159.9751 | 5.693053 |
| Indent_Data_010.hys | 36.29854 | 133.5485 | 5.637269 |
| Indent_Data_011.hys | 32.79905 | 180.4487 | 6.502261 |
| Indent_Data_012.hys | 19.6471 | 250.937 | 14.07094 |
| Indent_Data_013.hys | 27.95118 | 180.9661 | 8.151036 |
| Indent_Data_014.hys | 29.99756 | 219.389 | 7.373896 |
| Indent_Data_015.hys | 52.07026 | 111.6929 | 3.396959 |

4. BO 80PFC18-20SSC18

Number of Data Points = 0

| File | hc(nm) | Er(GPa) | H(GPa) |
|---|---|---|---|
| Indent_Data_000.hys | 23.41038 | 199.5113 | 10.60155 |
| Indent_Data_001.hys | 24.69487 | 179.9625 | 9.780528 |
| Indent_Data_002.hys | 22.58288 | 177.3134 | 11.2079 |
| Indent_Data_003.hys | 21.98404 | 179.8661 | 11.69133 |
| Indent_Data_004.hys | 23.00393 | 186.7106 | 10.89006 |
| Indent_Data_005.hys | 26.43266 | 151.2395 | 8.835886 |
| Indent_Data_006.hys | 23.46717 | 187.3147 | 10.57229 |
| Indent_Data_007.hys | 23.80623 | 187.0937 | 10.33756 |
| Indent_Data_008.hys | 27.29672 | 178.7983 | 8.433288 |
| Indent_Data_009.hys | 23.52295 | 190.3202 | 10.52344 |
| Indent_Data_010.hys | 20.11066 | 212.8998 | 13.53542 |

| | | | |
|---|---|---|---|
| Indent_Data_011.hys | 16.58066 | 248.9367 | 19.29765 |
| Indent_Data_012.hys | 25.55497 | 176.8563 | 9.294195 |
| Indent_Data_013.hys | 25.53767 | 166.5577 | 9.308039 |
| Indent_Data_014.hys | 29.36552 | 167.3028 | 7.599443 |
| Indent_Data_015.hys | 21.10155 | 210.6275 | 12.492 |

5. BO 60PFC18-40SSC18

Number of Data Points = 16

| File | hc(nm) | Er(GPa) | H(GPa) |
|---|---|---|---|
| Indent_data_000.hys | 16.99592 | 252.2801 | 18.35644 |
| Indent_data_001.hys | 70.92367 | 114.7031 | 2.147352 |
| Indent_data_002.hys | 33.18789 | 157.4626 | 6.387563 |
| Indent_data_003.hys | 47.27614 | 142.4312 | 3.894705 |
| Indent_data_004.hys | 38.08777 | 131.4265 | 5.27094 |
| Indent_data_005.hys | 38.58561 | 151.8851 | 5.177247 |
| Indent_data_006.hys | 25.14853 | 210.4353 | 9.517926 |
| Indent_data_007.hys | 41.00015 | 207.2719 | 4.767879 |
| Indent_data_008.hys | 44.62714 | 150.0979 | 4.22849 |
| Indent_data_009.hys | 42.84242 | 157.4603 | 4.474969 |
| Indent_data_010.hys | 41.50325 | 143.0762 | 4.67822 |
| Indent_data_011.hys | 41.63525 | 150.3717 | 4.658322 |
| Indent_data_012.hys | 32.23987 | 153.4023 | 6.652448 |
| Indent_data_013.hys | 43.34172 | 166.7425 | 4.404825 |
| Indent_data_014.hys | 34.9285 | 148.9497 | 5.946209 |
| Indent_data_015.hys | 37.02401 | 148.0216 | 5.488044 |

6. BO 40PFC18-60SSC18

Number of Data Points = 0

| File | hc(nm) | Er(GPa) | H(GPa) |
|---|---|---|---|
| Indent_Data_000.hys | 32.31939 | 197.8821 | 6.62528 |
| Indent_Data_001.hys | 28.18877 | 203.4403 | 8.051908 |
| Indent_Data_002.hys | 38.71888 | 160.5278 | 5.148573 |
| Indent_Data_003.hys | 35.05524 | 163.1635 | 5.921829 |
| Indent_Data_004.hys | 33.89786 | 165.3941 | 6.197361 |
| Indent_Data_005.hys | 35.4027 | 169.1081 | 5.837733 |
| Indent_Data_006.hys | 35.46053 | 149.2032 | 5.820028 |
| Indent_Data_007.hys | 41.0234 | 132.9438 | 4.750799 |

| | | | |
|---|---|---|---|
| Indent_Data_008.hys | 32.59704 | 167.4308 | 6.545464 |
| Indent_Data_009.hys | 48.77277 | 143.3176 | 3.725153 |
| Indent_Data_010.hys | 22.50995 | 244.5395 | 11.2733 |
| Indent_Data_011.hys | 29.54642 | 174.5016 | 7.525846 |
| Indent_Data_012.hys | 20.86794 | 211.0106 | 12.70922 |
| Indent_Data_013.hys | 29.32922 | 198.9577 | 7.609592 |
| Indent_Data_014.hys | 28.50266 | 168.7593 | 7.923175 |
| Indent_Data_015.hys | 34.0349 | 194.4186 | 6.176346 |

7. BO 20PFC18-80SSC18

Number of Data Points = 0

| File | hc(nm) | Er(GPa) | H(GPa) |
|---|---|---|---|
| Indent_Data_000.hys | 35.52744 | 173.2774 | 5.811697 |
| Indent_Data_001.hys | 36.34054 | 169.0171 | 5.630257 |
| Indent_Data_002.hys | 36.88091 | 168.0932 | 5.517495 |
| Indent_Data_003.hys | 30.58069 | 171.0856 | 7.167245 |
| Indent_Data_004.hys | 16.0953 | 256.1645 | 20.51455 |
| Indent_Data_005.hys | 29.40945 | 190.5547 | 7.580119 |
| Indent_Data_006.hys | 32.20999 | 177.8056 | 6.665046 |
| Indent_Data_007.hys | 26.37264 | 185.1289 | 8.864556 |
| Indent_Data_008.hys | 29.6498 | 161.9259 | 7.488616 |
| Indent_Data_009.hys | 29.1227 | 177.7114 | 7.68122 |
| Indent_Data_010.hys | 29.83164 | 166.0496 | 7.422363 |
| Indent_Data_011.hys | 32.87591 | 149.9495 | 6.474701 |
| Indent_Data_012.hys | 31.49549 | 173.0045 | 6.88266 |
| Indent_Data_013.hys | 32.1913 | 167.9927 | 6.665384 |
| Indent_Data_014.hys | 28.25192 | 160.8871 | 8.021602 |
| Indent_Data_015.hys | 27.34031 | 164.7126 | 8.413176 |

8. BO 20PFC18-80SSC18 Calcium Sulfonate

Number of Data Points = 16

| File | hc(nm) | Er(GPa) | H(GPa) |
|---|---|---|---|
| Indent_Data_000.hys | 28.2593 | 177.8779 | 8.025114 |
| Indent_Data_001.hys | 29.17828 | 170.3508 | 7.665627 |
| Indent_Data_002.hys | 29.41949 | 166.5823 | 7.57064 |

| | | | |
|---|---|---|---|
| Indent_Data_003.hys | 32.14272 | 156.8709 | 6.6817 |
| Indent_Data_004.hys | 35.38023 | 143 | 5.839727 |
| Indent_Data_005.hys | 23.94554 | 200.15 | 10.24513 |
| Indent_Data_006.hys | 31.81774 | 151.377 | 6.774334 |
| Indent_Data_007.hys | 33.64234 | 146.1652 | 6.271832 |
| Indent_Data_008.hys | 34.27348 | 151.2569 | 6.11272 |
| Indent_Data_009.hys | 33.78528 | 135.4662 | 6.230372 |
| Indent_Data_010.hys | 26.58951 | 169.4882 | 8.76288 |
| Indent_Data_011.hys | 29.5235 | 159.7468 | 7.538151 |
| Indent_Data_012.hys | 34.12359 | 143.4723 | 6.145169 |
| Indent_Data_013.hys | 34.29056 | 137.8505 | 6.10556 |
| Indent_Data_014.hys | 31.45319 | 186.5125 | 6.895772 |
| Indent_Data_015.hys | 29.07145 | 171.1405 | 7.697851 |

9. BO 20PFC18-80SSC18 DPA

Number of Data Points = 0

| File | hc(nm) | Er(GPa) | H(GPa) |
|---|---|---|---|
| Indent_data_000.hys | 42.43067 | 90.13404 | 4.533049 |
| Indent_data_001.hys | 34.28483 | 107.0992 | 6.100427 |
| Indent_data_002.hys | 43.95249 | 79.74245 | 4.309787 |
| Indent_data_003.hys | 28.29093 | 135.5384 | 8.008552 |
| Indent_data_004.hys | 39.70114 | 99.012 | 4.974075 |
| Indent_data_005.hys | 40.33282 | 91.43702 | 4.862582 |
| Indent_data_006.hys | 91.88151 | 36.92724 | 1.42563 |
| Indent_data_007.hys | 55.35987 | 67.4475 | 3.095303 |
| Indent_data_008.hys | 37.81471 | 103.1654 | 5.320878 |
| Indent_data_009.hys | 34.59133 | 115.7041 | 6.024312 |
| Indent_data_010.hys | 66.34159 | 78.72894 | 2.37034 |
| Indent_data_011.hys | 42.40558 | 91.33068 | 4.535981 |
| Indent_data_012.hys | 42.30907 | 108.4822 | 4.551078 |
| Indent_data_013.hys | 29.60731 | 111.9098 | 7.497408 |
| Indent_data_014.hys | 33.75948 | 101.6575 | 6.229524 |
| Indent_data_015.hys | 35.97406 | 106.0371 | 5.707418 |

10. BO 20PFC18-80SSC18 Phenolic

Number of Data Points = 16

| File | hc(nm) | Er(GPa) | H(GPa) |
|---|---|---|---|

| | | | |
|---|---|---|---|
| Indent_000.hys | 34.76629 | 161.6349 | 5.991497 |
| Indent_001.hys | 29.00426 | 193.7061 | 7.732145 |
| Indent_002.hys | 32.33341 | 169.3599 | 6.626825 |
| Indent_003.hys | 24.54007 | 234.6252 | 9.85963 |
| Indent_004.hys | 28.72303 | 203.7349 | 7.847386 |
| Indent_005.hys | 30.98902 | 215.6701 | 7.039885 |
| Indent_006.hys | 20.78137 | 246.5952 | 12.80883 |
| Indent_007.hys | 33.14477 | 199.3488 | 6.407198 |
| Indent_008.hys | 28.32292 | 209.149 | 7.998915 |
| Indent_009.hys | 32.43574 | 179.5737 | 6.600468 |
| Indent_010.hys | 37.41956 | 149.0901 | 5.406976 |
| Indent_011.hys | 34.30179 | 185.5935 | 6.107718 |
| Indent_012.hys | 30.71743 | 199.3117 | 7.130234 |
| Indent_013.hys | 31.79116 | 219.068 | 6.793347 |
| Indent_014.hys | 49.12418 | 95.27972 | 3.682156 |
| Indent_015.hys | 27.22431 | 171.1951 | 8.464224 |

11. BO 20PFC18-80SSC18 Straight OCP

Number of Data Points = 16

| File | hc(nm) | Er(GPa) | H(GPa) |
|---|---|---|---|
| Indent Data_000.hys | 68.61484 | 143.1596 | 2.260264 |
| Indent Data_001.hys | 30.67244 | 152.3689 | 7.132091 |
| Indent Data_002.hys | 36.84064 | 152.2931 | 5.525553 |
| Indent Data_003.hys | 31.48444 | 172.1609 | 6.877495 |
| Indent Data_004.hys | 47.55708 | 114.2597 | 3.862972 |
| Indent Data_005.hys | 33.71969 | 168.6239 | 6.251679 |
| Indent Data_006.hys | 21.96572 | 204.7835 | 11.70501 |
| Indent Data_007.hys | 36.28047 | 158.4413 | 5.646084 |
| Indent Data_008.hys | 46.25986 | 209.3712 | 4.023289 |
| Indent Data_009.hys | 47.8202 | 135.4354 | 3.833363 |
| Indent Data_010.hys | 63.73766 | 128.9447 | 2.521588 |
| Indent Data_011.hys | 42.45243 | 122.2147 | 4.531412 |
| Indent Data_012.hys | 46.00652 | 150.0373 | 4.05184 |
| Indent Data_013.hys | 47.29867 | 107.1869 | 3.890151 |
| Indent Data_014.hys | 38.00854 | 150.8724 | 5.290942 |
| Indent Data_015.hys | 39.92364 | 120.2961 | 4.932516 |

REFERENCES

[1] http://www.klubersolutions.com/pdfs/What_is_tribology.pdf. 2006;11/14/2012.

[2] Spikes H. Low- and zero-sulphated ash, phosphorus and sulphur anti-wear additives for engine oils. Lubr Sci 2008;20:103.

[3] Topolovec-Miklozic K, Forbus TR, Spikes HA. Film thickness and roughness of ZDDP antiwear films. Tribology Letters 2007;26:161-71.

[4] Fujita H, Spikes HA. The formation of zinc dithiophosphate antiwear films. Proc Inst Mech Eng Part J 2004;218:265-77.

[5] Jost P. Jost Report. House of Commons Official Report 1966;733 (74).

[6] Sheasby JS, Caughlin TA, Habeeb JJ. Observation of the antiwear activity of zinc dialkyldithiophosphate additives. Wear 1991;150:247-57.

[7] Spikes HA. The history and mechanisms of ZDDP. Trib Lett 2004;17:469-489.

[8] Willermet PA, Carter RO,III, Boulos EN. Lubricant-derived tribochemical films-An infra-red spectroscopic study. Tribology Int 1992;25:371,371-380.

[9] Willermet PA, Carter III RO, Schmitz PJ, Everson M, Scholl,D.J., Weber,W.H. Structure and properties of lubricant-derived anti-wear films. Lubrication Science 1997;9:325-348.

[10] Bancroft GM, Kasrai M, Fuller M, Yin Z, Fyfe K, Tan KH. Mechanisms of tribochemical film formation: stability of tribo- and thermally-generated ZDDP films. Trib Lett 1997;3:47,47-51.

[11] Fuller M, Yin Z, Kasrai M, Bancroft GM, Yamaguchi ES, Ryason PR et al. Chemical characterization of tribochemical and thermal films generated from neutral and basic ZDDPs using X-ray absorption spectroscopy. Tribology International 1997;30:305-15.

[12] Mourhatch R, Aswath PB. Nanoscale Properties of Tribofilms formed with Zinc Dialkyl Dithiophosphate (ZDDP) under Extreme Pressure Condition. Journal of Nanoscience and Nanotechnology 2008;9:2682-91.

[13] Nicholls M, Najman MN, Zhang Z, Kasrai M, Norton PR, Gilbert PUPA. The contribution of XANES spectroscopy to tribology. Canadian Journal of Chemistry 2007;85:816-30.

[14] Pereira G, Lachenwitzer A, Kasrai M, Bancroft GM, Norton PR, Abrecht M et al. Chemical and mechanical analysis of tribofilms from fully formulated oils Part 1 – Films on 52100 steel. Tribology 2007;1:48-61.

[15] Leslie R. Rudnick. Lubricants Additives: Chemistry and Applications. January 29, 2003;1:758.

[16] http://www.madehow.com/Volume-1/Lubricating-Oil.html#b. 2006;11/14/2012.

[17] G. Amontons . Hist Acad R Soc 1699:206.

[18] Angove DE, Cant NW. Position dependent phenomena during deactivation of three-way catalytic converters on vehicles. Catal Today 2000;63:371,371-378.

[19] M.V. van der Schoot, S.K. Bhargava, D.B. Akolekar, K. Foger, H. C. Watson. Soc Automot Eng 2001;01:3691.

[20] Loeser EH, Wiquist RC, Twiss SB. Cam and Tappet Lubrication III — Radioactive Study of Phosphorus in the EP Film. A S L E Transactions A S L E Transactions 1958;1:329-35.

[21] Brow RK, Tallant DR, Myers ST, Phifer CC. The short-range structure of zinc polyphosphate glass. J Non Cryst Solids 1995;191:45-55.

[22] G.W. Roper. J.C. Bell. Paper SAB 952473, Society of Automotive Engineers Fuels and Lubricants Meeting and Exposition, Toronto, Ontario+ 16-19 October 1995. . Society of Automotive Engineers 1995;1:16.

[23] http://www.movinggraphics.ca/Car_Illustrations.htm. 1999;2012/10/12.

[24] http://www.shell.com/home/content/products_services/on_the_road/oils_lubricants/cars/how_oil_works/. 2012;2012.

[25] http://www.agcoauto.com/content/news/p2_articleid/167. 2012;2012/10/12.

[26] Watkins RC. The antiwear mechanism of zddp's. Part II. Tribol Int 1982;15:13-5.

[27] H. J. Satrina. In: Anonymous Synthetic Oils and Lubricant Additives - Advances since 1979: Noyes Data Corporation; 1982, p. 70.

[28] Baird J. Great Britain Patent 1872;1516.

[29] Haas F. Lubricant U S Archer-Daniels-Midland Company 1939/06/13;2,162,398.

[30] Hu, S.M., C.L. Gao, J.J. Tang, J.C. Zhang, and H.F. Liang. Properties of mono- and dialkyldiphenyl sulfi des for high temperature lubricants and their molecular structures. Acta Petrolei Sinica (Shiyou Xuebao) 1997;S1:118–130.

[31] Askew, Herbert Frank (Bracknell, EN), Jayne, Gerald John Joseph (Bracknell, EN), Elliott, John Scotchford (Bracknell E. Edwin Cooper & Company Limited (Bracknell, EN) 1974;05/459,938.

[32] Spence, J. Ronald. Lubricating compositions containing normal-alkyl substituted 2-thiazoline disulfide antioxidants. Phillips Petroleum Company (Bartlesville, OK) 1984;06/525,912.

[33] So H, Lin RC. The combined effects of ZDDP, surface texture and hardness on the running-in of ferrous metals. Tribol Int 1999;32:243-53.

[34] Michael Cisson C, Rausina GA, Stonebraker PM. Human health and environmental hazard characterisation of lubricating oil additives. Lubr Sci 1996;8:145-77.

[35] Isaksson M, Frick M, Gruvberger B, Pontén A, Bruze M. Occupational allergic contact dermatitis from the extreme pressure (EP) additive zinc, bis ((O,O?-di-2-ethylhexyl) dithiophosphate) in neat oils. Contact Derm 2002;46:248-9.

[36] Kanerva L, Tupasela O, Jolanki R. Occupational allergic contact dermatitis from ethylhexylzinc dithiophosphate and fatty acid polydiethanolamide in cutting fluids. Contact Derm 2001;44:193-4.

[37] Reaction of Tributyl Phosphite with Oxidized Iron: Surface and Tribological Chemistry. Langmuir:7557.

[38] Najman MN, Kasrai M, Bancroft GM, Frazer BH, DeStatio G. The correlation of microchemical properties to antiwear (AW) performance in ashless thiophosphate oil additives. Tribol Lett 2004;17(4):811-22.

[39] Najman M, Kasrai M, Michael Bancroft G, Davidson R. Combination of ashless antiwear additives with metallic detergents: Interactions with neutral and overbased calcium sulfonates. Tribology International 2006;39:342-55.

[40] Gong Q, He W, Liu W. The tribological behavior of thiophosphates as additives in rapeseed oil. Tribol Int 2003;36:733-8.

[41] Brown AL. Treatment of Hydrocarbon oils. Westinghouse and Electric Manufacturing Company 1917;1,234,862.

[42] Ashburn HV. Lubricating Oil. The Texas Company 11/12/1940;2,221,162.

[43] Hall FW, Towne CC. Method of Lubrication. The Texas Company, New York 10/30/1941;2,257,601.

[44] Musher S. Lubricating Oil and method of making the same. The Musher Foundation, New York 12/3/1940;2,223,941.

[45] Loane CM, Hammond, Gayner JW. Lubricant. The Standard Oil Company, Chicago 6/29/1943;2,322,859.

[46] Moran RC, Evers WL, Fuller EW. Petroleum product and method of making same. Socony-Vacuum Oil Company Inc 10/20/1936;2,058,343.

[47] Moran RC, Kazacik AP. Mineral oil composition. Socony-Vacuum Oil Company Inc 3/21/1939;2,151,300.

[48] Smedler G, Eriksson S, Lindblad M, Bernler H, Lundgren S, Jobson E. Deterioration of Three-Way Automotive Catalysts, Part II - Oxygen Storage Capacity at Exhaust Conditions. Society of Automotive Engineers 1993;10.4271/930944.

[49] Angove DE, Cant NW. Position dependent phenomena during deactivation of three-way catalytic converters on vehicles. Catalysis Today 2000;63:371-8.

[50] C. F. Prutton, D. Turnbull, G. Dlouhy. Mechanism of action of organic chlorine and sulfur compounds in extreme-pressure lubrication. Journal of the Institute of Petroleum 1946;32:90-118.

[51] Kotvis PV, Huezo L, Millman WS, Tysoe WT. The surface decomposition and extreme-pressure tribological properties of highly chlorinated methanes and ethanes on ferrous surfaces. Wear 1991;147:401-19.

[52] Kotvis PV, Lara J, Surerus K, Tysoe WT. The nature of the lubricating films formed by carbon tetrachloride under conditions of extreme pressure. Wear 1996;201:10-4.

[53] Furlong O, Gao F, Kotvis P, Tysoe WT. Understanding the tribological chemistry of chlorine-, sulfur- and phosphorus-containing additives. Tribol Int 2007;40:699-708.

[54] Kaltchev M, Kotvis P,V., Blunt T,J., Laraa J, Tysoe W,T. A molecular beam study of the tribological chemistry of dialkyl disulfides. 2001.

[55] Barcroft FT. A technique for investigating reactions between E.P. additives and metal surfaces at high temperatures. Wear 1960;3:440-53.

[56] Rutherford T. J, Miller J. R. Compounded Hydrocarbon Oil. Standard Oil Company of California 08/19/1941;2,252,984.

[57] Rutherford T. J, Miller J. R. Compounded Oil. Standard Oil Company of California 08/19/1941;2,252,985.

[58] Asseff A. P. Lubricant. Lubri-Zol Corporation, Wickliffe, Ohio 10/28/1941;2,261,047.

[59] Cook W. E, Thomas D. William. Crankcase Lubricant and Chemical Compound therefore. 2,342,572 02/22/1944;2,342,572.

[60] Cook W. E, Thomas D. William. Crankcase Lubricant and chemical compound therefore. American Cyanamid Company 03/14/1944;2,344,392.

[61] Cook W. E, Thomas D. W. Lubricanting oil composition. American Cyanamid Company 03/14/1944;2,344,393.

[62] Cook W. E, Thomas D. W. Lubricanting Composition. American Cyanamid Company 09/19/1944;2,358,305.

[63] Cook W. E, Thomas D. W. Lubricating Compositions. American Cyanamid Company 01/23/1945;2,368,000.

[64] Mangolini F, Rossi A, Spencer ND. Influence of metallic and oxidized iron/steel on the reactivity of triphenyl phosphorothionate in oil solution. Tribol Int 2011;44:670-83.

[65] Zhang J, Liu W, Xue Q. The tribological properties of the heterocyclic compound containing S, N, O, and B as additive in liquid paraffin. Wear 1999;224:68-72.

[66] Sun Y, Hu L, Xue Q. Tribological properties and action mechanism of N,N-dialkyl dithiocarbamate-derived S-hydroxyethyl borate esters as additives in rapeseed oil. Wear 2009;266:917-24.

[67] McFadden C, Soto C, Spencer ND. Adsorption and surface chemistry in tribology. Tribol Int 1997;30:881-8.

[68] Klepper CC, Williams JM, Truhan Jr. JJ, Qu J, Riester L, Hazelton RC et al. Tribo-mechanical properties of thin boron coatings deposited on polished cobalt alloy surfaces for orthopedic applications. Thin Solid Films 2008;516:3070-80.

[69] Chung H, Weinberger MB, Levine JB, Kavner A, Yang J, Tolbert SH et al. Synthesis of Ultra-Incompressible Superhard Rhenium Diboride at Ambient Pressure. Science 2007;316:436-9.

[70] Ozdemir O, Usta M, Bindal C, Ucisik AH. Hard iron boride (Fe2B) on 99.97 wt% pure iron. Vacuum 2006;80:1391-5.

[71] Martini C, Palombarini G, Carbucicchio M. Mechanism of thermochemical growth of iron borides on iron. Journal of Materials Science 2004;39:933-7.

[72] Li Y, Pereira G, Lachenwitzer A, Kasrai M, Norton P. Studies on ZDDP Thermal Film Formation by XANES Spectroscopy, Atomic Force Microscopy, FIB/SEM and 31P NMR. Tribology Letters 2008;29:11-22.

[73] Ivanov AV, Antzutkin ON, Larsson A, Kritikos M, Forsling W. Polycrystalline and surface O,O′-dialkyldithiophosphate zinc(II) complexes: preparation, 31P CP/MAS NMR and single-crystal X-ray diffraction studies. Inorg Chim Acta 2001;315:26-35.

[74] - Correlations between 31P Chemical Shift Anisotropy and Molecular Structure in Polycrystalline O,O‘-Dialkyldithiophosphate Zinc(II) and Nickel(II) Complexes: 31P CP/MAS NMR and Ab Initio Quantum Mechanical Calculation Studies. - J Am Chem Soc:- 2218.

[75] Shah Ullah F, Glavatskih S, Antzutkin N. O. Novel Alkylborate–Dithiocarbamate Lubricant Additives: Synthesis and Tribophysical Characterization. :67-78.

[76] Jun D, Cyril A. M. Stabilized Lubricant Composition. Crompton Corporation 05/12/2005;128929.

[77] Martin JM, Belin M, Mansot JL, Dexpert H, Lagarde P. Friction-Induced Amorphization with Zddp - an EXAFS Study. ASLE Trans 1986;29:523-31.

[78] Penner-Hahn JE. 2.13 - X-ray Absorption Spectroscopy. In: Editors-in-Chief: J. A. McCleverty, T. J. Meyer, editors. Comprehensive Coordination Chemistry II, Oxford: Pergamon; 2003, p. 159-186.

[79] Morin C, Ikeura-Sekiguchi H, Tyliszczak T, Cornelius R, Brash JL, Hitchcock AP et al. X-ray spectromicroscopy of immiscible polymer blends: polystyrene–poly(methyl methacrylate). Journal of Electron Spectroscopy and Related Phenomena 2001;121:203-24.

[80] Croll M. L, Stöver D. H. H, Hitchcock P. A. Composite Tectocapsules Containing Porous Polymer Microspheres as Release Gates. Macromolecules:2903.

[81] Jacobsen, Wirick, Flynn, Zimba. Soft X-ray spectroscopy from image sequences with sub-100 nm spatial resolution. J Microsc 2000;197:173-84.

[82] Ade H, Smith AP, Zhang H, Zhuang GR, Kirz J, Rightor E et al. X-ray spectromicroscopy of polymers and tribological surfaces at beamline X1A at the NSLS. Journal of Electron Spectroscopy and Related Phenomena 1997;84:53-72.

[83] Bearden JA. Reevaluation of X-Ray Atomic Energy Levels. Reviews of Modern Physics 1967:125.

[84] James RW. The Dynamical Theory of X-Ray Diffraction. In: Anonymous Solid State Physics: Academic Press, p. 53-220.

[85] http://www-cxro.lbl.gov/optical_constants/web.html. 2010;10/27/2012.

[86] http://physics.nist.gov/PhysRefData/XrayMassCoef/cover.html. 2009;10/27/2012.

[87] Newville M, Ravel B, Haskel D, Rehr JJ, Stern EA, Yacoby Y. Analysis of multiple-scattering XAFS data using theoretical standards. Physica B: Condensed Matter 1995;208–209:154-6.

[88] Markowicz A. A. Handbook of X-ray Spectrometry. 2nd ed. New York: Marcel Dekker, 2002.

[89] The Synchrotron Radiation Center (SRC).

[90] The Canadian Light Source.

[91] Mourhatch R. Tribological and Antiwear Mechanisms of Fluorinated Zinc Dialkyl Dithiophosphate in Comparison to Zinc Dialkyl Dithiophosphate in Engine Oils. 2008:161.

[92] Bec S, Tonck A, Georges JM, Coy RC, Bell JC, Roper GW. Relationship between mechanical properties and structures of zinc dithiophosphate anti–wear films. Proceedings of

the Royal Society of London Series A: Mathematical, Physical and Engineering Sciences 1999;455:4181-203.

[93] http://www.hysitron.com/. 2010;10/27/2012.

[94] D. Nix W. Elastic and plastic properties of thin films on substrates: nanoindentation techniques. Materials Science and Engineering: A 1997;234–236:37-44.

[95] Oliver W,C., Pharr G,M. An improved technique for determining hardness and elastic modulus using load and displacement sensing indentation experiments. J Mater Res 1992;7:1564-83.

[96] Gatto V, Moehle W, Schneller E, Barris T, Cobb T, Featherstone M. A review of engine oil oxidation bench tests and their application in the screening of new antioxidant systems for low phosphorus engine oils. Journal of ASTM International 2007;4.

[97] Ribeaud M. Volatility of phosphorus-containing anti-wear agents for motor oils. Lubr Sci 2006;18:231-41.

[98] Vipper AB, Lashkhi VL, Belov PS, Parfenova VA, Blokhina IV. Antifriction and antiwear efficiency of ashless thiophosphates and dithiophosphates. Chemistry and Technology of Fuels and Oils 1983;19:136-9.

[99] Kai, Mizuno Y, Naoko. Fluorine-containing alkylsuccinic acid diester, process for preparing the same and use thereof. Matsushita Electric Industrial Co , Ltd 11/1/1994;08/333,296.

[100] Pardee P. R. Lubricant comprising fluoroalkyl esters. Ball Corporation 7/12/1978;05/924,025.

[101] Metro J. S, Plains S, Garbus J. A, Barnum E. Robert. Fluorine containing esters of poly-carboxylic acids. Esso Research and Engineering Company 2/25/1960;3124533.

[102] Najman M, Kasrai M, Michael Bancroft G, Davidson R. Combination of ashless antiwear additives with metallic detergents: interactions with neutral and overbased calcium sulfonates. Tribol Int 2006;39:342-55.

[103] Inhibition of Cumene Oxidation by Tetralin Hydroperoxide. J Am Chem Soc:2079.

[104] Gatto VJ, Elnagar HY, Moehle WE, Schneller ER. Redesigning alkylated diphenylamine antioxidants for modern lubricants. Lubr Sci 2007;19:25-40.

[105] Scott G. Oxidation and Antioxidants. Amsterdam: Elsevier, 1965.

[106] Brydson J A. Plastic Materials. 6th ed. Oxford (UK): Butter-worth-Heinemann Ltd., 1995.

[107] Spaleck W. Polypropylene Handbook. Polymerization, Characterization, Properties, Processing, Applications. Herausgegeben von E. P. Moore, Jr. Hanser-Gardner, Cincinnati, 1996. 419 S., geb. 136.00 $.?ISBN 1-56990-208-9. Angewandte Chemie 1997;109:1175-.

[108] Neyestanaki AK, Klingstedt F, Salmi T, Murzin DY. Deactivation of postcombustion catalysts, a review. Fuel 2004;83:395-408.

[109] Moulijn JA, van Diepen AE, Kapteijn F. Catalyst deactivation: is it predictable?: What to do? Applied Catalysis A: General 2001;212:3-16.

[110] Christou S, Gåsste J, Karlsson H, Fierro J, Efstathiou A. Regeneration of Aged Commercial Three-Way Catalytic Converters. Topics in Catalysis 2009;52:2029-34.

[111] Martin L, Arranz JL, Prieto O, Trujillani R, Holgado MJ, Galan MA et al. Simulation three-way catalyst ageing - Analysis of two conventional catalyst. Applied Catalysis B: Environmental 8/8/2003;44:41-52.

[112] Larese C, Galisteo FC, Granados ML, Mariscal R, Fierro JLG, Furio M et al. Deactivation of real three way catalysts by CePO4 formation. Applied Catalysis B: Environmental 2003;40:4.

[113] Larese C, Galisteo FC, Granados ML, Mariscal R, Fierro JLG, Lambrou PS et al. Effects of the CePO4 on the oxygen storage and release properties of CeO2 and Ce0.8Zr0.2O2 solid solution. Journal of Catalysis 2004;226:443-56.

[114] Larese C, López Granados M, Mariscal R, Fierro JLG, Lambrou PS, Efstathiou AM. The effect of calcination temperature on the oxygen storage and release properties of CeO2 and

Ce–Zr–O metal oxides modified by phosphorus incorporation. Applied Catalysis B: Environmental 2005;59:13-25.

[115] López Granados M, Galisteo FC, Lambrou PS, Mariscal R, Sanz J, Sobrados I et al. Role of P-containing species in phosphated CeO2 in the deterioration of its oxygen storage and release properties. Journal of Catalysis 2006;239:410-21.

[116] Subramanian B, Christou SY, Efstathiou AM, Namboodiri V, Dionysiou DD. Regeneration of three-way automobile catalysts using biodegradable metal chelating agent—S, S-ethylenediamine disuccinic acid (S, S-EDDS). J Hazard Mater 2011;186:999-1006.

[117] Chen X, Elsenbaumer RL, Aswath PB.

Synthesis and Tribological Behavior of Ashless Alkylphosphorofluoridothioates : Part 1: Synthesis and Wear Behavior. Tribol Int 2012;Under Review.

[118] Chen X, Kim B, Elsenbaumer R, Aswath PB, Aswath PB. Synthesis and Antiwear Behavior of Alkylthioperoxydiphosphates. Tribology - Materials, Surfaces and Interfaces 2012;Accepted for Publication.

[119] Sedlaček M, Podgornik B, Vižintin J. Influence of surface preparation on roughness parameters, friction and wear. Wear 2009;266:482-7.

[120] Jiang J, Arnell RD. The effect of substrate surface roughness on the wear of DLC coatings. Wear 2000;239:1-9.

[121] Hisakado T, Miyazaki K, Kameta A, Negishi S. Effects of surface roughness of roll metal pins on their friction and wear characteristics. Wear 2000;239:69-76.

[122] Kubiak KJ, Mathia TG. Influence of roughness on contact interface in fretting under dry and boundary lubricated sliding regimes. Wear 2009;267:315-21.

[123] Pereira G, Munoz-Paniagua D, Lachenwitzer A, Kasrai M, Norton PR, Capehart TW et al. A variable temperature mechanical analysis of ZDDP-derived antiwear films formed on 52100 steel. Wear 2007;262:461-70.

[124] Varlot K, Kasrai M, Martin JM, Vacher B, Bancroft GM, Yamaguchi ES et al. Antiwear film formation of neutral and basic ZDDP: influence of the reaction temperature and of the concentration. Tribology Letters 2000; 01;8:9-16.

[125] Suominen Fuller ML, Rodriguez Fernandez L, Massoumi GR, Lennard WN, Kasrai M, Bancroft GM. The use of Xâ€ray absorption spectroscopy for monitoring the thickness of antiwear films from ZDDP. Trib Lett 2000;8:187,187-192.

[126] Sutherland DGJ. Physical Review B:14989.

[127] Yin Z, Kasrai M, Fuller M, Bancroft GM, Fyfe K, Tan KH. Application of soft X-ray absorption spectroscopy in chemical characterization of antiwear films generated by ZDDP Part I: the effects of physical parameters. Wear 1997;202:172-91.

[128] Chemical characterization and nanomechanical properties of antiwear films fabricated fromZddp on a near hypereutectic Al-Si alloy. :411-427.

[129] Yin Z, Kasrai M, Bancroft GM, Tan KH. X-ray-absorption spectroscopic studies of sodium polyphosphate glasses. Physical Review B: Condensed Matter 1995;51:742.

[130] Mortier R, Orszulik S. Chemistry and Technology of Lubricant. 2nd ed. : Blackie Academic & Professional, 1997.

[131] Pospisil J. Advances in Polymer Science. 1995:87-190-124.

[132] Bearchell CA, Danks TN, Heyes DM, Moreton DJ, Taylor SE. Experimental and molecular modelling studies of overbased detergent particles. Phys Chem Chem Phys:5197.

[133] Koch P, Di Serio A. Compounds useful as detergent additives for lubricants and lubricating compositions. US Patent 1991;5,021,174.

[134] Can J Chem:842.

[135] Mechanism of Acid Neutralization by Overbased Colloidal Additives in Hydrocarbon Media. Langmuir:340.

[136] Rizvi SQA. A comprehensive review of lubricant chemistry, technology, selection, and design. : ASTM International, 2009.

## BIOGRAPHICAL INFORMATION

Pradip Sairam Pichumani completed his undergraduate in the field of Polymer Engineering from Amrita School of Engineering (Coimbatore, India). He has gained hands-on training in aircraft composite repair from Heatcon Composite Training (Philippines). He has pursued his Master's degree in the Materials Science and Engineering Department at the University of Texas at Arlington since 2010 under the supervision of Dr. Pranesh B. Aswath. During his master's program, at UTA, he got an opportunity to work as an intern at Advanced Micro Devices, Austin USA as a Failure Analysis Engineer from January 2012 to August 2012. Taking his consistent good academic performance into consideration, the department of Materials Science & Engineering awarded him Materials Science scholarship during multiple semesters. He's a part of ASM (American Society of Materials), Golden Key Member, STLE (Society of Tribologists and Lubrication Engineers) since 2010. His areas of interest include composites, semiconductor failure analysis & tribology.